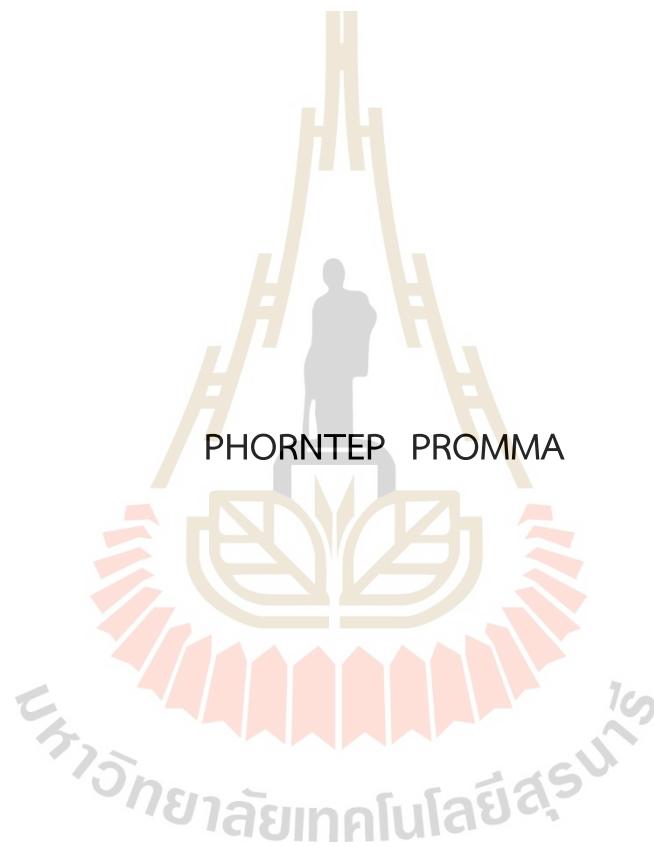# KINETICS AND THERMODYNAMICS OF ENZYMATIC DECARBOXYLATION OF α,β-UNSATURATED ACID: A THEORETICAL STUDY

PHORNTEP PROMMA

A Thesis Submitted in Partial Fulfillment of the Requirements for the
Degree of Doctor of Philosophy in Chemistry
Suranaree University of Technology
Academic Year 2023

จลนพลศาสตร์และอุณหพลศาสตร์ปฏิกิริยาดีคาร์บอกซิเลชันด้วยเอนไซม์ของกรดไม่อิ่มตัวแอลฟา บีตา: การศึกษาทางทฤษฎี

นายพรเทพ พรมมา

วิทยานิพนธ์นี้เป็นส่วนหนึ่งของการศึกษาตามหลักสูตรปริญญาวิทยาศาสตรดุษฎีบัณฑิต
สาขาวิชาเคมี
มหาวิทยาลัยเทคโนโลยีสุรนารี
ปีการศึกษา 2566

KINETICS AND THERMODYNAMICS OF ENZYMATIC DECARBOXYLATION OF α,β-UNSATURATED ACID: A THEORETICAL STUDY

Suranaree University of Technology has approved this thesis submitted in partial fulfillment of the requirements for the Degree of Doctor of Philosophy.

Thisis Examining Committee

_____
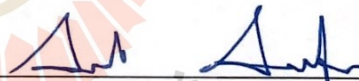
(Assoc. Prof. Dr. Viwat Vchirawongkwin)

Chairperson

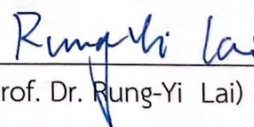_____

(Prof. Dr. Kritsana Sagarik)

Member (Thesis Advisor)

_____

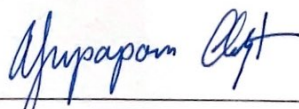(Assoc. Prof. Dr. Anyanee Kamkaew)

Member

_____

(Assoc. Prof. Dr. Suwit Suthirakun)

Member

_____

(Asst. Prof. Dr. Rung-Yi Lai)

Member

_____

(Assoc. Prof. Dr. Yupaporn Ruksakulpiwat)

Vice Rector for Academic Affairs

and Quality Assurance

_____

(Prof. Dr. Santi Maensiri)

Dean of Institute of Science

พรเทพ พรมมา : จลนพลศาสตร์และอุณหพลศาสตร์ปฏิกิริยาดีคาร์บอกซิเลชันด้วย
เอนไซม์ของกรดไม่อิ่มตัวแอลฟา บีตา: การศึกษาทางทฤษฎี (KINETICS AND
THERMODYNAMICS OF ENZYMATIC DECARBOXYLATION OF α,β-UNSATURATED
ACID: A THEORETICAL STUDY) อาจารย์ที่ปรึกษา : ศาสตราจารย์ ดร.กฤษณะ สาคริก,
96 หน้า

คำสำคัญ: ปฏิกิริยาดีคาร์บอกซิเลชันด้วยเอนไซม์, กรดไม่อิ่มตัวแอลฟา บีตา, วิธีการคำนวณเคมี
ควอนตัม, ทฤษฎีสถานการณ์เปลี่ยนแปลง, จลนพลศาสตร์และอุณหพลศาสตร์

        ปฏิกิริยาดีคาร์บอกซิเลชันของกรดไม่อิ่มตัวแอลฟา บีตา โดยใช้เอนไซม์ ferulic acid
decarboxylase (FDC1) และ prenylated flavin mononucleotide (PrFMN) เป็นโคแฟกเตอร์
เป็นที่สนใจเป็นอย่างมากในช่วงทศวรรษที่ผ่านมา เนื่องจากปฏิกิริยามีความเป็นมิตรต่อสิ่งแวดล้อมใน
กระบวนการผลิตสไตรีนและอนุพันธ์ของสไตรีนจากทรัพยากรที่มีอยู่ตามธรรมชาติ ที่ผ่านมาถึงแม้จะ
มีการศึกษากลไกการเกิดปฏิกิริยานี้ทั้งการทดลอง และทางทฤษฎี แต่ยังไม่พบว่ามีการศึกษาผลของ
ตัวทำละลายที่มีขั้วต่อปฏิกิริยาดังกล่าวในรายละเอียด ดังนั้นงานวิจัยเรื่องนี้จึงได้ทำการศึกษา
ปฏิกิริยาดีคาร์บอกซิเลชันเพื่อสังเคราะห์ β-methylstyrene (β-MeSt) ในสภาวะแวดล้อมไดอิเล็ก
ตริกสูงสุดและต่ำสุดที่เป็นไปได้ในสารละลายที่เป็นน้ำ (ε = 1 และ 78 ตามลำดับ) โดยใช้วิธี
การคำนวณเคมีควอนตัมที่ระดับ DFT/B3LYP/DZP ซึ่งผลการศึกษาพื้นผิวพลังงานศักย์ แสดงว่า
สันหลัง (backbone) ของเอนไซม์ FDC1 ไม่มีบทบาทสำคัญในกระบวนการนี้ ในขณะที่ความผันผวน
ของสภาพขั้วของตัวทำละลายส่งผลโดยตรงต่อการเปลี่ยนแปลงพลังงานกีดขวางอย่างมีนัยสำคัญ
โดยเฉพาะอย่างยิ่งในกระบวนการเกิดสถานะแทรนซิชันที่เกี่ยวข้องกับการถ่ายโอนโปรตอน (proton
transfer) ผลการคำนวณค่าคงที่อัตราโดยใช้ทฤษฎีสถานการณ์เปลี่ยนแปลง (transition state
theory, TST) ยืนยันว่าไม่มีผลของ quantum mechanical tunneling ต่อพลังงานกีดขวางในช่วง
อุณหภูมิที่ทำการศึกษา อย่างไรก็ตาม ในการคำนวณจำเป็นต้องพิจารณาผลของไดอิเล็กทริกเฉพาะที่
(local dielectric environment) ในกลไกการเกิดปฏิกิริยาร่วมด้วย เมื่อพิจารณาค่าคงที่อัตรา พบว่า
ในบางปฏิกิริยามูลฐาน ไม่สามารถเปรียบเทียบค่าที่คำนวณได้กับค่าที่วัดได้จากวิธีการทดลองโดยใช้
stopped-flow spectrophotometer แสดงว่าปฏิกิริยาการเกิด β-MeSt โดยตรงหลังจากการขจัด
คาร์บอนไดออกไซด์ (acid catalyst (2)) ที่มีผู้เสนอไว้ไม่น่าจะเกิดขึ้นได้ ทำให้ปฏิกิริยามูลฐาน
ไซโคลอิลิมิเนชัน (cycloelimination) ในไดอิเล็กทริกเฉพาะที่ต่ำ เป็นขั้นกำหนดปฏิกิริยา ผลการ
คำนวณอุณหพลศาสตร์แสดงว่าปฏิกิริยามูลฐานที่เกี่ยวข้องกับการถ่ายโอนโปรตอน ได้รับผลกระทบ
จากการผันผวนของสภาพขั้วของตัวทำละลาย นำไปสู่ข้อสรุปที่ว่าปฏิกิริยาดีคาร์บอกซิเลชันด้วย
เอนไซม์ของของกรดไม่อิ่มตัวแอลฟา บีตา โดยรวมเป็นปฏิกิริยาควบคุมทางอุณหพลศาสตร์
(thermodynamically controlled) โดยเฉพาะอย่างยิ่งในสภาวะแวดล้อมไดอิเล็กทริกเฉพาะที่สูง
โดยการเกิดเป็นโมเลกุลในบริเวณเร่ง มีผลต่อการเปลี่ยนแปลงเอนโทรปีมากกว่าการสลายหรือการ
สร้างพันธะโควาเลนต์ ตลอดจนการจัดเรียงตัวใหม่ของโมเลกุลในบริเวณเร่ง โดยงานวิจัยเรื่องนี้แสดง
การดำเนินไปของปฏิกิริยามูลฐานในรายละเอียดเป็นครั้งแรก และนำไปสู่องค์ความรู้เชิงลึกเกี่ยวกับผล

ของความผันผวนของไดอิเล็กทริกเฉพาะที่ต่อปฏิกิริยาดีคาร์บอกซิเลชันด้วยเอนไซม์ของของกรดไม่
อิ่มตัวแอลฟา บีตา ดังนั้นผลการวิจัยจึงสามารถใช้เป็นแนวทางในการศึกษาปฏิกิริยาปฏิกิริยาดีคาร์
บอกซิเลชันของกรดไม่อิ่มตัวแอลฟา บีตา ด้วยเอนไซม์อื่น ๆ ทั้งด้านการทดลองและทางทฤษฎีต่อไป
ในอนาคตได้

สาขาวิชาเคมี

ปีการศึกษา 2566

ลายมือชื่อนักศึกษา_____

ลายมือชื่ออาจารย์ที่ปรึกษา_____

PHORNTEP PROMMA : KINETICS AND THERMODYNAMICS OF ENZYMATIC DECARBOXYLATION OF α,β-UNSATURATED ACID: A THEORETICAL STUDY. THESIS ADVISOR : PROF. KRITSANA SAGARIK, Ph.D. 96 PP.

Keyword: enzymatic decarboxylation, 1,3-dipolar cycloaddition, α,β-unsaturated acid, the DFT method, transition state theory, kinetics and thermodynamics.

Enzymatic decarboxylation of α,β-unsaturated acid through ferulic acid decarboxylase (FDC1) has been of interest because this reaction has been anticipated to be a promising, environmentally friendly industrial process for producing styrene and its derivatives from natural resources. Because the local dielectric constant at the active site is not exactly known, enzymatic decarboxylation to generate β-methylstyrene (β—MeSt) was studied under two extreme conditions (ε = 1 and 78 in the gas phase and aqueous solution, respectively) using the B3LYP/DZP method and transition state theory (TST). The model molecular clusters consisted of an α-methylcinnamate (Cin) substrate, a prenylated flavin mononucleotide (PrFMN) cofactor and all relevant residues of FDC1. Analysis of the equilibrium structures showed that the FDC1 backbone does not play the most important role in the decarboxylation process. The potential energy profiles confirmed that the increase in the polarity of the solvent could lead to significant changes in the energy barriers, especially for the transition states that involve proton transfer. Analysis of the rate constants confirmed the low/no quantum mechanical tunneling effect in the studied temperature range and that inclusion of the fluctuation of the local dielectric environment in the mechanistic model was essential. Because the computed rate constants are not compatible with the time resolution of the stopped-flow spectrophotometric experiment, the direct route for generating β—MeSt after CO_2 elimination (acid catalyst (2)) is unlikely to be utilized, thereby confirming that indirect cycloelimination in a low local dielectric environment is the rate determining step. The thermodynamic results showed that the elementary reactions that involve charge (proton) transfer are affected by solvent polarity, thereby leading to the conclusion that overall, the enzymatic decarboxylation of α,β-unsaturated acid is thermodynamically controlled at high ε. The entropy changes due to the generation of molecules in the active site appeared more pronounced than that due to only covalent bond breaking/formation or structural reorientation. This work examined in detail for the first time the scenarios in each elementary reaction and provided insight into the effect of the fluctuations in the local dielectric environment on the enzymatic decarboxylation of α,β-unsaturated

acids. These results could be used as guidelines for further theoretical and experimental studies on the same and similar systems.

School of Chemistry

Academic Year 2023

Student's Signature_____

Advisor's Signature_____

ACKNOWLEDGEMENTS

CONTENTS

CONTENTS (Continued)

LIST OF TABLES

LIST OF FIGURES

LIST OF FIGURES (Continued)

LIST OF FIGURES (Continued)

LIST OF ABBREVIATIONS

UbiD	3-octaprenyl-4-hydroxybenzoate decarboxylase
UbiX	Flavin prenyltransferase
FDC1	Ferulic acid decarboxylases
PAD1	phenylacrylic acid decarboxylase
PrFMN	Prenylated flavin mononucleotide
Cin	α-methylcinnamate
C_α^{Cin}	α-carbon of α-methylcinnamate
C_{43}^{Cin}	Carbon atom number 43 in α-methylcinnamate
C_β^{Cin}	β-carbon of α-methylcinnamate
C_{29}^{PrFMN}	Carbon atom number 29 in PrFMN
C_{34}^{PrFMN}	Carbon atom number 34 in PrFMN
O_{30}^{PrFMN}	Oxygen atom number 30 in PrFMN
$\beta-MeSt$	β-methylstyrene
Arg173	Arginine role 173 in FDC1 enzyme
Gln190	Glutamine role 190 in FDC1 enzyme
Glu277	Glutamic acid role 277 in FDC1 enzyme
Glu282	Glutamic acid role 282 in FDC1 enzyme
FDC1^{Backbone}	Backbone atom of FDC1 enzyme
$R_{C_R^{Arg173H^+}-C_R^{Glu277}}$	The distance between the carbon atoms of the CH_3 groups that substituted the carbon atom of FDC1^{Backbone} of the residues Arg173 and Glu277
$R_{C_R^{Arg173H^+}-C_R^{Gln190}}$	The distance between the carbon atoms of the CH_3 groups that substituted the carbon atom of FDC1^{Backbone} of the residues Arg173 and Gln190
$R_{C_R^{Glu277}-C_R^{Gln190}}$	The distance between the carbon atoms of the CH_3 groups that substituted the carbon atom of FDC1^{Backbone} of the residues Glu277 and Gln190

LIST OF ABBREVIATIONS (Continued)

$R_{C_R^{Arg173H^+}-C_R^{Glu277}}$	The distance between the carbon atoms of the CH_3 groups that substituted the carbon atom of FDC1^{Backbone} of the residues Arg173 and Glu277
$R_{C_R^{Arg173H^+}-C_R^{Gln190}}$	The distance between the carbon atoms of the CH_3 groups that substituted the carbon atom of FDC1^{Backbone} of the residues Arg173 and Gln190
React	Model molecular cluster of the reactant in low local dielectric environment ($\varepsilon = 1$)
React$^{\varepsilon}$	Model molecular cluster of the reactant in high local dielectric environment ($\varepsilon = 78$)
TS	Model molecular cluster of the transition state in low local dielectric environment ($\varepsilon = 1$)
TS$^{\varepsilon}$	Model molecular cluster of the transition state in high dielectric environment ($\varepsilon = 78$)
Int	Model molecular cluster of the intermediate in low local dielectric environment ($\varepsilon = 1$)
Int$^{\varepsilon}$	Model molecular cluster of the intermediate in high dielectric environment ($\varepsilon = 78$)
Prod	Model molecular cluster of the product in low local dielectric environment ($\varepsilon = 1$)
Prod$^{\varepsilon}$	Model molecular cluster of the product in high local dielectric environment ($\varepsilon = 78$)
DFT	Density functional theory
B3LYP	Becke, 3-parameter, Lee–Yang–Parr
DZP	Double zeta polarized basis
COSMO	Conductor-like screening model
CPCM	Conductor-like polarizable continuum model
ε	Dielectric constant
HOMO	Highest occupied molecular orbital
LUMO	Lowest unoccupied molecular orbital
NEB	Nudged elastic band method
TST	Transition state theory

LIST OF ABBREVIATIONS (Continued)

ZPC	Zero point energy-corrected
kJ/mol	Kilo Joule per mole
E^{Total}	Total energy of the system in low local dielectric environment
$E^{Total,\varepsilon}$	Total energy of the system in high local dielectric environment
ΔE^{Solv}	Relative solvation energy
ΔE^{Rel}	Relative total energy with respect to the precursor in low local dielectric environment ($\varepsilon = 1$)
$\Delta E^{\ddagger}$	Energy barrier
ΔE^{ZPE}	Zero-point correction energy
$\Delta E^{\ddagger,ZPC}$	Zero point energy-corrected energy barrier
$\Delta E^{Rel,Solv}$	Relative total energy with respect to the precursor in high local dielectric environment ($\varepsilon = 78$)
k^{Arr}	Arrhenius rate constants
k^{Class}	Classical rate constants
$k^{Q\text{-}vib}$	Quantized-vibrational rate constants
$k^{S\text{-}Wig}$	Wigner corrected rate constants
$k^{F\text{-}Wig}$	Full Wigner corrected rate constants
T_c	Crossover temperature
$\Delta G^{\ddagger}$	The activation free energies
$\Delta H^{\ddagger}$	The activation enthalpy
$\Delta S^{\ddagger}$	The activation entropy
ΔG°	Standard free energy changes in low local dielectric environment ($\varepsilon = 1$)
$\Delta G^{\circ,\varepsilon}$	Standard free energy changes in high local dielectric environment ($\varepsilon = 78$)
ΔS°	Standard entropy changes of each elementary reaction in low local dielectric environment ($\varepsilon = 1$)
$\Delta S^{\circ,\varepsilon}$	Standard entropy changes of each elementary reaction in high local dielectric environment ($\varepsilon = 78$)
SD	Standard deviation

CHAPTER I

INTRODUCTION

1.1 Introduction

Decarboxylations of α,β-unsaturated acid are well-known as one of the most common and essential processes in chemical industries. Nevertheless, decarboxylation reactions are intrinsically difficult to utilize, due to the high energy of the transition state, involving the accretion of negative charge at the α-carbon of the substrate during formation of the transition structure (Ferguson et al., 2017; Payne et al., 2015). To overcome this problem, enzymatic decarboxylations have been of interest, because they are environmentally friendly reactions to produce important organic compounds from natural resources under mild reaction conditions (Ferguson et al., 2016; Ferguson et al., 2017; Lan and Chen, 2016; Payne et al., 2015). However, to enhance the reactions, cofactors such as pyridoxal phosphate (PLP), flavin mononucleotide (FMN), and Lewis acids (e.g., Mn^{2+}, Mg^{2+}, Fe^{2+}) must be used to stabilize the negative charge at the α-carbon.

Prenylated flavin mononucleotide (PrFMN) cofactor has been anticipated to be an appropriate cofactor for the enzymatic decarboxylations of α,β-unsaturated acid (Payne et al., 2015; White et al., 2015), due to ability of isoalloxazine ring system to serve as an electron sink to stabilize α-carbon by delocalized the negative charge to the extended π system in FMN moiety (Ferguson et al., 2016; Ferguson et al., 2017; Tian and Liu, 2017). Literature review showed that enzymatic decarboxylation of α,β-unsaturated acid via ferulic acid decarboxylase (FDC1) and PrFMN as a cofactor to produce styrene and their derivatives has received special attention in the last decade (Payne et al., 2015; White et al., 2015; Ferguson et al., 2016; Ferguson et al., 2017).

The reaction mechanism was first proposed by Payne et al. (2015), consisting of four consecutive elementary steps (Figure 1.1), namely, (I) 1,3-dipolar cycloaddition, (II) Grob-type decarboxylation, (III) protonation and (IV) retro 1,3-dipolarcycloaddition. Based on the results obtained from spectroscopic methods and kinetic isotope effects (Ferguson et al., 2016), cycloelimination (IV) has been suggested to represent the rate-determining step. To confirm the proposed mechanism, Kaneshiro et al. (2020) studied the kinetics of the proposed enzymatic decarboxylation in Figure 1.1, using stopped-flow UV–vis spectrophotometric method at 4°C and the half-of-sites kinetics model.

The results showed that formation of the PrFMN–styrene adduct monitored in the experiment represents the transient intermediate, which could determine the effectiveness of the FDC1 enzyme activity, and diffusion of the styrene product from the active site is the rate-determining process, with $k = 11$ s^{-1}. Therefore, cycloelimination is confirmed to the rate-determining step of the overall reaction.
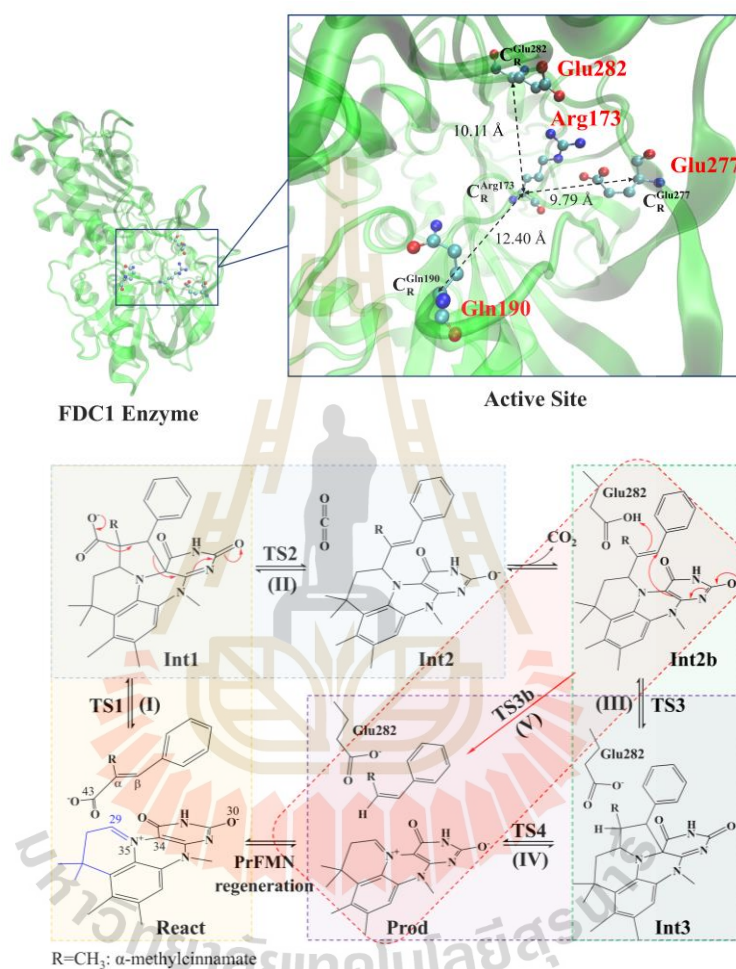
Figure 1.1 Structure of the FDC1 enzyme and the proposed catalytic pathways for the decarboxylation of α,β-unsaturated acid (Payne et al., 2015).

High-resolution crystal structure analysis showed that for the enzymatic decarboxylation of α,β-unsaturated acid via FDC1 and PrFMN cofactor to produce styrene, the active site residues of FDC1, Glu277, Arg173, and Glu282, are conserved during the reaction (Bailey et al., 2018). However, the results obtained from mass spectrometric technique and UV-visible spectroscopic method revealed that the photoisomerization of PrFMN with the iminium form (PrFMN[iminium]) to PrFMN with the

ketimine form (PrFMN^{ketimine}) is an irreversible process that reduces the catalytic activity of FDC1. Therefore, PrFMN^{ketimine} could be an inhibited cofactor for FDC1.

In this work, because the information on the kinetic and thermodynamic aspects was limited, the proposed elementary reactions of the enzymatic decarboxylation of α,β-unsaturated acid were further studied using the density functional theory with Becke, 3-parameter, Lee-Yang-Parr functional and double zeta polarized basis set (DFT/B3LYP/DZP) and transition state theory (TST). While previous theoretical studies focused only on potential energy profiles in low local dielectric environments, this theoretical study focused on the scenarios in the elementary reactions and on the kinetic and thermodynamic properties in two extreme local dielectric environments, namely, the gas phase and aqueous solution with ε = 1 and 78, respectively.

1.2 Research objectives

This work investigated kinetics and thermodynamics of enzymatic decarboxylation of α-methylcinnamate (Cin) via 1,3-dipolar cycloaddition reaction in Figure 1.1 The main objectives and scope of the present study are summarized as follows:

1. To study scenarios (progress) in the proposed elementary reactions in two extreme local dielectric environments namely, in the gas phase and aqueous solution with ε = 1 and 78, respectively.

2. To study the kinetic and thermodynamic aspects of the proposed elementary reactions in ε = 1 and 78 based on the TST method.

3. To study the effect of local dielectric environment in the proposed mechanisms.

CHAPTER II
LITERATURE REVIEWS

2.1 Enzyme-catalyzed decarboxylation reaction

Enzymatic decarboxylation reactions are one of the most important reactions in chemical industry and biological systems. They are usually applied in organic synthesis under mild reaction conditions, such as defunctionalization of organic molecules, for example, conversion of unsaturated carboxylic acids into alkene (Bhuiya et al., 2015; Ferguson et al., 2016; Ferguson et al., 2017). However, the reactions are not thermodynamically favorable, due to the accretion of negative charge at α-carbon during formation of transition states (Payne et al., 2015; Ferguson et al., 2017; Leys, 2017).

To overcome the high-energy transition state problem, cofactors such as pyridoxal phosphate (PLP), flavin, or metal ions were used as the Lewis acids to stabilize the negative charge at α-carbon. Experiments showed that PrFMN, which can be found in the 3-octaprenyl-4-hydroxybenzoate decarboxylase (UbiD) family, can also be used effectively in the decarboxylation reactions (Payne et al., 2015; Richard et al., 2015; White et al., 2015). This is due to the observation that the FMN isoalloxazine ring in the cofactor molecules can act as the electron sink that can dissipate negative charge from the α-carbon to extended π system as shown in Figure 2.1 (Tian and Liu, 2017; Leys, 2017). Similar to UbiD, ferulic acid decarboxylase (FDC1), as a class of PrFMN-dependent enzyme decarboxylase, has been used successfully to synthesize styrene and its derivatives from α,β-unsaturated acid precursor (Lin et al., 2015; McKenna and Nielsen, 2011; Marshall et al., 2017).
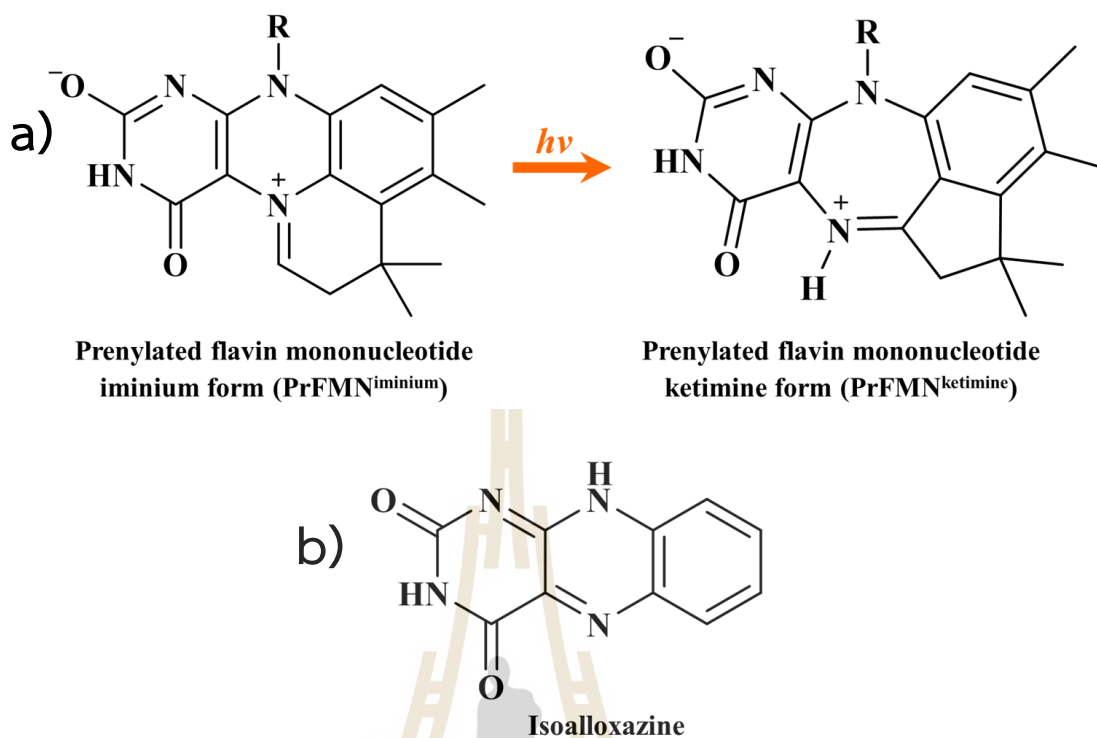
Figure 2.1 a) Structures of prenylated flavin mononucleotide with the iminium and ketimine forms (PrFMN[iminium] and PrFMN[ketimine]), respectively. b) isoalloxazine ring system (Payne et al., 2015; Rangarajan et al., 2004; White et al., 2015)

2.1.1 Enzymatic decarboxylation of α,β-unsaturated acid via FDC1

The mechanism of the enzymatic decarboxylation of α,β-unsaturated acid via FDC1 and PrFMN using cinnamic acid as the substrate was first proposed by Payne et al. (2015). The mechanism (Figure 1.1) involves four elementary steps, namely, (I) 1,3-dipolar cycloaddition, (II) Grob-type decarboxylation, (III) protonation and (IV) retro 1,3-dipolarcycloaddition, respectively. The proposed elementary reactions in the active site of FDC1 consist of the Arg173, Gln190, Glu277 and Glu282 residues and cinnamic acid located directly above the PrFMN ring with $\pi-\pi$ stacking interaction (Figure 2.2). The first elementary step is 1,3-dipolar cycloaddition (I), which involves simultaneous formation of covalent bonds between $C_{1'}$-C_α and C_{4a}-C_β, leading to the five-membered ring pyrrolidine cycloadduct intermediate.
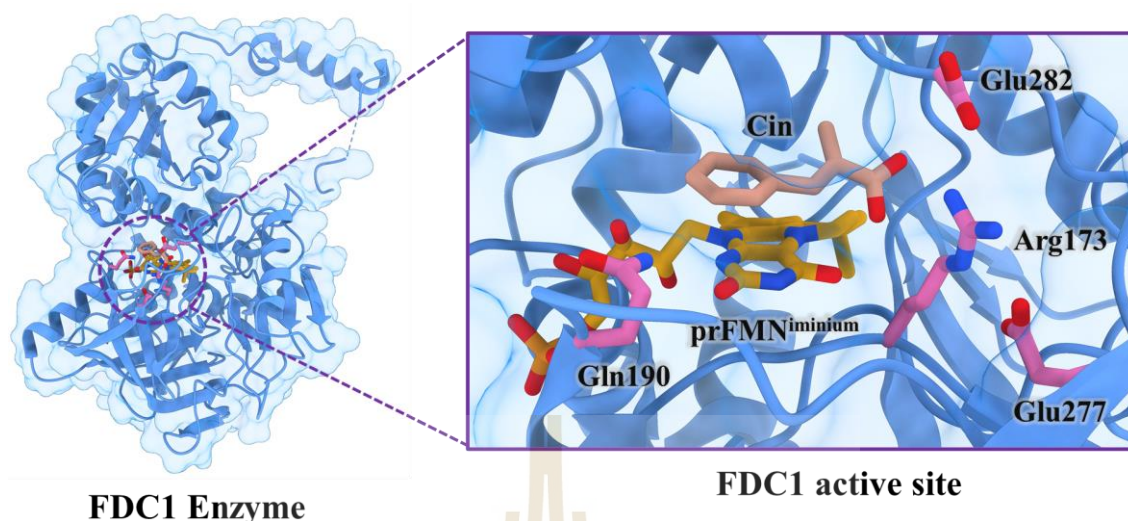
Figure 2.2 The structure of the active site of FDC1 enzyme and molecules involved in enzymatic decarboxylation of α,β-unsaturated acid.

In the second step, decarboxylation (II) occurs through C_{4a}-C_β bond dissociation, leading to breaking of the five-membered ring pyrrolidine, and CO_2 elimination from the substrate. In protonation (III), Glu282 acts as proton donor in the acid-base reaction, transferring its proton to C_α of the substrate moiety and leads to formation of the second pyrrolidine cycloadduct. The last step is retro 1,3-dipolar cycloaddition (IV), in which the $C_{1'}$-C_α and C_{4a}-C_β covalent bonds simultaneously dissociate to generate styrene through cycloelimination (IV).

The experimental results obtained from the high-resolution crystallographic data revealed that two forms of PrFMN could exist in the FDC1 active site (Payne et al., 2015; White et al., 2015), for which photoisomerization converts the iminium form of PrFMN (PrFMN[iminium]) into the ketimine form (PrFMN[ketimine]). PrFMN[ketimine] has a different form of isoalloxazine ring and is generally found in the wild-type of FDC1 (Marshall et al., 2017); photoisomerization transforms the six-membered heterocyclic ring in PrFMN[iminium] into seven-membered heterocyclic ring in PrFMN[ketimine] (Figure 2.1). Experiment also showed that to produce styrene, the enzymatic decarboxylation of cinnamic acid with PrFMN[ketimine] takes place via two consecutively elementary reactions, namely, Michael addition (I) and decarboxylation (II) (Payne et al., 2015; White et al., 2015).

2.1.2 Effects of PrFMN^{ketimine} on enzymatic decarboxylation of cinnamic acid

The enzymatic decarboxylation of cinnamic acid via FDC1 using the two forms of PrFMN cofactor was studied using quantum mechanics/molecular mechanics (QM/MM) method at the B3LYP/6-31G(d,p) level of theory (Tian and Liu, 2017). This theoretical study focused on the reaction mechanisms, in which PrFMN^{iminium} is replaced by PrFMN^{ketimine}. The results confirmed the mechanisms proposed by Payne et al. (2015), in which the reaction with PrFMN^{iminium} consists of four elementary steps, whereas a two-step process was observed for the reaction with PrFMN^{ketimine}. The QM/MM results further suggested that PrFMN^{ketimine} is not a reactive species in this enzymatic decarboxylation, because the overall energy barrier is higher (43.3 kcal/mol) compared with the reaction with PrFMN^{iminium} (23.5 kcal/mol). These theoretical results are in excellent agreement with previous experimental studies, in which UV-visible spectra decarboxylation assay revealed that for the reaction with PrFMN^{ketimine}, the catalytic activity decreases over time with significantly shorter half-life, ~30 min, compared with ~240 min for PrFMN^{iminium} (Bailey et al., 2018); while the reaction with PrFMN^{ketimine} ends in a very short time, the catalytic activity of the one with PrFMN^{iminium} remains for many hours.

These findings led to the conclusion that PrFMN^{iminium} is a more effective cofactor for the FDC1 enzymatic decarboxylation of cinnamic acid to produce styrene. To improve this enzymatic decarboxylation process, attempt was made to study the photoisomerization mechanism PrFMN^{iminium}→PrFMN^{ketimine}. Based on mass spectrometric technique and UV-visible spectroscopic method, Bailey et al. (2018) proposed isomerization pathways for PrFMN^{iminium}→PrFMN^{ketimine}, which involves (a) proton transfer, (b) photoexcitation, (c) ring expansion and (d) reverse protonation, respectively (Figure 2.3).
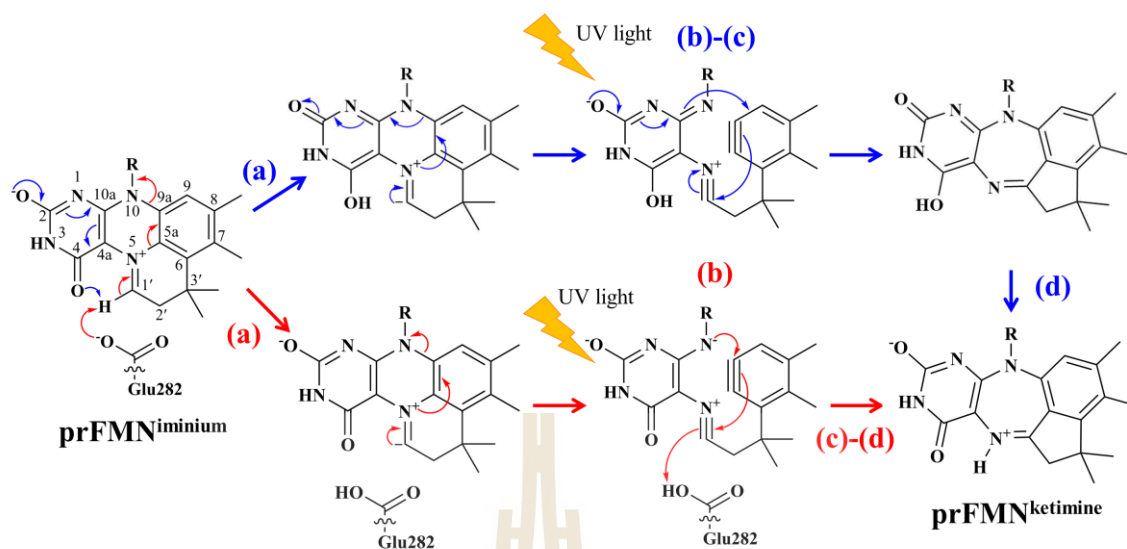
Figure 2.3 The proposed PrFMN^{iminium}→PrFMN^{ketimine} photoisomerization pathway (Bailey et al., 2018).

2.1.3 Enzymatic decarboxylation of α,β-unsaturated acids with alkene and alkyne

Bailey et al. (2019) studied enzymatic decarboxylation mechanisms for formations of styrene and its derivative from α,β-unsaturated acids with alkene and alkyne using the B3LYP/6-31G(d,p) method, using cinnamic (alkene) and phenylpropiolic (alkyne) acids as the precursors. This work focused on the reaction mechanisms when the alkene substrate is replaced by alkyne. The results (Figure 2.4) demonstrated that 1,3-dipolar cycloaddition (I) of cinnamic acid consists of two elementary steps, whereas only one elementary step was observed for the phenylpropiolic acid; the former produces pyrrolidine cycloadduct, whereas the latter generates 3-pyrroline cycloadduct.

The B3LYP/6-31G(d,p) geometry and reaction path optimizations (relaxed scan method) also revealed that the relative stability for the alkyne intermediate is significantly lower than that of the alkene intermediate (-40.0 kJ/mol and 5.9 kJ/mol, respectively). This suggests a higher stabilization effect of the π-π interaction between the dipolarophile and azomethine ylide moieties for the alkyne intermediate. Because the energy barrier for the cycloelimination (IV) involving the alkene intermediate is lower (64.1 kJ/mol) than the alkyne intermediate, the reaction using cinnamic acid is concluded to be energetically more favorable to produce styrene.

Figure 2.4 a)-b) The proposed mechanism and potential energy profile for the enzymatic decarboxylation of cinnamic acid (alkene type) and phenylpropiolic acid (alkyne type) via FDC1 enzyme (Bailey et al., 2019).
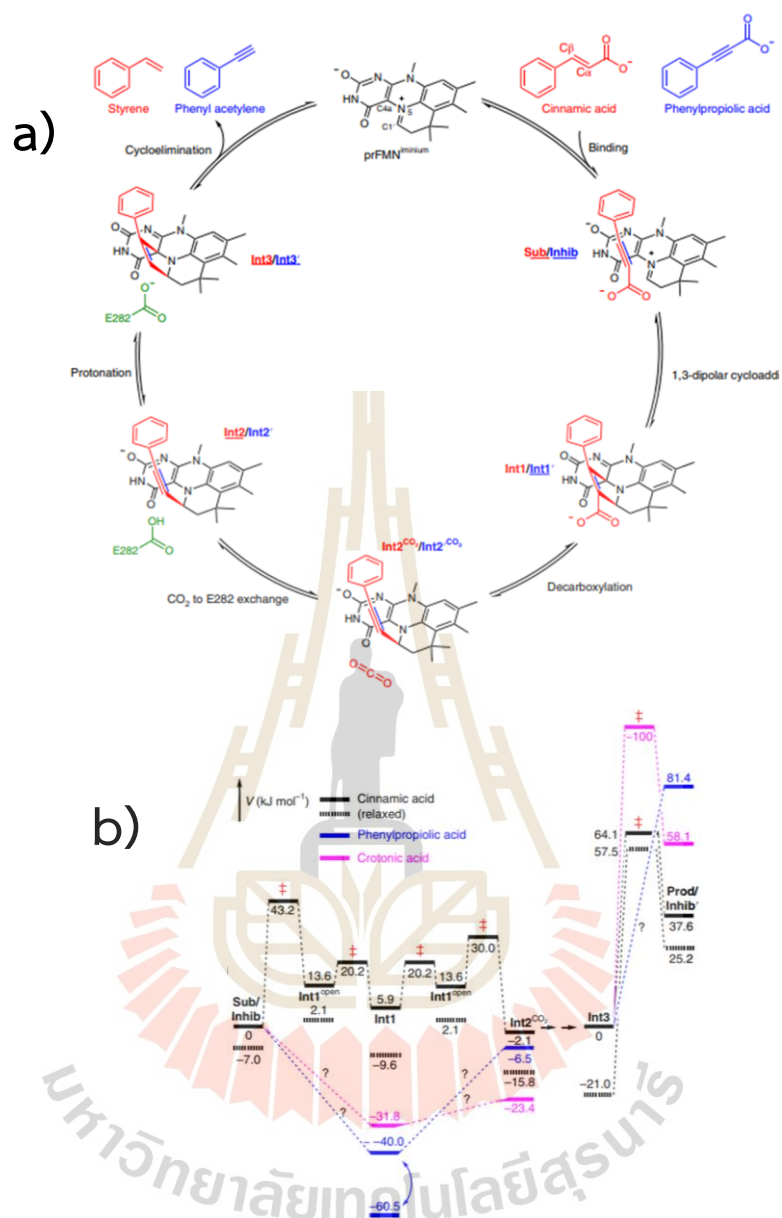
2.1.4 Influence of C_α Substituents on the enzymatic decarboxylation of α,β-unsaturated acids

The theoretical investigation was conducted on the biosynthesis of styrene from α,β-unsaturated acids, specifically α-methylcinnamic acid (R = CH₃), employing FDC1 with PrFMN^{iminium}. DFT/B3LYP/6-31G(d,p) method was employed to explore catalysis and inhibition pathways (Lan and Chen, 2016). The computational findings highlighted the crucial role of 1,3-dipolar cycloaddition (I) between PrFMN^{iminium} and the double bond of α-methylcinnamic acid as the key elementary step in all catalytic processes (Figure 2.5). The rate-limiting step in the catalysis pathway was identified as the protonation of the C_α of α-methylcinnamic acid (III), leading to the formation of styrene. However, the overall energy barrier for this step was significantly high (18.9 kcal mol⁻¹), suggesting that the cycloelimination (IV) process is the rate-limiting step. Additionally, the theoretical results revealed an inhibition pathway involving α-hydroxycinnamic acid substrate (R = OH), where protonation at the C_β carbon induces the conversion of the substrate moiety to its enol form, forming a more stable keto intermediate that leads to FDC1 enzyme inhibition due to high energy barrier of the reversible process.
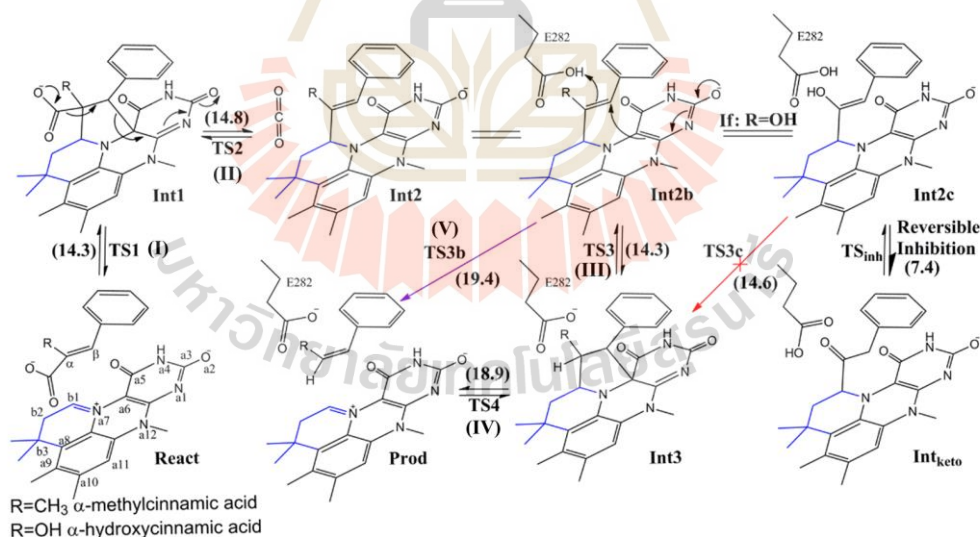
Figure 2.5 The proposed mechanism for the enzymatic decarboxylation of α-methylcinnamic and α-hydroxycinnamic acids via FDC1 (Lan and Chen, 2016).

2.1.5 The kinetic of transient intermediates in the enzymatic decarboxylation of α,β-unsaturated acids

The results from the stopped-flow spectroscopic experiment (Kaneshiro et al., 2020) showed that FDC1 plays a crucial role in the decarboxylation of various phenylacrylic acids to produce styrene derivatives through CO_2 elimination process, utilizing the cofactor PrFMN. The process involves 1,3-dipolar cycloaddition reaction between PrFMN and phenylacrylic acid, resulting in the formation of a five-membered ring cycloadduct that proceeds to the decarboxylation step, subsequent by the formation of PrFMN-styrene cycloadduct. Analysis of the kinetics in the pre-steady state model (Figure 2.6), conducted using ultraviolet-visible stopped-flow spectroscopy, shows that the cycloelimination of the PrFMN-styrene cycloadduct to produce styrene is the rate-determining step with $k_{cat} = 11.3$ s^{-1}.
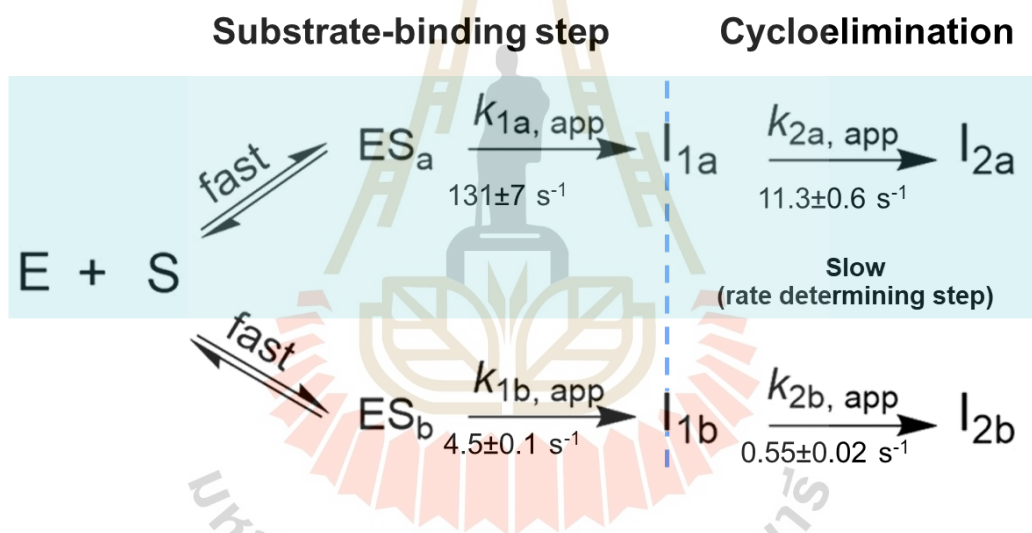
Figure 2.6 Pre-steady state kinetic data from half-of-sites model taken from stopped-flow spectroscopic experiment (Kaneshiro et al., 2020).

CHAPTER III
RESEARCH METHODOLOGY

3.1 Quantum chemical methods

Because the FDC1 enzyme is exceedingly large for high-level *ab initio* methods and because our previous studies showed that the mechanisms for proton transfer in heterocyclic aromatic systems can be studied reasonably well using the B3LYP method with the DZP basis set (Bua-ngern et al., 2016; Sagarik et al., 2015; Thisuwan and Sagarik, 2014), the B3LYP/DZP method was used in this study; our benchmark calculations on bifunctional proton transfers in poly(benzimidazole) (PBI) H-bond systems (Thisuwan et al., 2021) confirmed that the B3LYP/DZP method yields approximately the same equilibrium and transition structures and relative interaction energies as the B3LYP/TZP method with reasonable computational resources. In this study, the model molecular clusters that were hypothesized from Lan and Chen (2016) were chosen as model systems, which consist of all important active site residues, the substrate and the cofactor. The model molecular clusters were constructed by substituting the carbon atoms of FDC1$^{\text{Backbone}}$ that connect the residues with methyl (CH_3) groups (Table 3.1); for example, C_R^{Glu277} is the carbon atom of the CH_3 group that substitutes the carbon atom of the FDC1$^{\text{Backbone}}$ that connects the Glu277 residue (Figure 1.1).

Because our previous studies showed that the local dielectric environment (microenvironment) can affect the structures and energetics of elementary and because enzymatic decarboxylation occurs in aqueous solution, the conductor-like screening model (COSMO) was used to simulate the effect of the aqueous environment. COSMO was used successfully in our previous studies on proton transfer processes in H-bond systems. (Bua-ngern et al., 2016; Thisuwan and Sagarik, 2014; Thisuwan et al., 2021) Previous theoretical studies used ε = 4 (Lan and Chen, 2016) and 5.7 (Bailey et al., 2019) to model the local dielectric environment at the active site of FDC1. In this work, because the local dielectric constant was not exactly known and we wanted to study the elementary reactions in extreme local dielectric conditions, the lowest and highest possible values (and fluctuation) were used, namely, ε = 1 and 78, in the gas phase and bulk water, respectively. All B3LYP/DZP calculations were performed using the TURBOMOLE 7.50 software package (Ahlrichs et al., 1989; Furche et al., 2014).

3.2 Equilibrium structures and potential energy curves

Based on the proposed elementary reactions in Figure 1.1, to study the enzymatic decarboxylation reactions, six model molecular clusters in the FDC1 active site were taken from Lan and Chen (2016), consisting of a Cin-PrFMN^{iminuim} complex and four active site residues, namely, Arg173, Gln190, Glu277 and Glu282 (Table 3.1). To model the active site, the carbon atoms of the residues that connect with the backbone of FDC1 (FDC1^{Backbone}) were truncated and replaced by CH_3 groups. To ease the discussion, the symbols used by Lan and Chen (2016) (e.g., React, TS1 and Int1) are adopted in this work.

Table 3.1 Equilibrium structures, total energies in $\varepsilon = 1$ and 78 (E^{Total} and $E^{Total,\varepsilon}$, respectively), and solvation energies (ΔE^{Solv}) of the six model molecular clusters, obtained from B3LYP/DZP geometry optimizations. Spheres are the CH_3 groups substituting backbone atoms of the FDC1 enzyme. E^{Total} and $E^{Total,\varepsilon}$ are in au and (ΔE^{Solv} in kJ/mol. [...] = values computed in $\varepsilon = 78$.
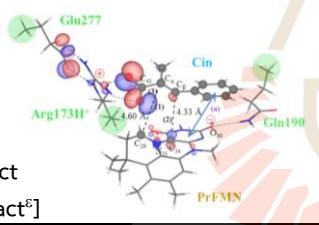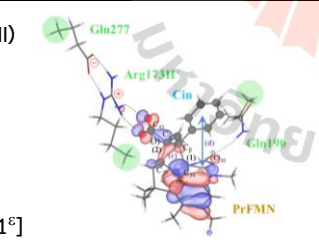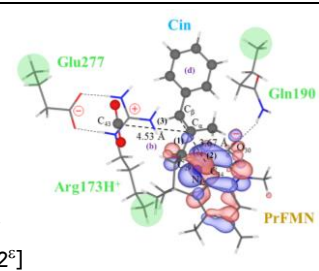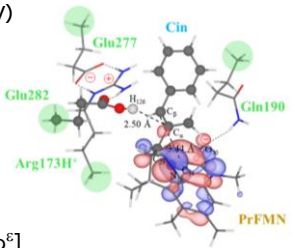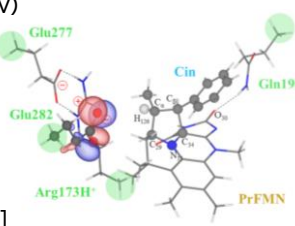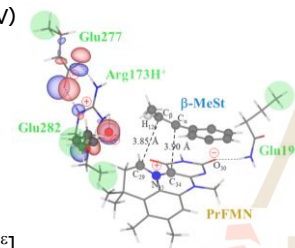
Model molecular cluster	E^{Total}	ΔE^{Solv}	R
(I) React [React$^{\varepsilon}$]	-2561.033273 [-2561.125954]	-243.3	(1) $R_{C_{\beta}^{Cin}-C_{34}^{PrFMN}} = 4.33\ [4.34]$ (2) $R_{C_{\alpha}^{Cin}-C_{29}^{PrFMN}} = 4.60\ [4.66]$ (3) $R_{C_{\alpha}^{Cin}-C_{43}^{Cin}} = 1.54\ [1.53]$ (a) formation of π-π stacking intermediate
(I)-(II) Int1 [Int1$^{\varepsilon}$]	-2561.033539 [-2561.123699]	-236.7	(1) $R_{C_{\beta}^{Cin}-C_{34}^{PrFMN}} = 1.64\ [1.64]$ (2) $R_{C_{\alpha}^{Cin}-C_{29}^{PrFMN}} = 1.56\ [1.56]$ (3) $R_{C_{\alpha}^{Cin}-C_{43}^{Cin}} = 1.58\ [1.57]$ (c) formation of pyrrolidine cycloadduct (d) relaxation of π-π stacking
(II) Int2 [Int2$^{\varepsilon}$]	-2561.055668 [-2561.135336]	-209.2	(1) $R_{C_{\beta}^{Cin}-C_{34}^{PrFMN}} = 3.67\ [3.67]$ (2) $R_{C_{\alpha}^{Cin}-C_{29}^{PrFMN}} = 1.53\ [1.53]$ (3) $R_{C_{\alpha}^{Cin}-C_{43}^{Cin}} = 4.52\ [4.53]$ (b) CO_2 elimination (c) $C_{\beta}^{Cin}-C_{34}^{PrFMN}$ dissociation (d) substrate moiety reorientation

Table 3.1 (Continued).

Model molecular cluster	E^{Total}	ΔE^{Solv}	R
(III)-(V) Int2b [Int2b$^\varepsilon$] 	-2680.075573 [-2680.159207]	-219.6	(1) $Rc_\beta^{Cin}-c_{34}^{PrFMN}$ = 3.44 [3.45] (2) $Rc_\alpha^{Cin}-c_{29}^{PrFMN}$ = 1.53 [1.53] (3) $Rc_\alpha^{Cin}-H_{126}^{Glu282}$ = 2.50 [2.55] (4) $Ro_{125}^{Glu282}-H_{126}^{Glu282}$ = 0.99 [0.99]
(III)-(IV) Int3 [Int3$^\varepsilon$] 	-2680.080390 [-2680.168887]	-232.3	(1) $Rc_\beta^{Cin}-c_{34}^{PrFMN}$ = 1.60 [1.60] (2) $Rc_\alpha^{Cin}-c_{29}^{PrFMN}$ = 1.57 [1.57] (3) $Rc_\alpha^{Cin}-H_{126}^{Glu282}$ = 1.10 [1.10] (4) $Ro_{125}^{Glu282}-H_{126}^{Glu282}$ = 3.89 [4.00] (c) formation of π-π stacking intermediate
(IV)-(V) Prod [Prod$^\varepsilon$] 	-2680.068672 [-2680.156268]	-230.0	(1) $Rc_\beta^{Cin}-c_{34}^{PrFMN}$ = 3.90 [3.89] (2) $Rc_\alpha^{Cin}-c_{29}^{PrFMN}$ = 3.85 [3.87] (d) formation of β-MeSt product

The model molecular clusters were optimized at the DFT/B3LYP/DZP level of theory, performed using TURBOMOLE 7.50 software package (Ahlrichs et al., 1989; Furche et al., 2014). The equilibrium structures in Table 3.1 were employed in the reaction path optimizations using the nudged elastic band (NEB) method with the limited-memory Broyden-Fletcher-Goldfarb-Shanno (L-BFGS) optimizer implemented in the ChemShell software package (Kästner et al., 2009; Metz et al., 2014).

For the reaction path optimizations ((I)-(IV) in Figure 1.1), fourteen replicas connecting the precursor, transition structure and product were optimized; (I) 1,3-dipolar cycloaddition, React→TS1→Int1; (II) decarboxylation, Int1→TS2→Int2; (III) acid catalyst (1), Int2b→TS3→Int3; (IV) cycloelimination Int3→TS4→Prod. In addition, because an alternative direct pathway to generate styrene from Int2b was proposed, acid catalyst (2) ((V) Int2b→TS3b→Prod in Figure 1.1) was also included in this study.

The conductor-like screening model (COSMO) was employed to study the effect of the aqueous environment. In this work, solvation energy (ΔE^{Solv}), defined as the difference between the total energies of the model molecular clusters in $\varepsilon = 78$ ($E^{Total,\varepsilon}$) and in $\varepsilon = 1$ (E^{Total}), were computed. Because the local dielectric constant was not exactly known, to study the elementary reactions in extreme local dielectric conditions, the lowest and highest possible values were used, namely, $\varepsilon = 1$ and 78, in the gas phase and bulk water, respectively.

The strength of the intermolecular interaction responsible for the transition state formation, especially in the acid catalysts (1) (III) and (2) (V), was approximated using the interaction energy between molecular fragments inside the model molecular cluster ($\Delta E^{Total,A...B}$), computed using $\Delta E^{Total,A...B} = E^{Total,AB} - (E^{Total,A} + E^{Total,B})$, where $E^{Total,AB}$ is the total energy of the model molecular cluster, and $E^{Total,A}$ and $E^{Total,B}$ are the total energies of the parts of the model molecular cluster containing molecular fragments A and B, respectively. Because the model molecular clusters considered in this work are large and the basis set used is restricted, to study the effect of basis set superposition error (BSSE), the counterpoise correction (Boys and Bernardi, 1970) was applied, for which $\Delta E^{Total,A...B/CP} = E^{Total,AB} - (E^{Total,A(B)} + E^{Total,B(A)})$; $E^{Total,A(B)}$ and $E^{Total,B(A)}$ denote the total energies of molecular fragment A computed with the "ghost" basis set (without electrons and nuclei) of molecular fragment B and vice versa. Because the hypothesized elementary reactions involved covalent bond breaking and formation, to study the characteristic electron density distributions (e.g., π-π and ion-pair characters), the highest occupy molecular orbitals (HOMO) of the model molecular clusters along the potential energy curves was plotted.

3.2.1 Density functional theory

The original density functional theory (DFT) idea begins from the Thomas-Fermi model (Thomas, 1927; Fermi, 1927). To simplify the complicated form of the *N*-electron wave function Ψ (x_1, x_2, ..., x_N) and the many-body Schrödinger equation, the electrons in the atom were considered as electron density n(**r**) for describe the approximate electrons distribution. Afterward, Hohenberg and Kohn (Hohenberg and Kohn, 1964) proposed the fundamental theorem for electronic ground state systems, namely the Hohenberg-Kohn existence theorem for which n(**r**) can be used to determine the electronic properties of atoms or molecules and their ground state energy that given by the variational principle. This procedure was further developed by Kohn and Sham (Kohn and Sham, 1965), in which the one-electron equations described by n(**r**) for considering the system that consists of *N* non-interacting

electrons, the total ground state energy of the non-interacting system can be obtained from Kohn–Sham equations as shown in equation (3.1).

$$\left[-\frac{1}{2}\nabla^2 - \sum_{\alpha} \frac{Z_\alpha}{r_{i\alpha}} + \int \frac{n(\mathbf{r}')}{|\mathbf{r} - \mathbf{r}'|}\, d\mathbf{r}' + \upsilon_{xc}(\mathbf{r}) \right] \psi_i(\mathbf{r}) = \varepsilon_i \psi_i(\mathbf{r}) \qquad (3.1)$$

Where the first term in Hamiltonian in operator equation (3.1) refers to the kinetic energy of *N* non-interacting electrons, the second term is the electron-nuclei attraction, the third term is electron-electron interaction energy operator, and the last term is the exchange-correlation potential which can be expressed as the following equation.

$$\upsilon_{xc}(\mathbf{r}) = \frac{\delta E_{xc}[n(\mathbf{r})]}{\delta n(\mathbf{r})} \qquad (3.2)$$

The ground-state electron density ($n(\mathbf{r})$) and the ground-state energy are obtained from single-electron wavefunction by solving the Kohn–Sham equations using the self-consistent field (SCF) method, as shown in the following procedures (Sholl and Steckel, 2009).

1. Establish an initial electron density, denoted as $n(\mathbf{r})$, for the trial.

2. Employ the trial electron density to solve the Kohn–Sham equations, determining the single-particle wave functions, $\psi_i(\mathbf{r})$.

3. Derive the electron density based on the Kohn–Sham single-particle wave functions obtained in step 2.

4. Compare the computed electron density, $n_{KS}(\mathbf{r})$, with the electron density utilized in solving the Kohn–Sham equations, $n(\mathbf{r})$. If the two densities match, it signifies the ground-state electron density, enabling the computation of the total energy.

5. In cases where the densities differ, the trial electron density necessitates adjustment. Following the adjustment, the process recommences from step 2.

3.2.2 Nudged elastic band method

To find the first-order saddle point (transition state; TS) between the reactant and product, the nudged elastic band method (NEB) was developed based on the chain-of-states calculations. The NEB method uses a series of harmonic restraints between replicas to find the first-order saddle point (transition state; TS) on the minimum energy path (MEP) as shown in Figure 3.1 (Sholl and Steckel, 2009; Plessow, 2013; Ghoreishi et al., 2019; Henkelman et al., 2000).
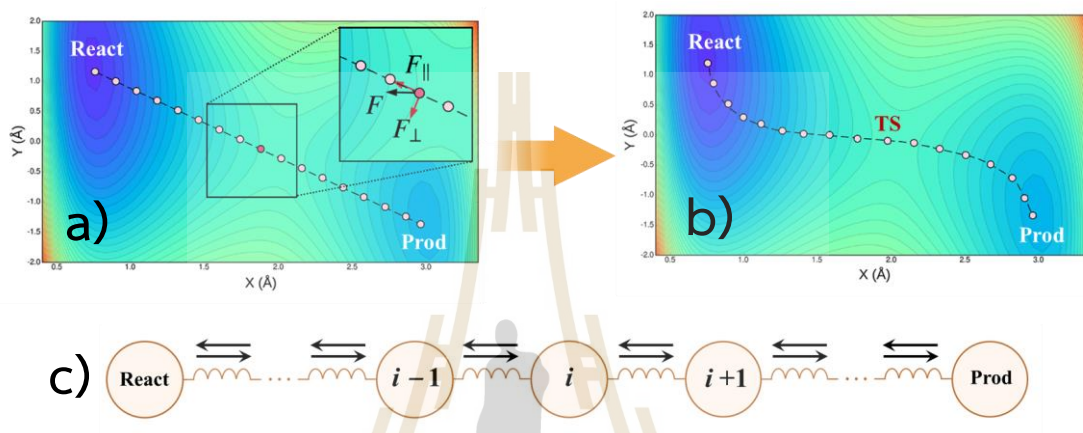
Figure 3.1 a)-b) Two-dimensional potential energy surfaces connecting reactant and product, initial guess, and NEB optimized reaction paths, respectively. c) mass-and-spring model used in the NEB method (Plessow, 2013; Ghoreishi et al., 2019).

The NEB method applies harmonic spring force (F_i^s) to find MEP, regarded as potential energy surface (PES). The total force (F_i^{NEB}) that acts on the replicas on the MEP can be considered as perpendicular forces ($F_i^\perp$) defined by force field parameters, whereas the spring forces are in the parallel direction with respect to the neighboring replicas ($F_i^\parallel$). The two orthogonal components are calculated using the following equations (Bergonzo et al., 2009; Ghoreishi et al., 2019).

$$F_i^{NEB} = F_i^\parallel + F_i^\perp \tag{3.3}$$

$$F_i^\perp = -\nabla V(R_i) + \nabla V((R_i) \cdot \tau_i) \cdot \tau_i \tag{3.4}$$

$$F_i^\parallel = (F_i^s \cdot \tau_i) \cdot \tau_i \tag{3.5}$$

F_i^s in equation (3.5) is the harmonic spring force at the position of the ith replicas. $\nabla V(R_i)$ is the potential force defined by the force field ($V(R_i)$) and τ_i is the tangent vector at each replica position.

3.2.3 Conductor-like screening model

The conductor-like screening model (COSMO) is the method to include solvent effects in the model calculation, from which thermodynamic properties of isolated molecules in solution, such as the solute-solvent interaction, can be studied.

COSMO is based on a dielectric screening concept, which explains the electrodynamic behavior of homogeneously polarizable macroscopic media (Klamt, 1995; Paduszyński, 2018; Tomasi et al., 2005). Electrostatic models describing the interaction between solute molecules and external electric fields (dielectric screening) are shown in Figure. 3.2.
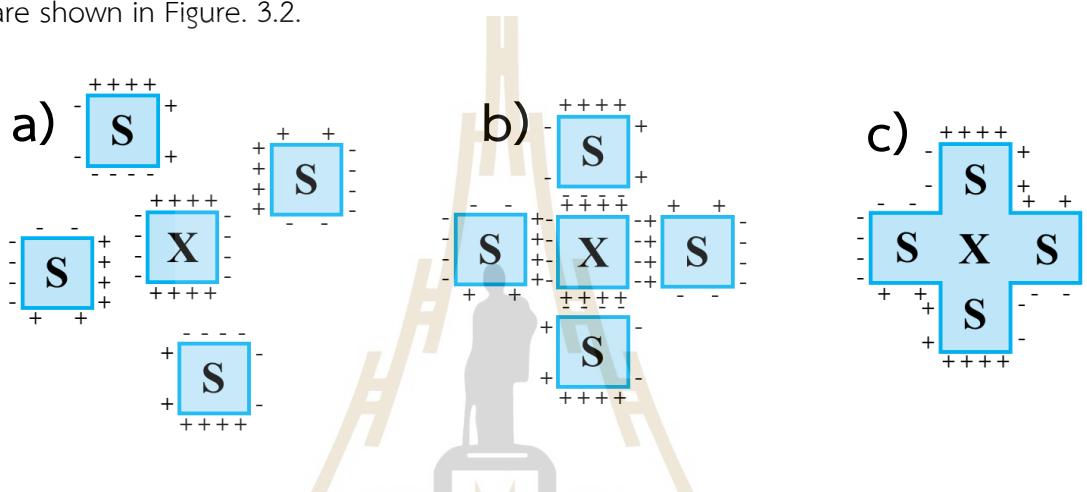
Figure 3.2 Virtual screening model describing the interaction between solute (X) and solvent (S) molecules. a) ensemble of surrounded molecules. b) pairing of surface charges. c) solute surrounded by solvent molecules (Klamt, 1995).

In Figure 3.2, COSMO considers solvent as a dielectric continuum of relative permittivity or dielectric constant (ε). Whereas solute molecule is embedded into the cavity surrounded by screening charges, leading to a change in the interaction energy between solute molecules (Klamt and Jonas, 1996).

3.3 Kinetics and thermodynamics of elementary reactions

3.3.1 Transition-state theory

The transition-state theory (TST) was developed by Henry Eyring in 1935 (Eyring, 1935). This method is based on the potential energy surface of the functional form in Figure 3.2, e.g., for AB + C $\longrightarrow$ [A—B—C]‡ $\longrightarrow$ A + BC. The TST method has been applied successfully on various types of chemical reactions (Laidler, 1983; Rooney, 1995; Truhlar et al., 1996).
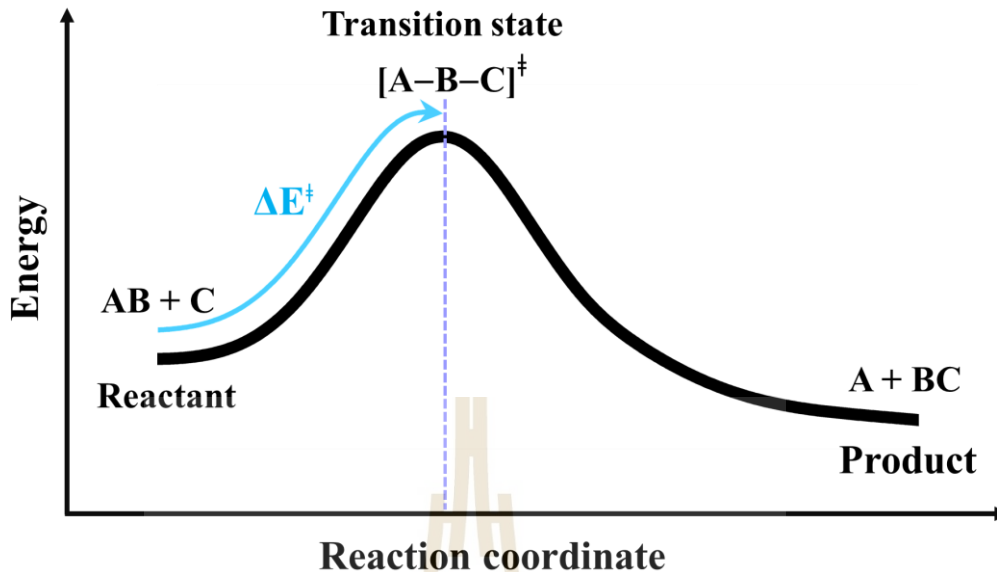
Figure 3.3 Example of the potential energy surface connecting reactant and product (AB + C $\longrightarrow$ [A−B−C]‡ $\longrightarrow$ A + BC) used in TST calculations.

In this work, the rate constants were computed using the TST method (Eyring, 1935; Kästner, 2014; Hänggi et al., 1990; Pollak and Talkner, 2005). To study the effect of quantum mechanical tunneling, the classical (k^{Class}) and quantized-vibrational (k^{Q-vib}) rate constants were initially computed over the temperature range of 200–371 K. k^{Class} was calculated using equation (3.6) (House, 2004):

$$k^{Class}(T) = \frac{k_B T}{h} \frac{Q^{\ddagger}}{Q^{R}} e^{-\Delta E^{\ddagger}/k_B T}.$$
(3.6)

Where Q^{R} and $Q^{\ddagger}$ are the partition functions of the reactant and transition structures, respectively. $\Delta E^{\ddagger}$ is the energy barrier obtained from the NEB potential energy curve. k_B and h are the Boltzmann and Planck constants, respectively. Then, k^{Q-vib} was obtained with the zero point energy-corrected energy barrier ($\Delta E^{\ddagger,ZPC}$):

$$k^{Q-vib}(T) = \frac{k_B T}{h} \frac{Q^{\ddagger,ZPC}}{Q^{R,ZPC}} e^{-\Delta E^{\ddagger,ZPC}/k_B T}.$$
(3.7)

$Q^{R,ZPC}$ and $Q^{\ddagger,ZPC}$ in equation (3.7) are the partition functions of the reactant and transition structures, respectively, that were obtained with zero point energy-corrected. $\Delta E^{\ddagger,ZPC}$ was obtained by including the zero-point correction energy (ΔE^{ZPE}) to $\Delta E^{\ddagger}$. The temperatures below which quantum mechanical tunneling dominates were

approximated using the crossover temperature (T_c) (Wigner, 1932; Wigner, 1937; Wigner, 1938):

$$T_c = \frac{\hbar\Omega^{\ddagger}}{2\pi k_B}. \tag{3.8}$$

$\Omega^{\ddagger}$ in equation (3.8) is the imaginary frequency of the transition structure. To approximate the effect of quantum mechanical tunneling, the Wigner corrections were made by multiplying $k^{Q\text{-vib}}(T)$ by the Wigner transmission coefficient ($\kappa^{F\text{-Wig}}$) in equation (3.9) (Wigner, 1932; Wigner, 1938):

$$\kappa^{F\text{-Wig}}(T) = \frac{\hbar\Omega^{\ddagger}/2k_BT}{\sin(\hbar\Omega^{\ddagger}/2k_BT)}. \tag{3.9}$$

In this work, $\kappa^{F\text{-Wig}}$ is regarded as the full Wigner transmission coefficient. Because $\kappa^{F\text{-Wig}}$ diverges near T_c, without a theoretical foundation, the simple Wigner transmission coefficient ($\kappa^{S\text{-Wig}}$) in equation (3.10) is recommended to avoid the divergence (Kästner, 2014):

$$\kappa^{S\text{-Wig}}(T) = 1 + \frac{1}{24}\left(\frac{\hbar\Omega^{\ddagger}}{k_BT}\right)^2. \tag{3.10}$$

$\kappa^{S\text{-Wig}}$ is a Taylor series expansion of $\kappa^{F\text{-Wig}}$ around $1/k_BT = 0$, maintaining only the first two terms. The Wigner corrected rate constants ($k^{F\text{-Wig}}$ and $k^{S\text{-Wig}}$) were computed using equation (3.11):

$$k^{F(S)\text{-Wig}}(T) = \kappa^{F(S)\text{-Wig}}(T)k^{Q\text{-vib}}(T). \tag{3.11}$$

$\kappa^{F\text{-Wig}}$ and $\kappa^{S\text{-Wig}}$ equal to 1 at the classical limit ($\hbar = 0$). The activation free energies ($\Delta G^{\ddagger}$) were computed from the rate constant using $k(T) = (k_BT/h)e^{-\Delta G^{\ddagger}/RT}$. To correlate $k^{S\text{-Wig}}$ with the experimental data (Kaneshiro et al., 2020), the Eyring equation (equation (3.12)) was primarily used to calculate the activation enthalpy ($\Delta H^{\ddagger}$) (House, 2007):

$$\ln k^{S\text{-Wig}}(T) = \ln A + \frac{\Delta S^{\ddagger}}{R} - \frac{\Delta H^{\ddagger}}{RT}. \tag{3.12}$$

$\Delta S^{\ddagger}$ is the activation entropy and R is the gas constant. $\Delta H^{\ddagger}$ in equation (3.12) was obtained from the linear relationship between $\ln k^{S\text{-Wig}}(T)$ and $1000/T$. $\Delta G^{\ddagger}$ obtained from the TST method were used to determine $\Delta S^{\ddagger}$ using $\Delta G^{\ddagger} = \Delta H^{\ddagger} - T\Delta S^{\ddagger}$. All the kinetic and thermodynamic calculations were performed using the DL-FIND program

(Kästner et al., 2009) included in the ChemShell software package (Smith and Forester, 1996; Metz et al., 2014).

3.3.2 Partition function

In quantum mechanics, the microscopic system is defined by a fundamental function known as the wave function. Similarly, in statistical mechanics, there exists a fundamental function with equivalent significance, referred to as the partition function (Cramer, 2013). In the case of the canonical ensemble, it is expressed as follows:

$$Q(N, V, T) = \sum_i e^{-E_i(N, V)/k_B T} \qquad (3.13)$$

Where i is all possible energy states of the system that have energy E_i. In the case of canonical ensemble, it can be employed to establish the thermodynamic definitions as shown in equations (3.14)—(3.17).

$$U = k_B T^2 \left(\frac{\partial \ln Q}{\partial T} \right)_{N, V} \qquad (3.14)$$

$$H = U + PV \qquad (3.15)$$

$$S = k_B \ln Q + k_B T \left(\frac{\partial \ln Q}{\partial T} \right)_{N, V} \qquad (3.16)$$

$$G = H - TS \qquad (3.17)$$

In equations (3.14) and (3.16), the notation for partial derivatives indicates that differentiation for temperature (T) is performed while keeping the values of N (number of particles) and V (volume) constant. Here, H represents enthalpy, P stands for pressure, S denotes entropy, and G signifies Gibbs free energy. For the ensemble that behaves as an ideal gas. The initial implication of this assumption is that, due to the lack of interactions among ideal gas molecules, we can express the partition function in a different form as shown in equations (3.18)—(3.20) (Cramer, 2013).

$$Q(N, V, T) = \frac{[q(V, T)]^N}{N!} \qquad (3.18)$$

$$q(V, T) = \left[\sum_{i}^{elect} g_i e^{-\varepsilon_i/k_BT}\right]\left[\sum_{j}^{trans} g_j e^{-\varepsilon_j(V)/k_BT}\right]\left[\sum_{k}^{rot} g_k e^{-\varepsilon_k/k_BT}\right]\left[\sum_{l}^{vib} g_l e^{-\varepsilon_l/k_BT}\right] \quad (3.19)$$

$$q(V, T) = q_{elec}(T)q_{trans}(V, T)q_{rot}(T)q_{vib}(T) \quad (3.20)$$

Where q is the molecular partition function, ε is the molecular energy, and $g_{i, j, k, l}$ is the degeneracy of energy levels i, j, k, and l, respectively.

CHAPTER IV
RESULTS AND DISCUSSION

4.1 Equilibrium structures of the model molecular clusters

The equilibrium structures and total energies of the model molecular clusters that are involved in the elementary reactions are presented in Table 3.1. The B3LYP/DZP results show that the equilibrium structures of the model molecular clusters and the shapes of the active sites therein are not significantly different at $\varepsilon = 1$ versus 78. The average residue-to-residue distances reveal small standard deviations (SD) for all elementary reactions; the average residue-to-residue distances were approximated using the distances between the carbon atoms of the CH_3 groups that substituted the carbon atom of $FDC1^{Backbone}$ (Figure 1.1). For example, for React→TS1→Int1 at $\varepsilon = 1$, $R_{C_R^{Arg173H^+}-C_R^{Glu277}} = 10.41\pm0.48$, $R_{C_R^{Arg173H^+}-C_R^{Gln190}} = 11.07\pm0.49$ and $R_{C_R^{Glu277}-C_R^{Gln190}} = 17.08\pm0.50$ Å (Table 4.1) and for Int2b→TS3→Int3, $R_{C_R^{Arg173H^+}-C_R^{Glu277}} = 10.78\pm0.04$, $R_{C_R^{Arg173H^+}-C_R^{Gln190}} = 13.00\pm0.59$ and $R_{C_R^{Arg173H^+}-C_R^{Glu282}} = 8.95\pm0.83$ Å. It appears that the highest SD are for elementary reactions that involve proton transfer, in which formation of π–π stacking leads to an increase in $R_{C_R^{Glu277}-C_R^{Gln190}}$. For example, at $\varepsilon = 1$, $R_{C_R^{Glu277}-C_R^{Gln190}} = 13.46\pm1.94$ and 13.43 ± 1.86 Å are for acid catalyst (1) (III) and acid catalyst (2) (V), respectively.

These average residue-to-residue distances (Tables 4.1 and 4.2) are in good agreement with the PDB crystallographic data (code 4ZA7) in Figure 1.1, in which $R_{C_R^{Arg173}-C_R^{Glu277}} = 9.79$, $R_{C_R^{Arg173}-C_R^{Gln190}} = 12.40$, $R_{C_R^{Glu277}-C_R^{Gln190}} = 17.47$ and $R_{C_R^{Arg173}-C_R^{Glu282}} = 10.11$ Å. Similar results were obtained from the analysis of the average residue-to-residue distances per each model molecular structure on the optimized reaction paths. They are also not significantly different; for example, for Structure 1 of elementary reactions (I)-(II) (Table 4.3), $R_{C_R^{Arg173H^+}-C_R^{Glu277}} = 10.31\pm0.99$ Å and that for elementary reactions (III)-(IV) is 10.82 ± 0.07 Å

Table 4.1 The residue-to-residue distances (Å) on the potential energy curves obtained based on the B3LYP/DZP and NEB methods and their average values. The distances are approximated using the distances between the carbon atoms of the CH_3 groups substituting the atoms of the FDC1 backbone (Figure 1.1) for elementary reactions (I)–(V) in $\varepsilon = 1$.

Elementary reaction ($\varepsilon = 1$)	Distance (Å)			
	$R_{C_R^{Arg173}\_C_R^{Glu277}}$	$R_{C_R^{Arg173}\_C_R^{Gln190}}$	$R_{C_R^{Glu277}\_C_R^{Gln190}}$	$R_{C_R^{Arg173}\_C_R^{Glu282}}$
1,3-dipolar cycloaddition (I)	10.41±0.48	11.07±0.49	17.08±0.50	–
Decarboxylation (II)	10.99±0.11	11.16±0.41	15.18±0.74	–
Acid catalyst (1) (III)	10.78±0.04	13.00±0.59	13.46±1.94	8.95±0.83
Cycloelimination (IV)	10.70±0.04	13.48±0.17	16.45±0.07	10.60±0.25
Acid catalyst (2) (V)	10.74±0.08	12.61±0.44	13.43±1.86	9.55±1.05

Table 4.2 The residue-to-residue distances (Å) on the potential energy curves obtained based on the B3LYP/DZP and NEB methods and their average values. The distances are approximated using the distances between the carbon atoms of the CH_3 groups substituting the atoms of the FDC1 backbone (Figure 1.1) for elementary reactions (I)–(V) in $\varepsilon = 78$.

Elementary reaction ($\varepsilon = 78$)	Distance (Å)			
	$R_{C_R^{Arg173}\_C_R^{Glu277}}$	$R_{C_R^{Arg173}\_C_R^{Gln190}}$	$R_{C_R^{Glu277}\_C_R^{Gln190}}$	$R_{C_R^{Arg173}\_C_R^{Glu282}}$
1,3-dipolar cycloaddition (I)	10.33±0.43	11.09±0.47	17.11±0.50	–
Decarboxylation (II)	10.96±0.29	11.04±0.38	15.27±0.75	–
Acid catalyst (1) (III)	10.79±0.05	12.94±0.58	13.60±1.96	9.06±0.83
Cycloelimination (IV)	10.75±0.05	13.47±0.16	16.41±0.25	10.62±0.27
Acid catalyst (2) (V)	10.77±0.07	12.59±0.45	13.35±1.98	9.50±1.12

The above results suggest that in the enzymatic decarboxylation reaction, the active site structure and volume do not significantly change. These results also imply that the motion of FDC1[Backbone] can be neglected in the model systems. These findings are in accordance with the results reported by Bailey et al. (2018), in which the Glu277—Arg173—Glu282 residue network was suggested to be conserved in the enzymatic decarboxylation reaction; the residues help immobilize the substrate and

cofactor in the active site. In addition, because the computed residue-to-residue distances are in good agreement with the PDB crystallographic data (code 4ZA7), one can conclude that the model molecular clusters are appropriate for representing the active site of FDC1. To facilitate discussion, additional character codes are used. To characterize the scenarios (progress) in the elementary reactions, lowercase letters in parentheses are used. For example, for 1,3-dipolar cycloaddition (React→TS1→Int1) in Figure 4.1, the three consecutive steps, namely, π–π stacking, dipolarophile iminium pair and pyrrolidine cycloadduct formations, are labeled (a), (b) and (c), respectively. The properties/processes with superscript "ε" correspond to a high local dielectric environment. For example, $TS1^{\varepsilon}$ in and $(a)^{\varepsilon}$ in Figure 4.2 is the transition structure and π–π stacking, respectively, that were observed on the potential energy curve at ε = 78.

4.2 Elementary reactions

The structures and energetics of the model molecular clusters on the potential energy curves of the elementary reactions (I)–(V) that were obtained via the NEB method at ε = 1 and ε = 78 are included in Figures 4.1–4.5, together with the relative total energies (ΔE^{Rel} and $\Delta E^{Rel,\varepsilon}$).

4.2.1 1,3-Dipolar cycloaddition (I)

The associative interactions between the residues, substrate and cofactor in React are represented by the salt bridges between Glu277 and Arg173H$^+$ and between Arg173H$^+$ and Cin and by the N–H...O$^-$ H-bond between Gln190 and PrFMN (Table 3.1), respectively. Because the aromatic rings are relatively close, the π–π interaction between Cin and PrFMN could help facilitate 1,3-dipolar cycloaddition. The HOMOs in Figure 4.2a show a significant difference between the electron density distributions in React at ε = 1 and 78. At ε = 1, the highest electron density is localized at the salt-bridge network that spans from the COO$^-$ group of Glu277 to Arg173H$^+$ to the COO$^-$ group of Cin, whereas at ε =78 (Figure 4.1b), the highest electron density distribution is at the PrFMN aromatic rings, thereby indicating higher aromaticity in the high local dielectric environment.

Figure 4.1 a)–b) Structures of the model molecular clusters involved in 1,3-dipolar cycloaddition (I) (Figure 1.1) obtained using the B3LYP/DZP and NEB methods in $\varepsilon = 1$ and 78, respectively. Distances are in Å and isosurface of HOMO is 0.042. c) Potential energy curves obtained using the B3LYP/DZP and NEB methods in $\varepsilon = 1$ and 78. ΔE^{Rel} = relative total energy with respect to the precursor React in $\varepsilon = 1$; $\Delta E^{Rel,\varepsilon}$ = relative total energy with respect to the precursor React$^{\varepsilon}$ in $\varepsilon = 78$; $\Delta E^{Rel,Solv}$ = relative solvation energy with respect to the precursor React$^{\varepsilon}$; $\Delta E^{\ddagger}$ = energy barrier; (…) and (…)$^{\varepsilon}$ = scenarios in the elementary reactions in $\varepsilon = 1$ and 78, respectively.

For 1,3-dipolar cycloaddition (I), the potential energy curve in Figure 4.1c reveals that at ε = 1, React→TS1 is a two-step process, in which the formation of π–π stacking (a) occurs first ($\Delta E^{\ddagger}$ = 24 kJ/mol), followed by dipolarophile-iminum pair formation (b) in the transition structure TS1 ($\Delta E^{\ddagger}$ = 50 kJ/mol). TS1 is characterized by the α,β-double bond of Cin staying exactly above the iminium ion (C_{29}^{PrFMN}—$N_{35}^{PrFMN,+}$—C_{34}^{PrFMN}, 1,3–dipole) of PrFMN ($R_{C_{\alpha}^{Cin}-C_{29}^{PrFMN}}$ = 2.78 and $R_{C_{\beta}^{Cin}-C_{34}^{PrFMN}}$ = 3.30 Å).

It appears that pyrrolidine cycloadduct formation (c) and relaxation of π–π stacking (d) occur instantly in TS1→Int1, thereby leading to the transformation of the enolate anion to a C=O group at the O_{30}^{PrFMN} atom. Figure 4.1c also shows that Int1 possesses approximately the same stability as React. The HOMO plots along the potential energy curve (Figure 4.1a) show electron density redistribution upon pyrrolidine cycloadduct formation and relaxation of the π–π stacking interaction, thereby leading to a considerable increase in the π–character spanning from the enoate group of Cin to the heteroaromatic rings (the isoalloxazine ring) of PrFMN. The electron density redistribution is due to neutralization of the iminium ion and is accompanied by an increase in the C_{α}^{Cin}–C_{43}^{Cin} bond distance from $R_{C_{\alpha}^{Cin}-C_{43}^{Cin}}$ = 1.54 to 1.58 Å, which reflects a weaker C_{α}^{Cin}–C_{43}^{Cin} covalent bond in Int1 (precursor for CO_2 elimination) compared with the precursor React.

At ε = 78, the potential energy curve is almost the same as that at ε = 1 (Figure 4.1c). The energy barriers for π–π stacking $(a)^{\varepsilon}$ and $TS1^{\varepsilon}$ formation $(b)^{\varepsilon}$ are slightly different, namely, $\Delta E^{\ddagger}$ = 26 and 48 kJ/mol, respectively. This could be because cycloadduct formation ($React^{\varepsilon} \rightarrow TS1^{\varepsilon} \rightarrow Int1^{\varepsilon}$) does not involve direct charge (proton) transfer. Therefore, the electric field that is induced by the aqueous solvent (ε = 78) does not have a strong influence on the energy barriers. The relative solvation energies ($\Delta E^{Rel,Solv}$) in Figure 4.1c, which were computed with respect to the solvation energy (ΔE^{Solv}) of the precursor React, show that because the charges in the active site (e.g., $N_{35}^{PrFMN,+}$ in Figure 4.1b) are not directly hydrated, the stability of $TS1^{\varepsilon}$ is only slightly increased (~-8 kJ/mol) and that of $Int1^{\varepsilon}$ is slightly decreased (~6 kJ/mol); the latter is due to the neutralization of the iminium charge ($N_{35}^{PrFMN,+}$) upon pyrrolidine cycloadduct formation.

4.2.2 Decarboxylation (II)

At $\varepsilon = 1$, the structures of the model molecular clusters on the potential energy curve in Figure 4.2 reveal that decarboxylation (II) (Int1→TS2→Int2) is a three-step process, in which the C_{α}^{Cin}–C_{43}^{Cin} bond extension (a) continues in Int1→TS2 ($R_{C_{\alpha}^{Cin}-C_{43}^{Cin}}$ = 1.62 Å and $\Delta E^{\ddagger}$ = 60 kJ/mol), followed by CO_2 elimination (b), $C_{\beta}^{Cin} - C_{34}^{PrFMN}$ dissociation (c) and reorientation of the aromatic ring of Cin away from PrFMN (d) in TS2→Int2, with $R_{C_{\alpha}^{Cin}-C_{43}^{Cin}}$ = 4.52 and $R_{C_{\beta}^{Cin}-C_{34}^{PrFMN}}$ = 3.67 Å, respectively. The potential energy curve in Figure 4.2c shows that at $\varepsilon = 78$, although the consecutive reaction scheme is not different from that at $\varepsilon = 1$, the C_{α}^{Cin}–C_{43}^{Cin} bond extension $(a)^{\varepsilon}$, CO_2 elimination $(b)^{\varepsilon}$ and C_{β}^{Cin}–C_{34}^{PrFMN} dissociation $(c)^{\varepsilon}$ occur readily in Int1$^{\varepsilon}$→TS2$^{\varepsilon}$ with a significantly lower energy barrier ($\Delta E^{\ddagger}$ = 39 kJ/mol). It appears that the transfer of the negative charge from the COO^{-} group of Cin to form the enolate anion (enolization) at the O_{30}^{PrFMN} atom (Figure 4.2b), which accompanies $(a)^{\varepsilon}$, $(b)^{\varepsilon}$ and $(c)^{\varepsilon}$, leads to a decrease in the relative solvation energy (stabilization of TS2$^{\varepsilon}$) to $\Delta E^{Rel,Solv}$ = -12 kJ/mol (Figure 4.2c), whereas the substrate moiety reorientation $(d)^{\varepsilon}$ ($R_{C_{\beta}^{Cin}-C_{34}^{PrFMN}}$ = 3.67 Å) results in an increase in $\Delta E^{Rel,Solv}$ to 26 kJ/mol; Int2$^{\varepsilon}$ (e.g., the aromatic ring of Cin) is moderately destabilized by the electric field of the aqueous solvent.
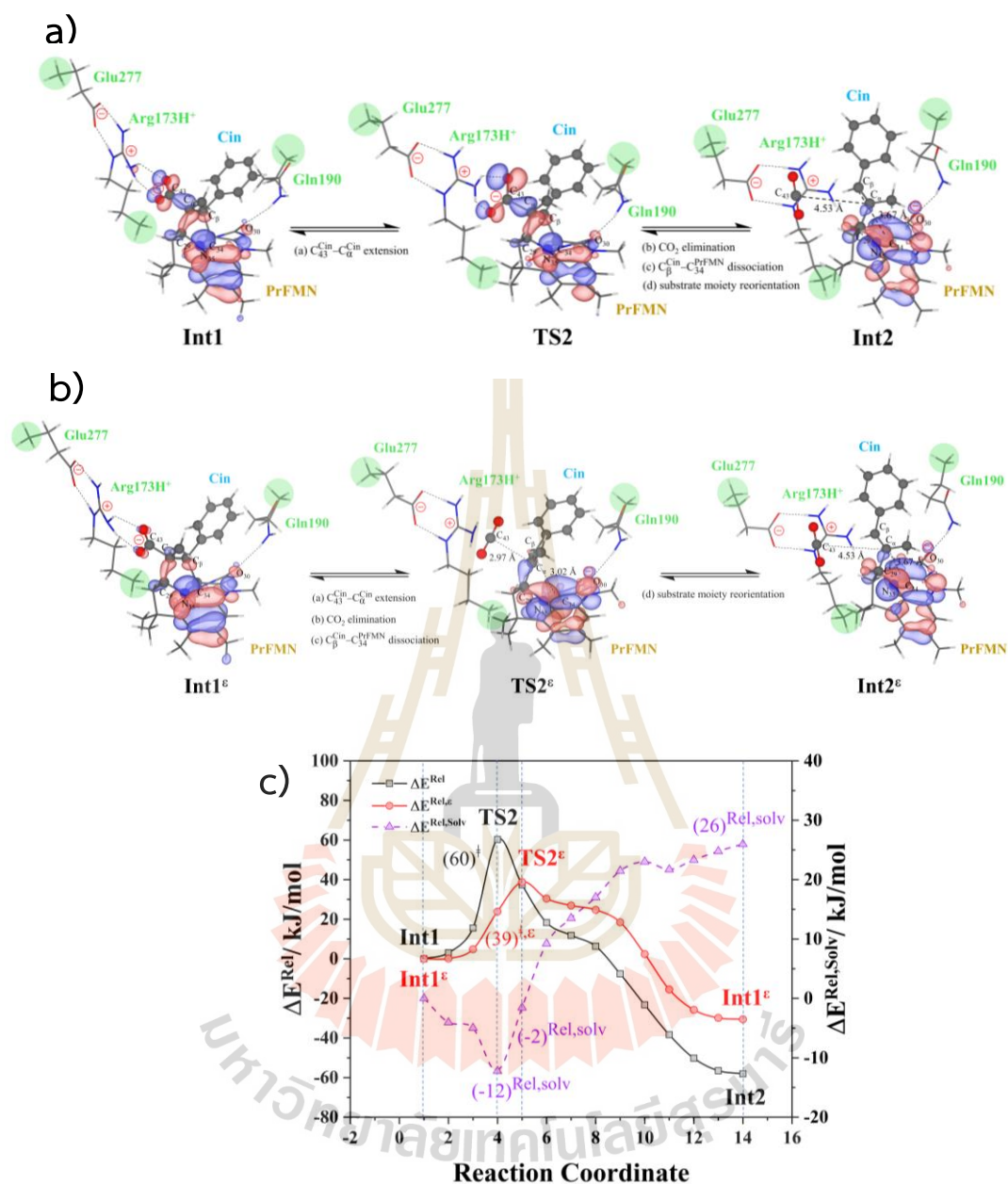
Figure 4.2 a)–b) Structures of the model molecular clusters involved in decarboxylation (II) (Figure 1.1) obtained using the B3LYP/DZP and NEB methods in ε = 1 and 78, respectively. Distances are in Å and isosurface of HOMO is 0.042. c) Potential energy curves obtained using the B3LYP/DZP and NEB methods in ε = 1 and 78.

4.2.3 Acid catalyst (1) (III)

The precursor and transition structures of the model molecular clusters on the potential energy curves in Figure 4.3a indicate that at $\varepsilon = 1$, proton transfer from the COOH group of Glu282 to C_α^{Cin} (a) and formation of the pyrrolidine cycloadduct (b) are associated with a low energy barrier; for Int2b→TS3, $R_{C_\alpha^{Cin}-H_{126}^{Glu282}} = 1.10$, $R_{C_\alpha^{Cin}-C_{29}^{PrFMN}} = 1.53$ and $R_{C_\beta^{Cin}-C_{34}^{PrFMN}} = 1.64$ Å with $\Delta E^{\ddagger} = 42$ kJ/mol. The low energy barrier suggests that proton transfer from the COOH group of Glu282 to C_α^{Cin} could occur without a water bridge in the active site, as suggested by Tian and Liu (2017). The formation of $\pi-\pi$ stacking between Cin and PrFMN (c) is partly responsible for the stability of Int3.

The scenario is slightly different at $\varepsilon = 78$ (Figures 4.3b and 4.3c), in which proton transfer from the COOH group of Glu282 to C_α^{Cin} (a)$^{\varepsilon}$ instantly produces the transition state (TS3$^{\varepsilon}$); for Int2b$^{\varepsilon}$→TS3$^{\varepsilon}$, $R_{C_\alpha^{Cin}-H_{126}^{Glu282}} = 1.26$ (shared proton structure), $R_{C_\alpha^{Cin}-C_{29}^{PrFMN}} = 1.55$ and $R_{C_\beta^{Cin}-C_{34}^{PrFMN}} = 2.31$ Å with a considerably higher energy barrier ($\Delta E^{\ddagger} = 137$ kJ/mol) and destabilized relative solvation energy ($\Delta E^{Rel,Solv} = 5$ kJ/mol). At $\varepsilon = 78$, acid catalyst (1) is accomplished through the formation of pyrrolidine cycloadduct (b)$^{\varepsilon}$ and $\pi-\pi$ stacking intermediate (c)$^{\varepsilon}$ (Int3$^{\varepsilon}$).

The increase in $\Delta E^{\ddagger}$ at $\varepsilon = 78$ is opposite the situation in decarboxylation (II) because proton transfer in this case leads to an increase in the number of the positive and negative charges (acid-base ion pairs in TS3$^{\varepsilon}$ with $R_{C_\alpha^{Cin}-H_{126}^{Glu282}} = 1.26$ Å), which are partly stabilized by the high local dielectric environment; the "dipolar" interaction (a)$^{\varepsilon}$ in TS3$^{\varepsilon}$ forms a "dipolar energy trap", which increases $\Delta E^{\ddagger}$ at $\varepsilon = 78$.[14] Analysis of the $O_{125}^{Glu282,-}...H_{126}^{Glu282}-C_\alpha^{Cin}$ H-bond and $O_{125}^{Glu282,-}...H_{126}^{Glu282,+}...C_\alpha^{Cin}$ ion-pair interaction energies (at (a) and (a)$^{\varepsilon}$ in TS3 and TS3$^{\varepsilon}$, respectively) suggests that with respect to the precursor, the H-bond is strongly destabilized at $\varepsilon = 1$ ($\Delta E^{Rel,H-bond/CP} = 39$ kJ/mol), whereas at $\varepsilon = 78$, the ion pair is only weakly destabilized ($\Delta E^{Rel,H-bond/CP,\varepsilon} = 2$ kJ/mol).
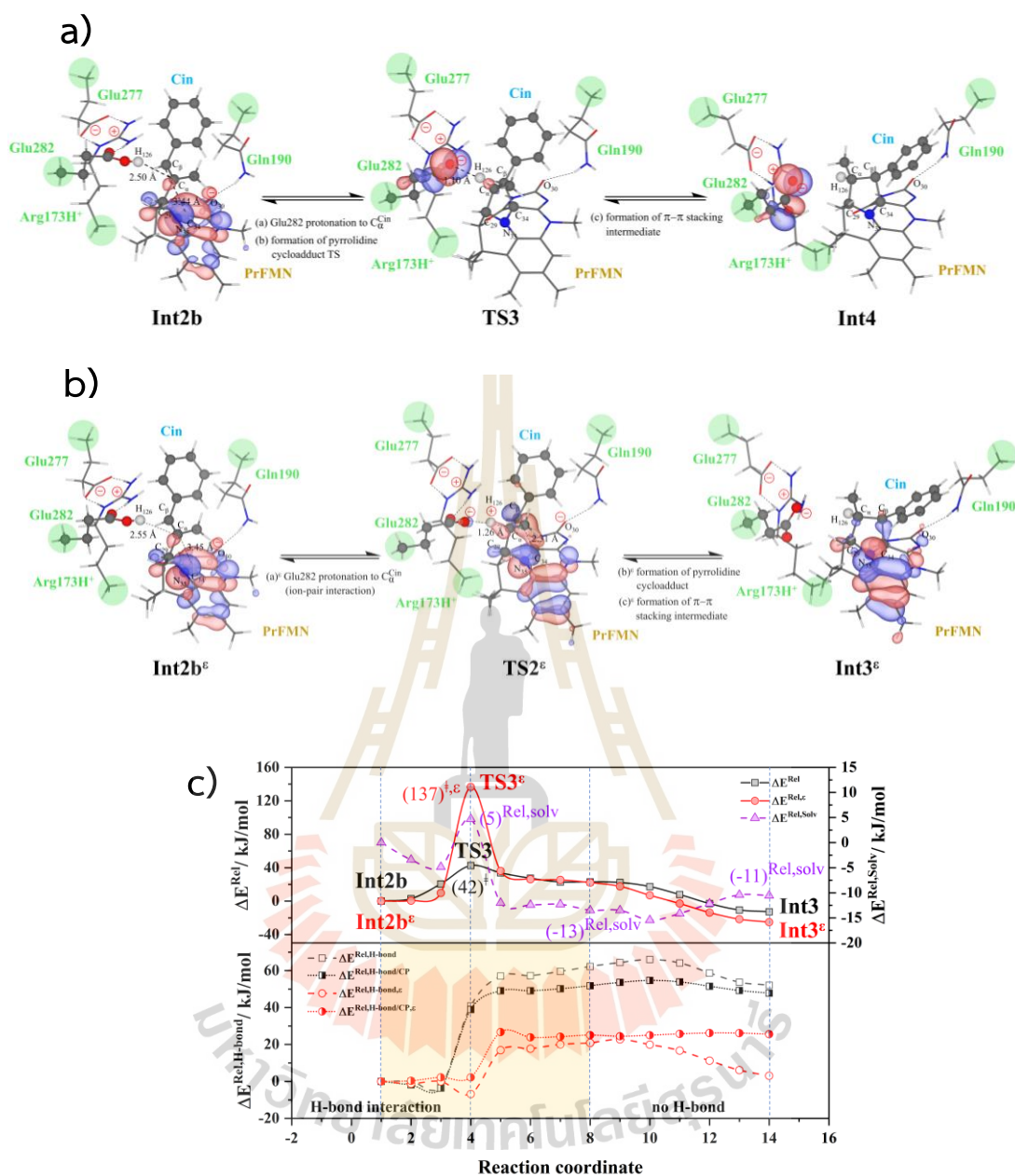
Figure 4.3 a)–b) Structures of the model molecular clusters involved in acid catalyst (1) (III) (Figure 1.1) obtained using the B3LYP/DZP and NEB methods in $\varepsilon = 1$ and 78, respectively. Distances are in Å and isosurface of HOMO is 0.042. c) Potential energy curves obtained using the B3LYP/DZP and NEB methods in $\varepsilon = 1$ and 78. The calculations of the H-bond interaction energies ($\Delta E^{Rel,H-bond}$, $\Delta E^{Rel,H-bond/CP}$, $\Delta E^{Rel,H-bond,\varepsilon}$ and $\Delta E^{Rel,H-bond/CP,\varepsilon}$).

4.2.4 Cycloelimination (IV)

To complete the enzymatic reaction cycle, β-methylstyrene (β–MeSt) and PrFMN are formed through cycloelimination (IV). In Int3→TS4→Prod at $\varepsilon = 1$ (Figure 4.4a), the $C_\beta^{Cin}-C_{34}^{PrFMN}$ extension (a) and dissociation (b) ($R_{C_\beta^{Cin}-C_{34}^{PrFMN}} = 2.93$ Å) and $C_\alpha^{Cin}-C_{29}^{PrFMN}$ dissociation (c) ($R_{C_\alpha^{Cin}-C_{29}^{PrFMN}} = 2.69$ Å) occur consecutively in Int3→TS4 ($\Delta E^\ddagger = 81$ kJ/mol, Figure 4.4c), whereas β–MeSt leaves the iminium ion (TS4→Prod) on a barrierless potential curve ($R_{C_\alpha^{Cin}-C_{29}^{PrFMN}} = 3.85$ and $R_{C_\beta^{Cin}-C_{34}^{PrFMN}} = 3.90$ Å); the model molecular cluster Prod consists of free β–MeSt and the regenerated PrFMN, Glu277, Arg173H^{+} and Gln190, as in React.

The scenarios are slightly different at $\varepsilon = 78$ (Figure 4.4b), in which the $C_\beta^{Cin}-C_{34}^{PrFMN}$ extension (a)$^\varepsilon$ takes place first in Int3$^\varepsilon$→TS4$^\varepsilon$ ($R_{C_\beta^{Cin}-C_{34}^{PrFMN}} = 2.93$ Å) with a comparable energy barrier ($\Delta E^\ddagger = 77$ kJ/mol), followed by the $C_\beta^{Cin}-C_{34}^{PrFMN}$ (b)$^\varepsilon$ and $C_\alpha^{Cin}-C_{29}^{PrFMN}$ dissociations (c)$^\varepsilon$ ($R_{C_\beta^{Cin}-C_{34}^{PrFMN}} = 3.89$ Å and $R_{C_\alpha^{Cin}-C_{29}^{PrFMN}} = 3.87$ Å, respectively). Analysis of $\Delta E^{Rel,Solv}$ on the potential energy curve in Figure 4.4c suggests similar stabilization and destabilization effects of the aqueous solvent as in decarboxylation (II), in which the transition structure TS4$^\varepsilon$ is stabilized and Prod$^\varepsilon$ is slightly destabilized by the local dielectric environment; TS4$^\varepsilon$→Prod$^\varepsilon$ results in β–MeSt and PrFMN.
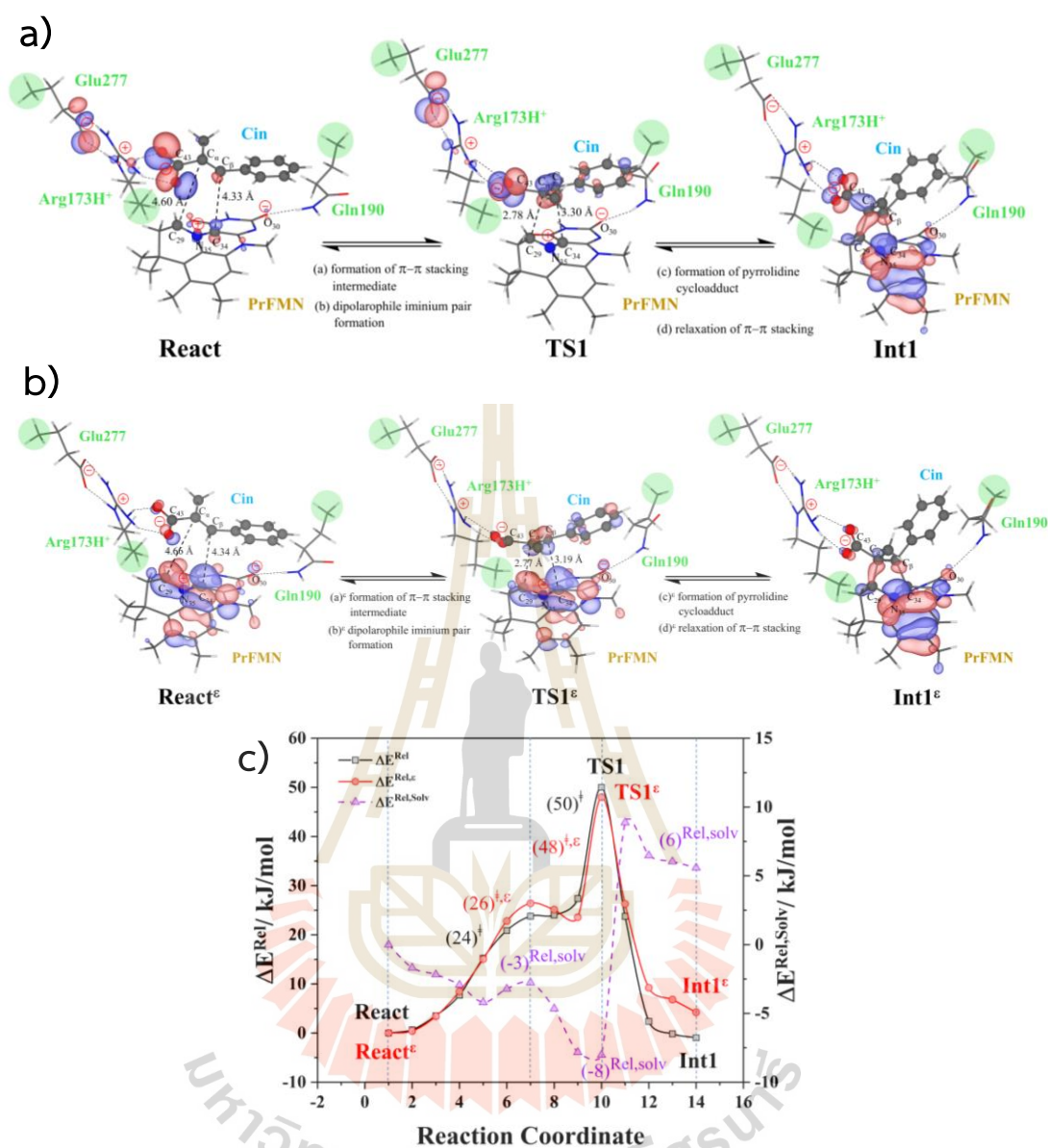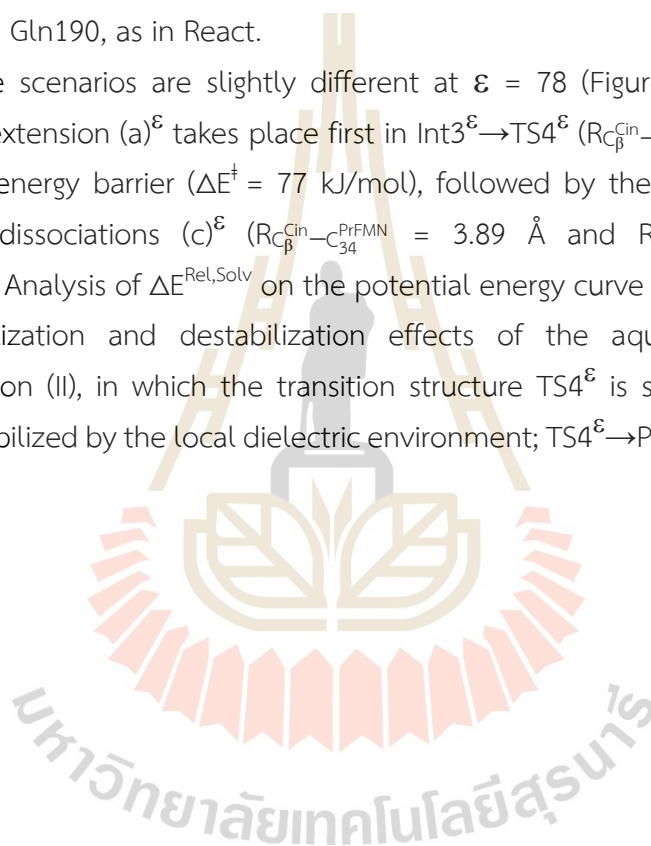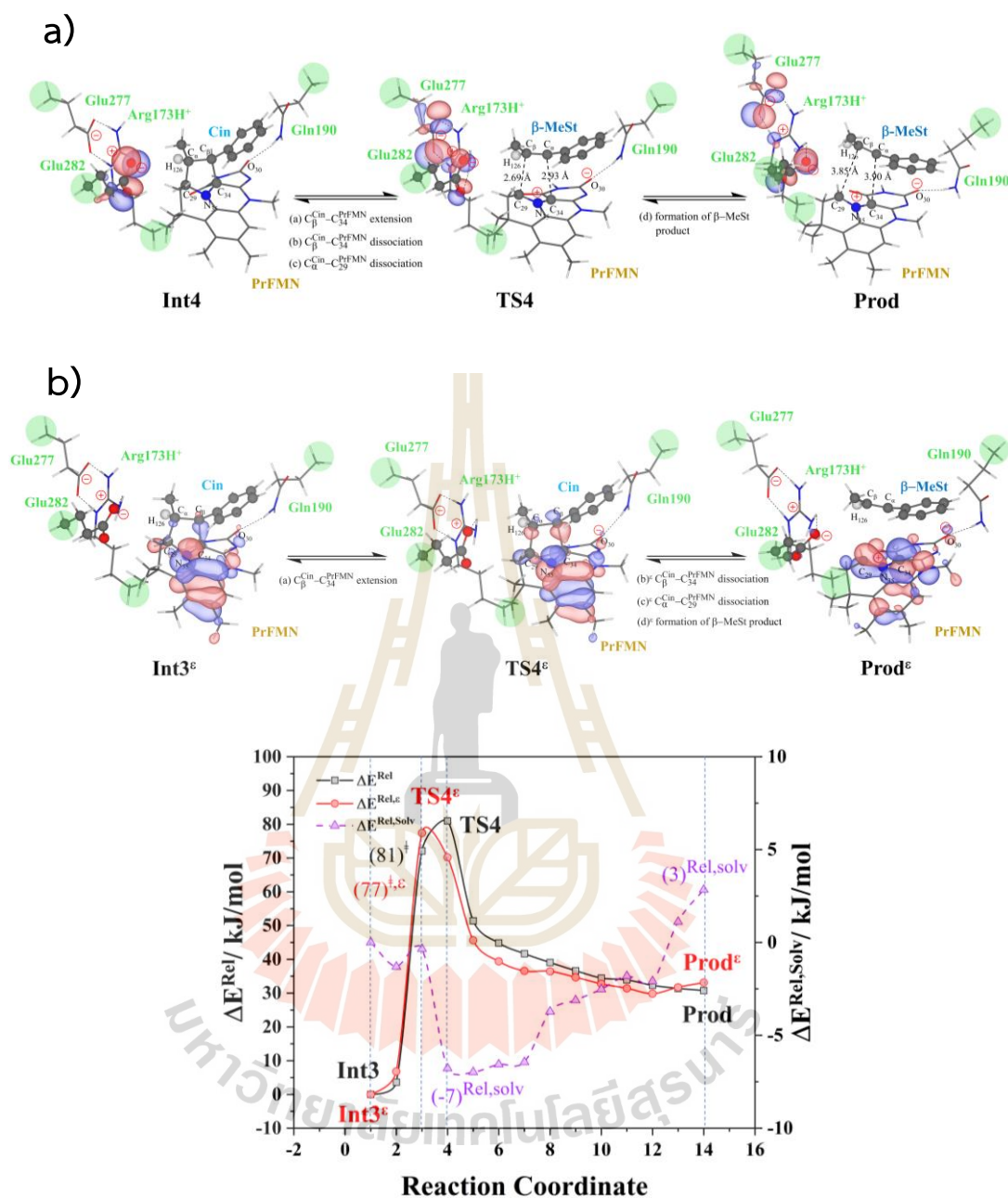
Figure 4.4 a)–b) Structures of the model molecular clusters involved in cycloelimination (IV) (Figure 1.1) obtained using the B3LYP/DZP and NEB methods in ε = 1 and 78, respectively. Distances are in Å and the isosurface of HOMO is 0.042. c) Potential energy curves obtained using the B3LYP/DZP and NEB methods in ε = 1 and 78.

4.2.5 Acid catalyst (2) (V)

Based on the potential energy curves that have been discussed up to this point, the highest energy barrier at $\varepsilon = 1$ is for cycloelimination (IV) ($\Delta E^{\ddagger} = 81$ kJ/mol), whereas that at $\varepsilon = 78$ is for acid catalyst (1) (III) ($\Delta E^{\ddagger} = 137$ kJ/mol). To complete the discussion on the potential energy curves of the elementary reactions, the route for generating Prod directly from Int2b (without the formation of pyrrolidine cycloadduct) is discussed. At $\varepsilon = 1$ (Figure 4.5a), the proton transfer from the COOH group of Glu282 to C_{α}^{Cin} (a) instantly leads to $C_{\alpha}^{Cin}-C_{29}^{PrFMN}$ dissociation (b) ($R_{C_{\alpha}^{Cin}-C_{29}^{PrFMN}} = 2.95$ and $R_{C_{\alpha}^{Cin}-C_{43}^{Cin}} = 4.18$ Å) and the formation of β—MeSt (c) with a slightly lower energy barrier ($\Delta E^{\ddagger} = 73$ kJ/mol) compared with Int3$\rightarrow$TS4$\rightarrow$Prod ($\Delta E^{\ddagger} = 81$ kJ/mol), whereas at $\varepsilon = 78$, Int2b$^{\varepsilon}\rightarrow$TS3b$^{\varepsilon}\rightarrow$Prod$^{\varepsilon}$ as shown in Figure 4.5b involves a considerably lower energy barrier ($\Delta E^{\ddagger} = 47$ kJ/mol; Figure 4.5c). Therefore, the direct route at $\varepsilon = 78$ should also be considered in further discussion.
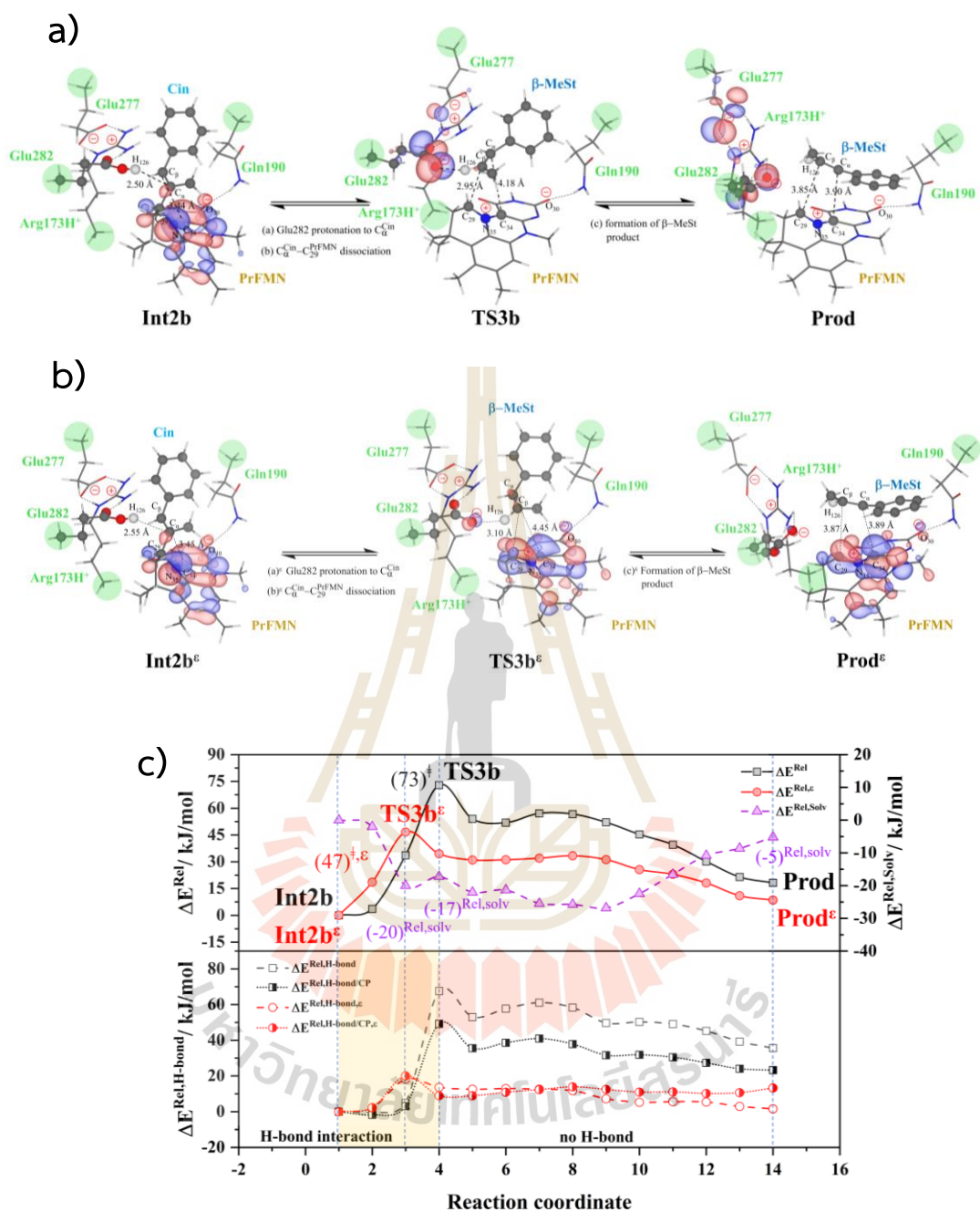
Figure 4.5 a)–b) Structures of the model molecular clusters involved in acid catalyst (2) (V) (Figure 1.1) obtained using the B3LYP/DZP and NEB methods in $\varepsilon = 1$ and 78, respectively. Distances are in Å and isosurface of HOMO is 0.042. c) Potential energy curves obtained using the B3LYP/DZP and NEB methods in $\varepsilon = 1$ and 78.

4.3 The effect of high local dielectric environment

The potential energy profiles for the enzymatic decarboxylation of α,β-unsaturated acid that were obtained in this and previous studies are presented in Figure 4.6. To verify the theoretical results, our potential energy profiles at $\varepsilon = 1$ are compared with profiles at $\varepsilon = 4$ (Lan and Chen, 2016) (Figure 4.6a) that were obtained from B3LYP/6-311+G(2d,2p)//6-31G(d,p) calculations with the intrinsic reaction coordinate (IRC) and conductor-like polarizable continuum model (CPCM) methods. Based on the number of atoms in the model molecular clusters, the elementary reactions are categorized into two groups, namely, the decarboxylation/CO_2 elimination (React→TS1→Int1→TS2→Int2) and β—MeSt formation/cofactor regeneration on the indirect (Int2b→TS3→Int3→TS4→Prod) and direct routes (Int2b→TS3b→Prod), which involve 115 and 126 atoms, respectively.

Comparison of the potential energy profiles in Figure 4.6a reveals similar energy barriers at $\varepsilon = 1$ and 4 (Lan and Chen, 2016), except for acid catalyst (1) (III), for which $\Delta E^{\ddagger}$ at $\varepsilon = 4$ is ~17 kJ/mol higher than that at $\varepsilon = 1$, thereby implying that a slight increase in ε could result in a significant change in the energy barrier for the elementary reaction involving proton transfer.

The potential energy profiles in Figure 4.6b confirm the above observation by showing that the increase in the polarity of the solvent from $\varepsilon = 1$ to 78 leads to significant changes in $\Delta E^{\ddagger}$, especially for the transition states that involve proton transfer; $\Delta E^{\ddagger}$ for acid catalyst (1) (III) increases from 42 to 137 kJ/mol, whereas that of acid catalyst (2) (V) decreases from 73 to 47 kJ/mol. It appears that due to the regeneration of the positive and negative charges at PrFMN, the Glu277, Arg173H$^+$ and Gln190 residues, the end-product cluster (Prod) is more stable at $\varepsilon = 78$ than at $\varepsilon = 1$.
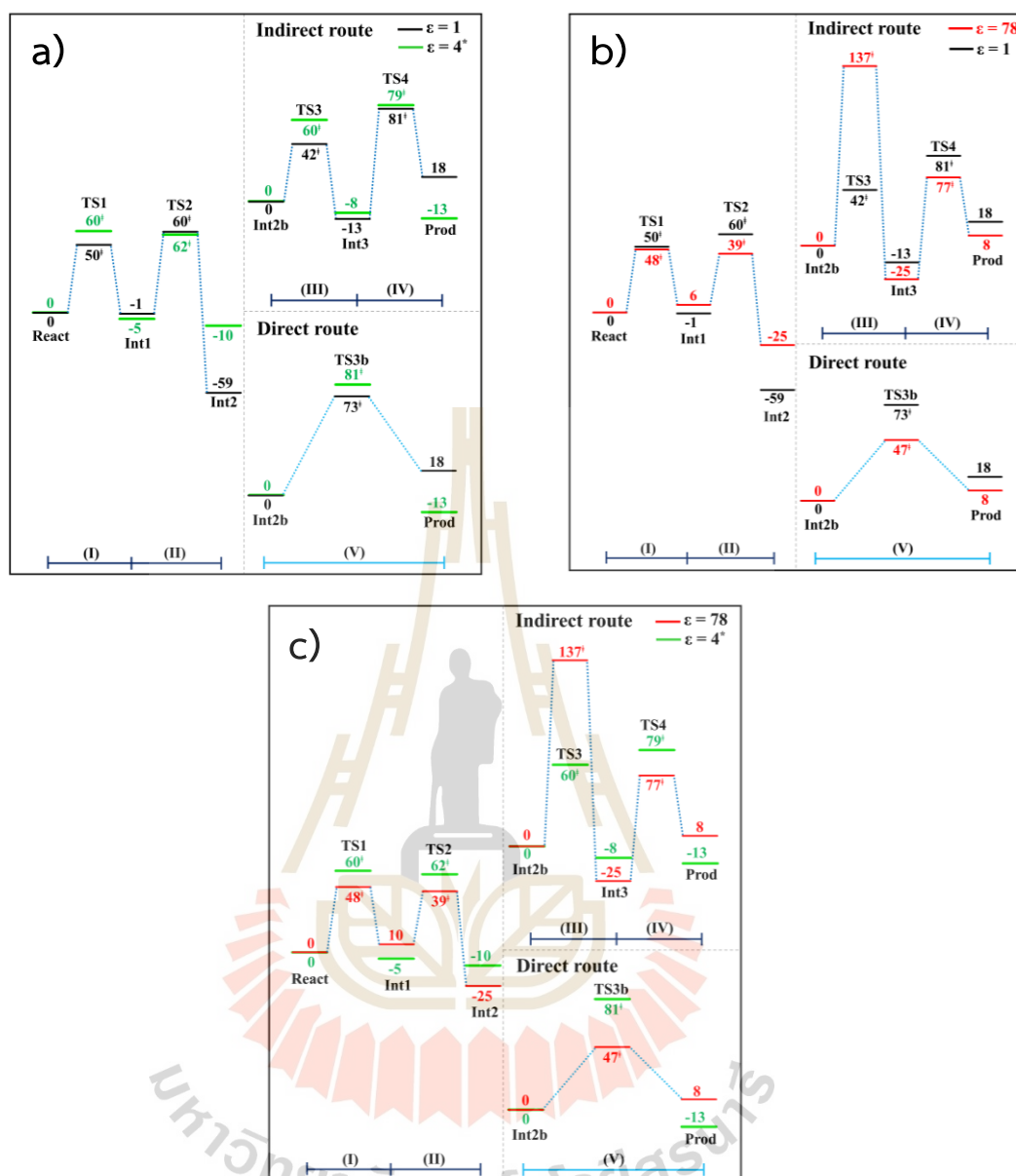
Figure 4.6 Potential energy profiles for enzymatic decarboxylation of α,β-unsaturated acid. Energy barriers are in kJ/mol. (I) = 1,3-dipolar cycloaddition; (II) = decarboxylation; (III) = acid catalyst (1); (IV) = cycloelimination; (V) = acid catalyst (2). a) The B3LYP/DZP results in ε = 1 (black solid lines) compared with those obtained using the B3LYP/6-311+G(2d,2p)//6-31G(d,p) and CPCM methods (ε = 4) reported by Lan and Chen (2016) (green solid lines). b) The B3LYP/DZP results in ε = 1 and 78 (black and red solid lines, respectively). c) The B3LYP/DZP results in ε = 78 compared with those obtained using the B3LYP/6-311+G(2d,2p)//6-31G(d,p) and CPCM methods (ε = 4) reported by Lan and Chen (2016) (red and green solid lines, respectively).

4.4 Kinetics and thermodynamics of the elementary reactions

All the kinetic and thermodynamic results at $\varepsilon = 1$ and 78 that were obtained based on the TST method are presented in Tables 4.3 and 4.4, respectively. The emphasis will be on the results at 277 K in Tables A5.1 and A5.2, which is the temperature at which the stopped-flow spectrophotometric experiment (Kaneshiro et al., 2020) was performed. Comparison of the rate constants that were obtained using different methods reveals considerable differences only for $k_{f/r}^{Class}$. This confirms that for large biological molecules, at least the zero-point vibrational energies must be included in TST calculations. The values for $T_c = 3-123$ K suggest a low/no quantum mechanical tunneling effect in the studied temperature range. At $\varepsilon = 1$, $k_{f/r}^{Q-vib}$, $k_{f/r}^{S-Wig}$ and $k_{f/r}^{F-Wig}$ are almost the same over the temperature range of 200-371 K. At $\varepsilon = 78$, $k_{f/r}^{Q-vib}$, $k_{f/r}^{S-Wig}$ and $k_{f/r}^{F-Wig}$ are approximately the same, except for 1,3-dipolar cycloaddition (I) and acid catalyst (1) (III), for which $k_{f/r}^{S-Wig}$ and $k_{f/r}^{F-Wig}$ are slightly higher than $k_{f/r}^{Q-vib}$ at low temperatures. Therefore, further discussion focuses only on $k_{f/r}^{S-Wig}$.

Analysis of k_f^{S-Wig} at 277 K confirms that the fluctuation of the local dielectric environment must be included in the mechanistic model; otherwise, some of the hypothesized elementary reactions are too slow to be monitored in the stopped-flow spectroscopic experiment. For example, decarboxylation (II) ($Int1^\varepsilon \rightarrow TS2^\varepsilon \rightarrow Int2^\varepsilon$) is kinetically favorable at $\varepsilon = 78$, with $k_f^{S-Wig,\varepsilon} = 1.21 \times 10^{10}$ s^{-1}, whereas at $\varepsilon = 1$, $k_f^{S-Wig} = 1.26 \times 10^{-2}$ s^{-1}. In contrast, for acid catalyst (1) (III) at $\varepsilon = 78$ ($Int2b^\varepsilon \rightarrow TS3^\varepsilon \rightarrow Int3^\varepsilon$), $k_f^{S-Wig,\varepsilon} = 9.60 \times 10^{-14}$ s^{-1}, whereas for the same reaction at $\varepsilon = 1$ ($Int2b \rightarrow TS3 \rightarrow Int3$), $k_f^{S-Wig} = 1.71 \times 10^8$ s^{-1}, which indicates that acid catalyst (1) (III) is kinetically favorable in a low local dielectric environment. This is in accordance with our previous work (Bua-ngern et al., 2016; Thisuwan et al., 2021; Suwannakham and Sagarik, 2017), in which the fluctuation of the local dielectric environment was confirmed to govern the kinetics of proton transfer processes; based on this analysis, React$\rightarrow$TS1$\rightarrow$Int1 (1,3-dipolar cycloaddition (I)) is kinetically more favorable than React$^\varepsilon \rightarrow$TS1$^\varepsilon \rightarrow$Int1$^\varepsilon$ ($k_f^{S-Wig} = 3.44 \times 10^3$ and $k_f^{S-Wig,\varepsilon} = 2.44 \times 10^3$ s^{-1}, respectively).

Table 4.3 Thermodynamics and kinetics of the elementary reactions of the enzymatic decarboxylation of α,β-unsaturated acid in $\varepsilon = 1$ at 277 K. Rate constants, temperatures and energies are in s^{-1}, K and kJ/mol, respectively; $\Delta E^{\ddagger}$ = energy barriers; $\Delta E^{\ddagger,ZPE}$ = difference between $E^{\ddagger,ZPE}$ of the transition structure and precursor; $\Delta E^{\ddagger,ZPC}$ = zero point energy-corrected energy barrier; $\Delta H^{\ddagger}$ = activation enthalpy; T_c = crossover temperature; T = temperature; $k_{f/r}^{S-Wig}$ = rate constant obtained with quantized vibrations and quantum mechanical tunneling through the simplified Wigner correction to the second order; $k_{f/r}^{Arr}$ = Arrhenius rate constant; $\Delta G^{\ddagger}$ = activation free energies; $\Delta S^{\ddagger}$ = activation entropy; f/r = forward or reverse direction.

Elementary reaction ($\varepsilon = 1$)	$\Delta E^{\ddagger}$	$\Delta E^{\ddagger,ZPE}$	$\Delta E^{\ddagger,ZPC}$	$\Delta H^{\ddagger}$	T_c	$k_{f/r}^{S-Wig}$	$k_{f/r}^{Arr}$	$\Delta G^{\ddagger}$	$\Delta S^{\ddagger}$
1,3-dipolar cycloaddition (React → TS1)	50.0	6.1	56.1	58.2	3	3.44×10^3	2.75×10^2	49.0	3.3×10^{-2}
1,3-dipolar cycloaddition (React ← TS1)	51.0	-9.3	41.7	58.0	3	4.77×10^8	3.72×10^5	32.4	9.2×10^{-2}
Decarboxylation (Int1 → TS2)	60.2	-5.0	55.2	56.1	4	1.26×10^{-2}	1.02×10^{-3}	77.8	-7.8×10^{-2}
Decarboxylation (Int1 ← TS2)	118.3	7.9	126.2	119.8	4	2.49×10^{-18}	1.91×10^{-19}	161.2	-1.5×10^{-1}
Acid catalyst (1) (Int2b → TS3)	42.4	7.2	49.6	46.9	15	1.71×10^8	1.37×10^7	24.1	8.2×10^{-2}
Acid catalyst (1) (Int2b ← TS3)	55.2	-2.9	52.3	53.9	15	1.29×10^{11}	1.05×10^{10}	8.8	1.6×10^{-1}
Cycloelimination (Int3 → TS4)	81.0	-11.5	69.5	75.2	7	1.31×10^2	1.06×10^1	56.5	6.8×10^{-2}
Cycloelimination (Int3 ← TS4)	50.2	3.5	53.7	52.8	7	1.46×10^1	1.16×10^0	61.6	-3.2×10^{-2}
Acid catalyst (2) (Int2b → TS3)	72.9	-7.5	65.4	71.0	31	6.86×10^{10}	5.47×10^9	10.3	2.2×10^{-1}
Acid catalyst (2) (Int2b ← TS3)	54.7	-2.3	52.4	55.8	31	5.27×10^{10}	4.22×10^9	10.9	1.6×10^{-1}

Table 4.4 Thermodynamics and kinetics of the elementary reactions of the enzymatic decarboxylation of α,β-unsaturated acid in ε = 78 at 277 K. Rate constants, temperatures and energies are in s^{-1}, K and kJ/mol, respectively; $\Delta E^{\ddagger}$ = energy barriers; $\Delta E^{\ddagger,ZPE}$ = difference between $E^{\ddagger,ZPE}$ of the transition structure and precursor; $\Delta E^{\ddagger,ZPC}$ = zero point energy-corrected energy barrier; $\Delta H^{\ddagger}$ = activation enthalpy; T_c = crossover temperature; T = temperature; $k_{f/r}^{S-Wig}$ = rate constant obtained with quantized vibrations and quantum mechanical tunneling through the simplified Wigner correction to the second order; $k_{f/r}^{Arr}$ = Arrhenius rate constant; $\Delta G^{\ddagger}$ = activation free energies; $\Delta S^{\ddagger}$ = activation entropy; f/r = forward or reverse direction.

Elementary reaction (ε = 78)	$\Delta E^{\ddagger,\varepsilon}$	$\Delta E^{\ddagger,ZPE,\varepsilon}$	$\Delta E^{\ddagger,ZPC,\varepsilon}$	$\Delta H^{\ddagger,\varepsilon}$	T_c	$k_{f/r}^{S-Wig,\varepsilon}$	$k_{f/r}^{Arr,\varepsilon}$	$\Delta G^{\ddagger,\varepsilon}$	$\Delta S^{\ddagger,\varepsilon}$
1,3-dipolar cycloaddition (React$^{\varepsilon}$ → TS1$^{\varepsilon}$)	48.0	-0.4	47.6	48.0	123	2.44×10^{3}	1.50×10^{2}	50.4	-8.7×10^{-3}
1,3-dipolar cycloaddition (React$^{\varepsilon}$ ← TS1$^{\varepsilon}$)	43.8	-0.3	43.5	43.8	43	8.14×10^{3}	6.28×10^{2}	47.1	-1.2×10^{-2}
Decarboxylation (Int1$^{\varepsilon}$ → TS2$^{\varepsilon}$)	38.8	-14.7	24.1	31.7	44	1.21×10^{10}	9.63×10^{8}	14.3	6.3×10^{-2}
Decarboxylation (Int1$^{\varepsilon}$ ← TS2$^{\varepsilon}$)	69.3	5.9	75.2	75.0	44	5.12×10^{-5}	3.94×10^{-6}	90.6	-5.6×10^{-2}
Acid catalyst (1) (Int2b$^{\varepsilon}$ → TS3$^{\varepsilon}$)	136.6	-7.4	129.2	127.9	61	9.60×10^{-14}	7.00×10^{-15}	137.0	-3.3×10^{-2}
Acid catalyst (1) (Int2b$^{\varepsilon}$ ← TS3$^{\varepsilon}$)	161.7	-22.1	139.6	142.5	61	2.29×10^{-15}	1.60×10^{-16}	145.7	-1.2×10^{-2}
Cycloelimination (Int3$^{\varepsilon}$ → TS4$^{\varepsilon}$)	77.4	-10.0	67.4	69.8	51	5.34×10^{-1}	4.09×10^{-2}	69.3	1.8×10^{-3}
Cycloelimination (Int3$^{\varepsilon}$ ← TS4$^{\varepsilon}$)	44.3	6.9	51.2	47.3	51	2.09×10^{-1}	1.57×10^{-2}	71.5	-8.7×10^{-2}
Acid catalyst (2) (Int2b$^{\varepsilon}$ → TS3$^{\varepsilon}$)	46.6	-5.2	41.4	44.5	55	4.53×10^{6}	3.41×10^{5}	32.6	4.3×10^{-2}
Acid catalyst (2) (Int2b$^{\varepsilon}$ ← TS3$^{\varepsilon}$)	38.1	-1.7	36.4	37.3	55	7.31×10^{5}	5.50×10^{4}	36.8	1.8×10^{-3}

Attempt was made to correlate the rate constants obtained from the TST method with the experimental data (Kaneshiro et al., 2020). Because the experiments on enzyme kinetics are complex due to several factors, such as experimental conditions (e.g., temperature, pH and ionic strength), sensitivity of the spectroscopic equipment and measurement timescale (time resolution), it is not straightforward to compare our theoretical results with the experimental data. In this work, the Arrhenius rate constants (k^{Arr}) were calculated in terms of $\Delta G^{\ddagger}$, which were obtained from the TST method (Tables A5.1 and A5.2), using $k^{Arr} = Ae^{-\Delta G^{\ddagger}/k_B T}$.

Because the pre-exponential constant (A) in the Arrhenius equation is not known for this enzyme system, the value was tentatively approximated using the highest rate constants ($\sim 10^{11}$ s^{-1}) with low $\Delta G^{\ddagger}$. Investigation of Tables A5.1 and A5.2 revealed that the highest rate constants at 277 and 300 K are $k_{f/r}^{S\text{-}Wig} = 7.56 \times 10^{11}$, 7.02×10^{11}, 3.28×10^{11} and 1.29×10^{11} s^{-1}, and the average value is 4.79×10^{11} s^{-1}. Based on this approximated pre-exponential constant and the values of $\Delta G^{\ddagger}$, $k_{f/r}^{Arr}$ were computed and included in Tables 4.3 and 4.4.

To correlate k_f^{Arr} and $k_f^{Arr,e}$ with the experimental rate constants (Kaneshiro et al., 2020), the elementary reactions that occur within the time resolution of stopped-flow spectrophotometry ($\sim 10^{-3}$ s) are considered. Based on the assumption that the two active sites on FDC1 react with different rates (denoted (a) and (b) for the fast and slow sites, respectively), the stopped-flow spectrophotometric results at 277 K and the half-of-sites model suggested that for the fast site (a), the PrFMN^{iminium}-cinnamic acid cycloadduct is formed with $k_{1(a)} = 131$ s^{-1} and is converted to the PrFMN^{iminium}—styrene cycloadduct with $k_{2(a)} = 75$ s^{-1}. However, cycloelimination to generate the styrene product and free FDC1 appeared to be the slowest process, with $k_{cat} = 11$ s^{-1}. Because the observed rete constants were reported to be in the range of $k_{obs} = 0.75\text{-}2.0 \times 10^{2}$ s^{-1}, only the elementary reactions with k_f^{Arr} larger than k_{obs} are included in the proposed mechanism. Based on the analysis of all the rate constants (k_f^{Arr} and $k_f^{Arr,\varepsilon}$) and activation free energies ($\Delta G^{\ddagger}$) in Tables 4.3 and 4.4, the kinetically controlled paths for the enzymatic decarboxylation of α,β-unsaturated acid (long rightwards blue arrows) are proposed in Figure 4.7.
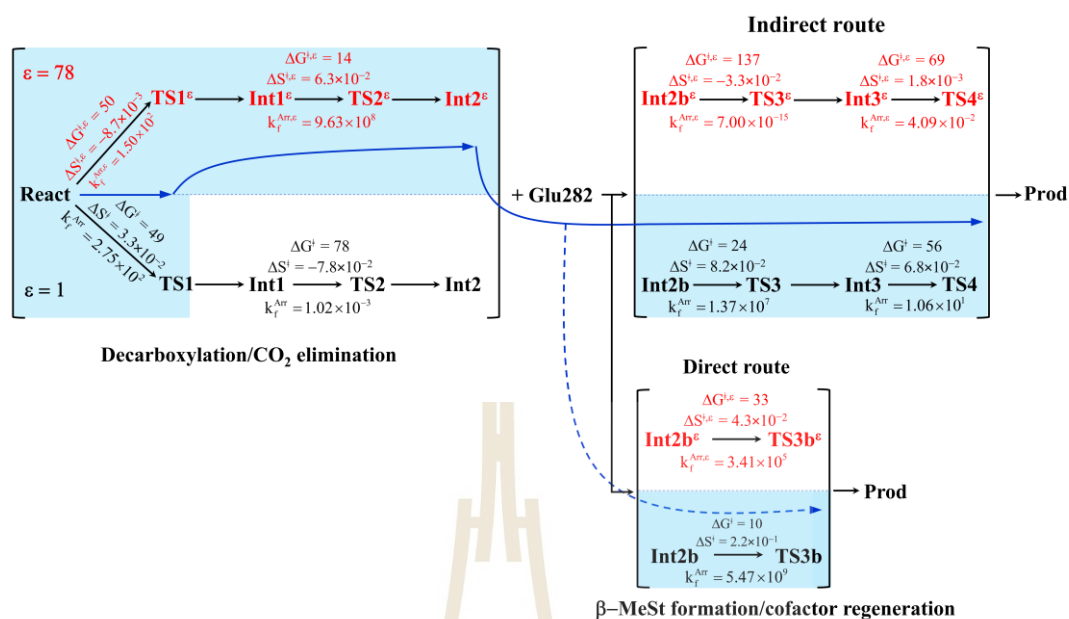
Figure 4.7 The kinetically controlled paths (long rightwards blue arrows) for the enzymatic decarboxylation of α,β-unsaturated acid at 277 K, proposed based on the potential energy profiles (Figure 4.6), Arrhenius rate constants (k_f^{Arr} and $k_f^{Arr,\varepsilon}$) and activation free energies ($\Delta G^{\ddagger}$ and $\Delta G^{\ddagger,\varepsilon}$) obtained from the TST method. Energies and rate constants are in kJ/mol and s^{-1}, respectively. Long rightwards blue dashed line arrow is an alternative kinetically controlled path, which is too fast to be monitored using the stopped-flow spectroscopic method.

Comparison of the rate constants of the proposed elementary reactions (long rightwards blue arrows in Figure 4.7) with those that were obtained in the experiment suggests that within the time resolution of stopped-flow spectrophotometry, k_f^{Arr} of 1,3-dipolar cycloaddition (I) is compatible (associated) with $k_{1(a)}$; for $React^{\varepsilon} \rightarrow TS1^{\varepsilon} \rightarrow Int1^{\varepsilon}$ and $React \rightarrow TS1 \rightarrow Int1$, $k_f^{Arr,e} = 1.50 \times 10^2$ and $k_f^{Arr} = 2.75 \times 10^2$ s^{-1} at $\varepsilon = 78$ and 1, respectively. However, because decarboxylation (II) at $\varepsilon = 1$ is slower than the time resolution of stopped-flow spectrophotometry ($k_f^{Arr} = 1.02 \times 10^{-3}$ s^{-1}), decarboxylation (II) is likely to occur in a high local dielectric environment. Likewise, although the direct route for generating β−MeSt (acid catalyst (2) (V)) is kinetically very favorable ($k_f^{Arr,e} = 3.41 \times 10^5$ and $k_f^{Arr} = 5.47 \times 10^9$ s^{-1} at $\varepsilon = 78$ and 1, respectively), it is too fast to be monitored in the stopped-flow spectroscopic experiment. Because the indirect route at $\varepsilon = 1$ ($Int3 \rightarrow TS4 \rightarrow Prod$) is within the time resolution of stopped-flow

spectrophotometry (k_f^{Arr} = 1.06×10^1 s^{-1}), cycloelimination (IV), which includes β—MeSt formation and cofactor regeneration, could be the rate-determining step. This analysis is in accordance with the conclusion by Ferguson et al. (2016) and is in good agreement with the kinetics results reported by Kaneshiro et al. (2020), in which cycloelimination (IV) of the PrFMN^{iminium}—β—MeSt cycloadduct and diffusion from the active site represent the slowest processes, k_{cat} = 1.13×10^1 s^{-1}.

To examine whether the proposed kinetically controlled (favorable) mechanisms in Figure 4.7 (long rightward blue arrows) are also thermodynamically controlled, the standard free energy changes ($\Delta G°$ and $\Delta G°^{,ε}$) of each elementary reaction were calculated from the difference between the activation free energies ($\Delta G^‡$) in the forward and reverse directions. In addition, because the entropic effect has been suggested to play an important role in enzymatic reactions (Villà et al., 2000), an attempt was made to study the entropy changes of the system (the model molecular clusters); although several known and unknown factors contribute to the entropy change, e.g., the entropy change of the surrounding, we tentatively consider only the entropy change in the system. The standard entropy changes of each elementary reaction ($\Delta S°$ and $\Delta S°^{,ε}$) were computed in the studied temperature range (200—371 K). These thermodynamic data are listed in Tables A5.1 and A5.2, and the values at 277 K are presented in Figure 4.8.
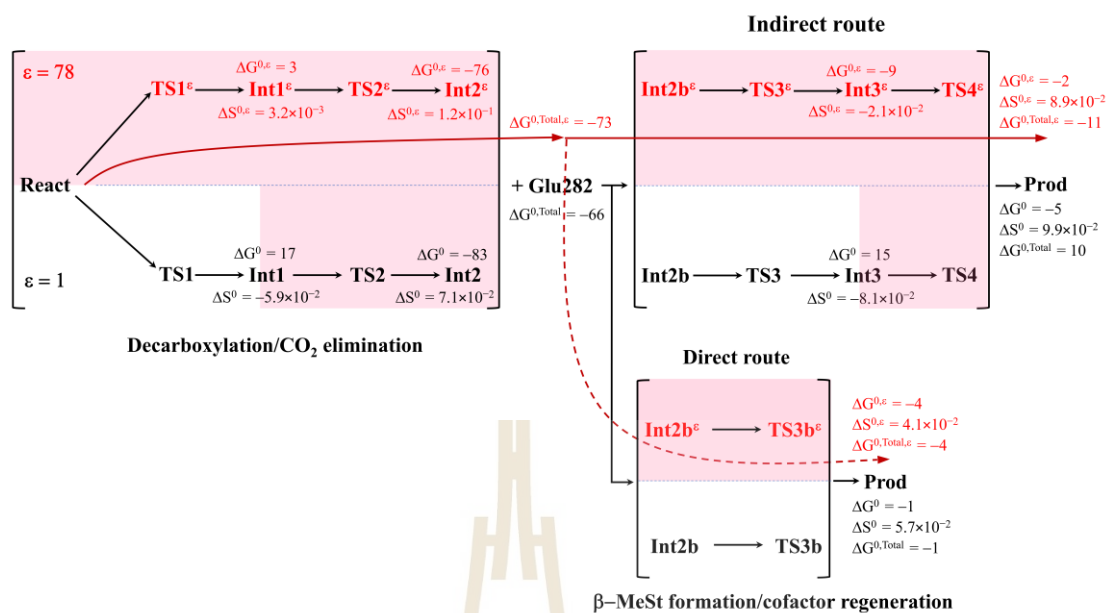
Figure 4.8 The thermodynamically controlled paths (long rightwards red arrows) for the enzymatic decarboxylation of α,β-unsaturated acid at 277 K, proposed based on the standard free energy ($\Delta G°$ and $\Delta G^{°,\varepsilon}$) and entropy ($\Delta S°$ and $\Delta S^{°,\varepsilon}$) changes of the elementary reactions. Energies are in kJ/mol. Long rightwards red dashed line arrow is an alternative thermodynamic controlled path.

The results reveal similar trends for $\Delta G°$ and $\Delta G^{°,\varepsilon}$ (Table 4.5), except for acid catalyst (1) (III), in which $\Delta G^{°,\varepsilon}$ is negative, whereas $\Delta G°$ is positive; at 277 K, $\Delta G°$ and $\Delta G^{°,\varepsilon}$ for 1,3-dipolar cycloaddition (I) are both positive, whereas those for decarboxylation (II), cycloelimination (IV) and acid catalyst (2) (V) are all negative. Analysis of the scenarios in the elementary reactions in Figures 4.1—4.5 suggests that at least three factors affect the standard free energy and entropy changes of the systems, namely, the disorder/order due to breaking/formation of covalent bonds, increase/decrease in the number of molecules, and charge (proton) transfer at the active site. For example, for 1,3-dipolar cycloaddition (I), $\Delta S°$ and $\Delta S^{°,\varepsilon}$ are only slightly changed due to the formation of the pyrrolidine cycloadduct, whereas the values for decarboxylation (II), cycloelimination (IV) and acid catalyst (2) (V) are all positive because these elementary reactions involve both net covalent bond breaking and an increase in the number of molecules in the active site, e.g., decarboxylation (II) involving $C_\alpha^{Cin}-C_{43}^{Cin}$ and $C_\beta^{Cin}-C_{34}^{PrFMN}$ covalent bond dissociations and formations of free CO_2 molecule.

Table 4.5 Standard free energies and entropies of the elementary reactions in $\varepsilon = 1$ and 78, obtained from TST calculations. Energies and temperatures are in kJ/mol and K, respectively. $\Delta G°$ and $\Delta G°^{,\varepsilon}$ = standard free energies; $\Delta S°$ and $\Delta S°^{,\varepsilon}$ = standard entropies.

Elementary reaction	T	$\Delta G°$	$\Delta G°^{,\varepsilon}$	$\Delta S°$	$\Delta S°^{,\varepsilon}$
1,3-dipolar cycloaddition (I)	200	15.7	3.4	-7.8×10^{-2}	3.0×10^{-3}
	277	16.6	3.3	-5.9×10^{-2}	3.3×10^{-3}
	300	16.9	3.3	-6.0×10^{-2}	3.0×10^{-3}
	371	18.1	3.0	-4.8×10^{-2}	3.2×10^{-3}
Decarboxylation (II)	200	-78.2	-67.5	7.2×10^{-2}	1.2×10^{-1}
	277	-83.4	-76.3	7.1×10^{-2}	1.2×10^{-1}
	300	-85.0	-79.0	7.1×10^{-2}	1.2×10^{-1}
	371	-90.1	-87.6	7.1×10^{-2}	1.2×10^{-1}
Acid catalyst (1) (III)	200	9.3	-10.0	-8.2×10^{-2}	-2.3×10^{-2}
	277	15.3	-8.6	-8.1×10^{-2}	-2.1×10^{-2}
	300	17.1	-8.1	-8.0×10^{-2}	-2.2×10^{-2}
	371	22.9	-6.5	-8.1×10^{-2}	-2.2×10^{-2}
Cycloelimination (IV)	200	2.3	4.4	1.0×10^{-1}	9.1×10^{-2}
	277	-5.1	-2.2	9.9×10^{-2}	8.9×10^{-2}
	300	-7.3	-4.2	9.9×10^{-2}	8.9×10^{-2}
	371	-14.4	-10.6	9.9×10^{-2}	8.9×10^{-2}
Acid catalyst (2) (V)	200	3.7	-1.1	5.8×10^{-2}	4.2×10^{-2}
	277	-0.6	-4.2	5.7×10^{-2}	4.1×10^{-2}
	300	-1.9	-5.1	5.7×10^{-2}	4.1×10^{-2}
	371	-6.0	-8.1	5.7×10^{-2}	4.1×10^{-2}

It appears that the entropy changes for the elementary reactions that generate molecules, e.g., decarboxylation (II) and cycloelimination (IV), are more pronounced than those for the reactions that involve only charge (proton) transfer, covalent bond breaking/formation and structural reorientation, e.g., 1,3-dipolar cycloaddition (I) and catalyst (1) (III) at $\varepsilon = 78$. Based on the total free energy changes ($\Delta G°^{,Total}$ and $\Delta G°^{,Total,\varepsilon}$

in Figure 4.8), the decarboxylation/CO_2 elimination reaction ((I) and (II)) at ε = 78 is slightly more favorable than at ε = 1 ($\Delta G^{\circ,Total,\varepsilon}$ = -73 and $\Delta G^{\circ,Total}$ = -66 kJ/mol). Likewise, the β—MeSt formation/cofactor regenerations in the indirect route ((III) and (IV)) at ε = 78 are significantly more favorable than at ε = 1, ($\Delta G^{\circ,Total,\varepsilon}$ = -11 and $\Delta G^{\circ,Total}$ = 10 kJ/mol). These results lead to the conclusion that elementary reactions that involve charge (proton) transfer favor a high local dielectric environment. The proposed thermodynamically favorable paths are illustrated in Figure 4.8 (long rightwards red arrows).

PCHAPTER V
CONCLUSIONS

Enzymatic decarboxylation of α,β-unsaturated acid through ferulic acid decarboxylase (FDC1) has been of interest because the reaction is anticipated to be a promising, environmentally friendly industrial process for producing styrene and its derivatives from natural resources. In this study, the proposed mechanisms for the enzymatic decarboxylation of α,β-unsaturated acid were theoretically studied using the B3LYP/DZP method and TST. The present study began with geometry optimizations of the proposed model molecular clusters in extreme local dielectric environments (ε = 1 and 78). The model molecular clusters consisted of the Cin substrate, PrFMN cofactor and all relevant residues of FDC1 at the active site. These moderate model molecular clusters made it possible to calculate kinetic and thermodynamic properties with reasonable computational resources.

Analysis of the B3LYP/DZP results showed that the active site structure and volume are not significantly changed in the enzymatic decarboxylation reaction, which suggested that the FDC1 backbone does not play the most important role in enzymatic decarboxylation processes. These findings are in accordance with the experimental result that the Glu277—Arg173—Glu282 residue network was conserved in the enzymatic decarboxylation reaction. These findings confirmed that the selected model molecular clusters (including the active site) are reasonable.

Comparison of the potential energy profiles that were obtained via the NEB method revealed similar energy barriers at ε = 1 and 4 (Lan and Chen, 2016), except for acid catalyst (1), for which $\Delta E^{\ddagger}$ at ε = 4 is higher than that at ε = 1, thereby implying that an increase in the local dielectric environment could result in a significant change in the energy barrier for the elementary reaction that involves proton transfer. The potential energy profiles at ε = 78 confirmed that the increase in the polarity of the solvent could lead to significant changes in $\Delta E^{\ddagger}$, especially for the transition states that involve charge (proton) transfer. Comparison of the rate constants that were obtained based on various methods revealed that the zero-point vibrational energies are important and cannot be neglected in TST calculations.

Although the values of the crossover temperatures suggested a low or no quantum mechanical tunneling effect on the enzymatic decarboxylation of α,β-unsaturated acid it is advisable to include this effect in the theoretical study on every enzymatic reaction

to assure that the effect can be neglected at least in the studied temperature range. Analysis of the rate constants at $\varepsilon = 1$ and 78 confirmed that the inclusion of the fluctuation of the local dielectric environment in the mechanistic model is essential; otherwise, some of the hypothesized elementary reactions are too slow to be monitored using the stopped-flow spectroscopic method. Because the rate constants at $\varepsilon = 1$ and 78 are not compatible with the time resolution of stopped-flow spectrophotometry, the direct route for generating Prod through acid catalyst (2) is unlikely to be utilized, whereas the cycloelimination that occurs in the indirect route in a low local dielectric environment is the rate determining step.

To examine the entropic effect and determine whether the proposed kinetically controlled (favorable) mechanisms are also thermodynamically controlled, the standard free energy and entropy changes of the elementary reactions were calculated. The results showed that at 277 K, the thermodynamic properties of the elementary reactions that involve charge (proton) transfer ((III) and (IV)) are strongly affected by a high local dielectric environment, which led to the conclusion that overall, the enzymatic decarboxylation of α,β-unsaturated acid is thermodynamically controlled in a high local dielectric environment. It appeared that the factors that affect the standard entropy changes are the disorder/order due to breaking/formation of covalent bonds and charge (proton) transfer in the active site; the standard entropy changes due to generation of molecules are the most significant (pronounced). The results that are reported in this work illustrate for the first time scenarios in each elementary reaction and provide insight into the effect of the local dielectric environment on the kinetics and thermodynamics of the enzymatic decarboxylation process of α,β-unsaturated acid, which could be used as guidelines for further theoretical and experimental studies on the same and similar systems.

REFERENCES

REFERENCES

Ahlrichs, R., Bär, M., Häser, M., Horn, H., and Kölmel, C. (1989). Electronic structure calculations on workstation computers: The program system turbomole. *Chemical Physics Letters*, *162*(3), 165-169.

Ásgeirsson, V., Birgisson, B. O., Bjornsson, R., Becker, U., Neese, F., Riplinger, C., and Jónsson, H. (2021). Nudged elastic band method for molecular reactions using energy-weighted springs combined with eigenvector following. *Journal of Chemical Theory and Computation*, *17*(8), 4929-4945.

Bailey, S. S., Payne, K. A., Fisher, K., Marshall, S. A., Cliff, M. J., Spiess, R., Parker, D. A., Rigby, S. E. J., and Leys, D. (2018). The role of conserved residues in Fdc decarboxylase in prenylated flavin mononucleotide oxidative maturation, cofactor isomerization, and catalysis. *Journal of Biological Chemistry*, *293*(7), 2272-2287.

Bailey, S. S., Payne, K. A., Saaret, A., Marshall, S. A., Gostimskaya, I., Kosov, I., Fisher, K., Hay, S., and Leys, D. (2019). Enzymatic control of cycloadduct conformation ensures reversible 1, 3-dipolar cycloaddition in a prFMN-dependent decarboxylase. *Nature Chemistry*, *11*(11), 1049-1057.

Bergonzo, C., Campbell, A. J., Walker, R. C., and Simmerling, C. (2009). A partial nudged elastic band implementation for use with large or explicitly solvated systems. *International Journal of Quantum Chemistry*, *109*(15), 3781-3790.

Bhuiya, M. W., Lee, S. G., Jez, J. M., and Yu, O. (2015). Structure and mechanism of ferulic acid decarboxylase (FDC1) from Saccharomyces cerevisiae. *Applied and Environmental Microbiology*, *81*(12), 4216-4223.

Boys, S. F., and Bernardi, F. J. M. P. (1970). The calculation of small molecular interactions by the differences of separate total energies. Some procedures with reduced errors. *Molecular Physics*, *19*(4), 553-566.

Cramer, C. J. (2013). Essentials of computational chemistry: theories and models. *John Wiley & Sons*.

Eyring, H. (1935). The activated complex in chemical reactions. *The Journal of Chemical Physics*, *3*(2), 107-115.

Ferguson, K. L., Arunrattanamook, N., and Marsh, E. N. G. (2016). Mechanism of the novel prenylated flavin-containing enzyme ferulic acid decarboxylase probed by isotope effects and linear free-energy relationships. *Biochemistry*. *55*(20), 2857-2863.

Ferguson, K. L., Eschweiler, J. D., Ruotolo, B. T., and Marsh, E. N. G. (2017). Evidence for a 1, 3-dipolar cyclo-addition mechanism in the decarboxylation of phenylacrylic acids catalyzed by ferulic acid decarboxylase. *Journal of the American Chemical Society*, *139*(32), 10972-10975.

Fermi, E. (1927). Statistical method to determine some properties of atoms. *Rendiconti lincei*, *6*, 602-607.

Furche, F., Ahlrichs, R., Hättig, C., Klopper, W., Sierka, M., and Weigend, F. (2014). Turbomole. *Wiley Interdisciplinary Reviews: Computational Molecular Science*, *4*(2), 91-100.

Ghoreishi, D., Cerutti, D. S., Fallon, Z., Simmerling, C., and Roitberg, A. E. (2019). Fast implementation of the nudged elastic band method in AMBER. *Journal of Chemical Theory and Computation*, *15*(8), 4699-4707.

Hänggi, P., Talkner, P., and Borkovec, M. (1990). Reaction-rate theory: fifty years after Kramers. *Reviews of Modern Physics*, *62*(2), 251.

Henkelman, G., Uberuaga, B. P., and Jónsson, H. (2000). A climbing image nudged elastic band method for finding saddle points and minimum energy paths. *The Journal of Chemical Physics*, *113*(22), 9901-9904.

Hohenberg, P., and Kohn, W. (1964). Inhomogeneous electron gas. *Physical review*, *136*(3B), B864.

House, J. E. (2007). Principles of chemical kinetics. *Academic Press*.

Kaneshiro, A. K., Koebke, K. J., Zhao, C., Ferguson, K. L., Ballou, D. P., Palfey, B. A., Ruotolo, B. T., and Marsh, E. N. G. (2020). Kinetic analysis of transient intermediates in the mechanism of prenyl-flavin-dependent ferulic acid decarboxylase. *Biochemistry*, *60*(2), 125-134.

Kästner, J., Carr, J. M., Keal, T. W., Thiel, W., Wander, A., and Sherwood, P. (2009). DL-FIND: an open-source geometry optimizer for atomistic simulations. *The Journal of Physical Chemistry A*, *113*(43), 11856-11865.

Kästner, J. (2014). Theory and simulation of atom tunneling in chemical reactions. *Wiley Interdisciplinary Reviews: Computational Molecular Science*, *4*(2), 158-168.

Klamt, A. (1995). Conductor-like screening model for real solvents: a new approach to the quantitative calculation of solvation phenomena. *The Journal of Physical Chemistry*, *99*(7), 2224-2235.

Klamt, A., and Jonas, V. (1996). Treatment of the outlying charge in continuum solvation models. *The Journal of Chemical Physics*, *105*(22), 9972-9981.

Kohn, W., and Sham, L. J. (1965). Self-consistent equations including exchange and correlation effects. *Physical review*, *140*(4A), A1133.

Laidler, K. J., and King, M. C. (1983). The development of transition-state theory. *Journal of Physical Chemistry*, *87*(15), 2657-2664.

Lan, C. L., and Chen, S. L. (2016). The decarboxylation of α,β-unsaturated acid catalyzed by prenylated FMN-dependent ferulic acid decarboxylase and the enzyme inhibition. *The Journal of Organic Chemistry*, *81*(19), 9289-9295.

Leys, D. (2018). Flavin metamorphosis: cofactor transformation through prenylation. *Current Opinion in Chemical Biology*, *47*, 117-125.

Lin, F., Ferguson, K. L., Boyer, D. R., Lin, X. N., and Marsh, E. N. G. (2015). Isofunctional enzymes PAD1 and UbiX catalyze formation of a novel cofactor required by ferulic acid decarboxylase and 4-hydroxy-3-polyprenylbenzoic acid decarboxylase. *ACS Chemical Biology*, *10*(4), 1137-1144.

Marshall, S. A., Fisher, K., Cheallaigh, A. N., White, M. D., Payne, K. A., Parker, D. A., Rigby, S. E. J., and Leys, D. (2017). Oxidative maturation and structural characterization of prenylated FMN binding by UbiD, a decarboxylase involved in bacterial ubiquinone biosynthesis. *Journal of Biological Chemistry*, *292*(11), 4623-4637.

McKenna, R., and Nielsen, D. R. (2011). Styrene biosynthesis from glucose by engineered E. coli. *Metabolic Engineering*, *13*(5), 544-554.

Metz, S., Kästner, J., Sokol, A. A., Keal, T. W., and Sherwood, P. (2014). ChemShell-a modular software package for QM/MM simulations. *Wiley Interdisciplinary Reviews: Computational Molecular Science*, *4*(2), 101-110.

Paduszyński, K., and Domańska, U. (2018). COSMO-RS screening for ionic liquid to be applied in extraction of 2-phenylethanol from aqueous solutions. *Journal of Molecular Liquids*, *271*, 305-312.

Payne, K. A., White, M. D., Fisher, K., Khara, B., Bailey, S. S., Parker, D., Rattray, N. J. W., Trivedi, D. K., Goodacre, R., Beveridge, R., Barran, P., Rigby, S. E. J., Scrutton, N. S., Hay, S., and Leys, D. (2015). New cofactor supports α,β-unsaturated acid decarboxylation via 1, 3-dipolar cycloaddition. *Nature*, *522*(7557), 497-501.

Plessow, P. (2013). Reaction path optimization without NEB springs or interpolation algorithms. *Journal of Chemical Theory and Computation*, *9*(3), 1305-1310.

Pollak, E., and Talkner, P. (2005). Reaction rate theory: What it was, where is it today, and where is it going?. *Chaos: An Interdisciplinary Journal of Nonlinear Science*, *15*(2).

Rangarajan, E. S., Li, Y., Iannuzzi, P., Tocilj, A., Hung, L. W., Matte, A., and Cygler, M. (2004). Crystal structure of a dodecameric FMN-dependent UbiX-like decarboxylase (Pad1) from Escherichia coli O157: H7. *Protein Science*, *13*(11), 3006-3016

Richard, P., Viljanen, K., and Penttilä, M. (2015). Overexpression of PAD1 and FDC1 results in significant cinnamic acid decarboxylase activity in Saccharomyces cerevisiae. *AMB Express*, *5*, 1-5.

Rooney, J. J. (1995). Eyring transition-state theory and kinetics in catalysis. *Journal of Molecular Catalysis A: Chemical*, *96*(1), L1-L3.

Smith, W., and Forester, T. R. (1996). ChemShell-amodular software package for QM/MM simulation. *Journal of Molecular Graphics and Modelling*, *14*, 136-141.

Steckel, J. A., and Sholl, D. (2009). Density functional theory. *A John Wiley & Sons*, Inc., Publication, Wiley, 1-33.

Thomas, L. H. (1927). The calculation of atomic fields. *Cambridge university press.*, *23*, 542-548.

Tian, G., and Liu, Y. (2017). Mechanistic insights into the catalytic reaction of ferulic acid decarboxylase from Aspergillus niger: a QM/MM study. *Physical Chemistry Chemical Physics*, *19*(11), 7733-7742.

Tomasi, J., Mennucci, B., and Cammi, R. (2005). Quantum mechanical continuum solvation models. *Chemical Reviews*, *105*(8), 2999-3094.

Truhlar, D. G., Garrett, B. C., and Klippenstein, S. J. (1996). Current status of transition-state theory. *The Journal of Physical Chemistry*, *100*(31), 12771-12800.

White, M. D., Payne, K. A., Fisher, K., Marshall, S. A., Parker, D., Rattray, N. J., Rattray, N. J. W., Trivedi, D. K., Goodacre, R., Rigby, S. E. J., Scrutton, N. S., Hay, S., and Leys, D. (2015). UbiX is a flavin prenyltransferase required for bacterial ubiquinone biosynthesis. *Nature*, *522*(7557), 502-506.

Wigner, E. (1932). On the quantum correction for thermodynamic equilibrium. *Physical Review*, *40*(5), 749.

Wigner, E. (1937). Calculation of the rate of elementary association reactions. *The Journal of Chemical Physics*, *5*(9), 720-725.

Wigner, E. (1938). The transition state method. *Transactions of the Faraday Society*, *34*, 29-41.

APPENDICES
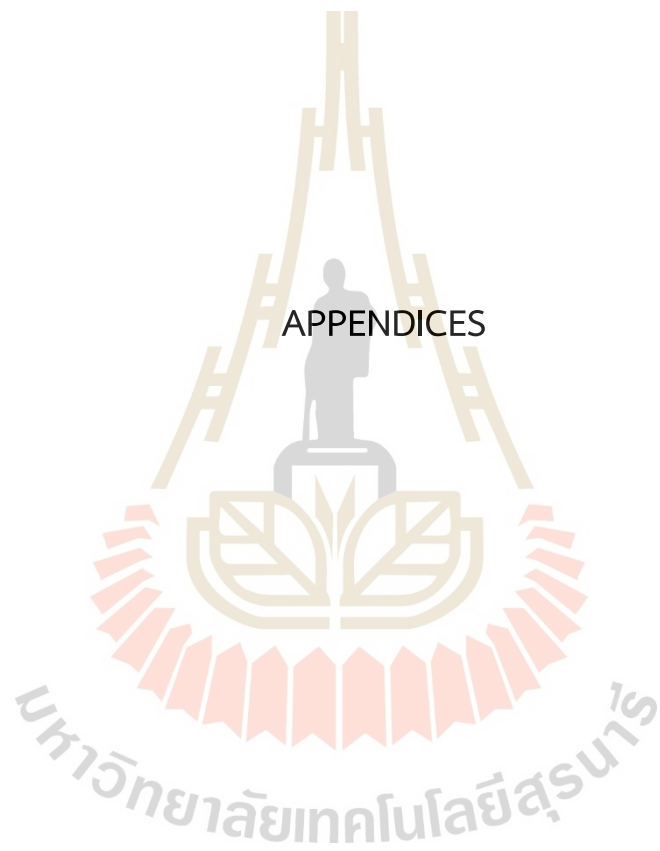
APPENDIX A
ADDITIONAL STATIC RESULTS

A1 The residue-to-residue distances (Å) on the potential energy curves obtained based on the B3LYP/DZP and NEB methods and their average values. The distances are approximated using the distances between the carbon atoms of the CH₃ groups substituting the atoms of the FDC1 backbone (Figure 1.1)

   Table A1.1 For elementary reactions (I)→(V) in ε = 1 and 78, respectively. The averages are made per elementary reaction.

   Table A1.2 The average residue-to-residue distances made per each model molecular cluster on the optimized reaction paths (I)→(II) and (III)→(V), in ε = 1 and 78, respectively. SD = standard deviation computed based on Equations (A1)─(A2); Structure number = structure on the optimized reaction path; * = transition structure.

   Table A1.3 An example for the calculations of the average residue-to-residue distances ($R_{C_R^{Arg173H^+}-C_R^{Glu277}}$ in Tables A1.1 and A1.2) and their SD, Equations (A1) and (A2), respectively.

Table A1.1

Elementary reaction ($\varepsilon = 1$)	Structure number	Distance (Å)			
		$R_{C_R^{Arg173H^+}-C_R^{Glu277}}$	$R_{C_R^{Arg173H^+}-C_R^{Gln190}}$	$R_{C_R^{Glu277}-C_R^{Gln190}}$	$R_{C_R^{Arg173H^+}-C_R^{Glu282}}$
	1	9.61	12.02	18.01	-
	2	9.73	11.85	17.83	-
	3	9.86	11.69	17.67	-
	4	9.90	11.43	17.40	-
	5	10.08	11.21	17.25	-
	6	10.28	11.00	17.13	-
1,3-dipolar	7	10.48	10.84	17.02	-
cycloaddition	8	10.65	10.74	16.89	-
(I)	9	10.76	10.70	16.78	-
	10*	10.81	10.71	16.78	-
	11	10.80	10.72	16.78	-
	12	10.79	10.77	16.84	-
	13	10.91	10.69	16.55	-
	14	11.01	10.56	16.23	-
Average±SD		10.41±0.48	11.07±0.49	17.08±0.50	-

Table A1.1 (Continued).

Elementary reaction ($\varepsilon = 1$)	Structure number	Distance (Å)			
		$R_{C_R}^{Arg173H^+}-C_R^{Glu277}$	$R_{C_R}^{Arg173H^+}-C_R^{Gln190}$	$R_{C_R}^{Glu277}-C_R^{Gln190}$	$R_{C_R}^{Arg173H^+}-C_R^{Glu282}$
	1	11.01	10.56	16.23	-
	2	11.00	10.74	16.01	-
	3	11.01	10.90	15.82	-
	4*	11.04	10.95	15.70	-
	5	11.07	10.87	15.78	-
	6	11.08	10.97	15.62	-
Decarboxylation	7	11.07	11.09	15.40	-
(II)	8	11.07	11.23	15.18	-
	9	11.05	11.32	15.01	-
	10	11.01	11.45	14.81	-
	11	10.96	11.59	14.58	-
	12	10.89	11.74	14.34	-
	13	10.81	10.88	14.10	-
	14	10.72	12.00	13.87	-
Average±SD		10.99±0.11	11.16±0.41	15.18±0.74	-

Table A1.1 (Continued).

Elementary reaction ($\varepsilon = 1$)	Structure number	Distance (Å)			
		$R_{C_R}^{Arg173H^+}$-C_R^{Glu277}	$R_{C_R}^{Arg173H^+}$-C_R^{Gln190}	$R_{C_R}^{Glu277}$-C_R^{Gln190}	$R_{C_R}^{Arg173H^+}$-C_R^{Glu282}
	1	10.86	11.79	10.23	7.61
	2	10.84	12.11	11.07	7.94
	3	10.82	12.41	11.51	8.06
	4*	10.81	12.59	11.74	8.07
	5	10.79	12.78	12.08	8.43
	6	10.78	12.98	12.83	8.76
Acid catalyst (1)	7	10.78	13.13	13.41	8.99
(III)	8	10.77	13.24	13.87	9.16
	9	10.76	13.33	14.26	9.31
	10	10.75	13.39	14.62	9.45
	11	10.74	13.45	14.98	9.61
	12	10.73	13.51	15.40	9.78
	13	10.73	13.60	15.93	9.97
	14	10.74	13.72	16.56	10.21
Average±SD		10.78±0.04	13.00±0.59	13.46±1.94	8.95±0.83

59

Table A1.1 (Continued).

Elementary reaction ($\varepsilon = 1$)	Structure number	Distance (Å)			
		$RC_R^{Arg173H^+}-C_R^{Glu277}$	$RC_R^{Arg173H^+}-C_R^{Gln190}$	$RC_R^{Glu277}-C_R^{Gln190}$	$RC_R^{Arg173H^+}-C_R^{Glu282}$
	1	10.74	13.72	16.56	10.21
	2	10.74	13.65	16.53	10.32
	3	10.74	13.63	16.52	10.34
	4*	10.73	13.63	16.52	10.34
	5	10.73	13.62	16.51	10.37
	6	10.73	13.57	16.50	10.48
Cycloelimination	7	10.72	13.52	16.48	10.57
(IV)	8	10.71	13.47	16.46	10.66
	9	10.69	13.42	16.43	10.73
	10	10.68	13.37	16.41	10.79
	11	10.66	13.33	16.39	10.82
	12	10.65	13.29	16.37	10.86
	13	10.63	13.24	16.35	10.90
	14	10.62	13.20	16.33	10.95
Average±SD		10.70±0.04	13.48±0.17	16.45±0.07	10.60±0.25

Table A1.1 (Continued).

Elementary reaction ($\varepsilon = 1$)	Structure number	Distance (Å)			
		$RC_R^{Arg173H^+}-C_R^{Glu277}$	$RC_R^{Arg173H^+}-C_R^{Gln190}$	$RC_R^{Glu277}-C_R^{Gln190}$	$RC_R^{Arg173H^+}-C_R^{Glu282}$
	1	10.86	11.79	10.23	7.61
	2	10.82	11.97	11.05	8.12
	3	10.81	12.15	11.68	8.53
	4*	10.80	12.25	11.85	8.66
	5	10.79	12.38	12.14	8.88
	6	10.78	12.54	12.84	9.29
Acid catalyst (2)	7	10.77	12.67	13.39	9.66
(V)	8	10.74	12.76	13.79	9.88
	9	10.71	12.85	14.21	10.04
	10	10.69	12.92	14.58	10.18
	11	10.67	12.97	14.91	10.31
	12	10.65	13.02	15.27	10.84
	13	10.63	13.10	15.73	10.70
	14	10.62	13.20	16.33	10.95
Average±SD		10.74±0.08	12.61±0.44	13.43±1.86	9.55±0.57

Table A1.2

Elementary reaction ($\varepsilon = 78$)	Structure number	Distance (Å)			
		$R_{C_R^{Arg173H^+}}$-C_R^{Glu277}	$R_{C_R^{Arg173H^+}}$-C_R^{Gln190}	$R_{C_R^{Glu277}}$-C_R^{Gln190}	$R_{C_R^{Arg173H^+}}$-C_R^{Glu282}
	1	9.63	12.02	18.02	-
	2	9.76	11.84	17.85	-
	3	9.86	11.62	17.61	-
	4	9.99	11.43	17.44	-
	5	10.13	11.25	17.30	-
1,3-dipolar	6	10.29	11.08	17.19	-
cycloaddition	7	10.47	10.92	17.06	-
(I)	8	10.62	10.80	16.93	-
	9	10.73	10.75	16.81	-
	10*	10.71	10.78	16.88	-
	11	10.72	10.78	16.85	-
	12	10.77	10.77	16.79	-
	13	10.92	10.66	16.49	-
	14	10.04	10.55	16.25	-
Average±SD		10.33±0.43	11.09±0.47	17.11±0.50	-

Table A1.2 (Continued).

Elementary reaction (ε = 78)	Structure number	Distance (Å)			
		$R_{C_R}^{Arg173H^+}$-C_R^{Glu277}	$R_{C_R}^{Arg173H^+}$-C_R^{Gln190}	$R_{C_R}^{Glu277}$-C_R^{Gln190}	$R_{C_R}^{Arg173H^+}$-C_R^{Glu282}
	1	10.04	10.55	16.23	-
	2	10.99	10.77	16.01	-
	3	10.98	10.91	15.86	-
	4	11.07	10.84	15.88	-
	5*	11.07	10.84	15.86	-
	6	11.09	10.83	15.78	-
Decarboxylation (II)	7	11.09	10.97	15.55	-
	8	11.11	11.13	15.31	-
	9	11.15	11.22	15.20	-
	10	11.14	11.36	15.01	-
	11	11.09	11.52	14.75	-
	12	10.98	10.71	14.26	-
	13	10.86	10.87	14.18	-
	14	10.74	12.01	13.89	-
Average±SD		10.96±0.29	11.04±0.38	15.27±0.75	-

Table A1.2 (Continued).

Elementary reaction ($\varepsilon = 78$)	Structure number	Distance (Å)			
		$RC_R^{Arg173H^+}-C_R^{Glu277}$	$RC_R^{Arg173H^+}-C_R^{Gln190}$	$RC_R^{Glu277}-C_R^{Gln190}$	$RC_R^{Arg173H^+}-C_R^{Glu282}$
	1	10.90	11.81	10.24	7.60
	2	10.86	12.12	11.00	7.94
	3	10.84	12.38	11.67	8.22
	4*	10.81	12.48	11.89	8.33
	5	10.80	12.67	12.39	8.59
	6	10.80	12.87	13.03	8.87
Acid catalyst (1)	7	10.78	13.01	13.55	9.08
(III)	8	10.76	13.12	14.01	9.26
	9	10.75	13.22	14.41	9.41
	10	10.74	13.30	14.78	9.56
	11	10.74	13.39	15.17	9.72
	12	10.74	13.48	15.59	9.89
	13	10.75	13.59	16.06	10.06
	14	10.77	13.71	16.58	10.27
Average±SD		10.79±0.05	12.94±0.58	13.60±1.96	9.06±0.83

Table A1.2 (Continued).

Elementary reaction ($\varepsilon = 78$)	Structure number	Distance (Å)			
		$R_{C_R^{Arg173H^+}-C_R^{Glu277}}$	$R_{C_R^{Arg173H^+}-C_R^{Gln190}}$	$R_{C_R^{Glu277}-C_R^{Gln190}}$	$R_{C_R^{Arg173H^+}-C_R^{Glu282}}$
	1	10.77	13.71	16.58	10.27
	2	10.79	13.63	16.56	10.37
	3*	10.79	13.61	16.54	10.32
	4	10.79	13.61	16.54	10.32
	5	10.79	13.59	16.54	10.36
	6	10.79	13.56	16.53	10.46
Cycloelimination	7	10.77	13.51	16.51	10.58
(IV)	8	10.76	13.46	16.48	10.67
	9	10.75	13.41	16.46	10.76
	10	10.74	13.37	16.43	10.84
	11	10.72	13.32	16.40	10.90
	12	10.70	13.28	16.38	10.96
	13	10.67	13.25	16.37	10.95
	14	10.65	13.20	16.35	10.97
Average±SD		10.75±0.05	13.47±0.16	16.48±0.08	10.62±0.27

Table A1.2 (Continued).

Elementary reaction ($\varepsilon = 78$)	Structure number	Distance (Å)			
		$RC_R^{Arg173H^+}-C_R^{Glu277}$	$RC_R^{Arg173H^+}-C_R^{Gln190}$	$RC_R^{Glu277}-C_R^{Gln190}$	$RC_R^{Arg173H^+}-C_R^{Glu282}$
	1	10.90	11.81	10.24	7.60
	2	10.85	12.03	10.97	8.10
	3*	10.86	12.02	10.81	8.00
	4	10.83	12.18	11.53	8.48
	5	10.82	12.35	12.13	8.8
	6	10.80	12.51	12.79	9.30
Acid catalyst (2) (V)	7	10.79	12.63	13.36	9.68
	8	10.76	12.73	13.80	9.92
	9	10.74	12.82	14.22	10.09
	10	10.73	12.89	14.61	10.25
	11	10.72	12.95	14.98	10.40
	12	10.70	13.01	15.34	10.58
	13	10.68	13.10	15.80	10.80
	14	10.65	13.20	16.34	10.97
Average±SD		10.77±0.07	12.59±0.45	13.35±1.98	9.50±1.12

Table A1.3

Elementary reaction ($\varepsilon = 1$)	Structure number	Distance (Å)		
		$RC_R^{Arg173H^+}\text{-}C_R^{Glu277}$	$RC_R^{Arg173H^+}\text{-}C_R^{Gln190}$	$RC_R^{Arg173H^+}\text{-}C_R^{Glu282}$
	1	10.31±0.99	11.29±1.03	-
	2	10.37±0.90	11.30±0.78	-
	3	10.44±0.81	11.30±0.56	-
	4	10.47±0.81	11.19±0.34	-
	5	10.58±0.70	11.04±0.24	-
	6	10.68±0.57	10.99±0.02	-
	7	10.78±0.42	10.97±0.18	-
(I)→(II)	8	10.86±0.30	10.99±0.35	-
	9	10.91±0.21	11.01±0.44	-
	10	10.91±0.14	11.08±0.52	-
	11	10.88±0.11	11.16±0.62	-
	12	10.84±0.07	11.26±0.69	-
	13	10.86±0.07	10.79±0.13	-
	14	10.87±0.21	11.28±1.02	-

67

Table A1.3 (Continued).

Elementary reaction ($\varepsilon = 1$)	Structure number	Distance (Å)		
		$R_{C_R^{Arg173H^+}-C_R^{Glu277}}$	$R_{C_R^{Arg173H^+}-C_R^{Gln190}}$	$R_{C_R^{Arg173H^+}-C_R^{Glu282}}$
	1	10.82±0.07	12.43±1.11	8.48±1.50
	2	10.80±0.05	12.58±0.93	8.79±1.33
	3	10.79±0.04	12.73±0.79	8.98±1.20
	4	10.78±0.04	12.82±0.72	9.02±1.18
	5	10.77±0.03	12.93±0.63	9.23±1.02
	6	10.76±0.03	13.03±0.52	9.51±0.88
	7	10.76±0.03	13.11±0.43	9.74±0.79
(III)⟶(V)	8	10.74±0.03	13.16±0.36	9.90±0.75
	9	10.72±0.04	13.20±0.31	10.03±0.71
	10	10.71±0.04	13.23±0.27	10.14±0.67
	11	10.69±0.04	13.25±0.25	10.25±0.61
	12	10.68±0.05	13.27±0.25	10.49±0.62
	13	10.66±0.06	13.31±0.26	10.52±0.49
	14	10.66±0.07	13.37±0.36	10.70±0.43

Table A1.3 (Continued).

Elementary reaction ($\varepsilon = 78$)	Structure number	Distance (Å)		
		$RC_R^{Arg173H^+}-C_R^{Glu277}$	$RC_R^{Arg173H^+}-C_R^{Gln190}$	$RC_R^{Arg173H^+}-C_R^{Glu282}$
(I)→(II)	1	9.84±0.29	11.29±1.04	-
	2	10.38±0.87	11.31±0.76	-
	3	10.42±0.79	11.27±0.50	-
	4	10.53±0.76	11.14±0.42	-
	5	10.60±0.66	11.05±0.29	-
	6	10.69±0.57	10.96±0.18	-
	7	10.78±0.44	10.95±0.04	-
	8	10.87±0.35	10.97±0.23	-
	9	10.94±0.30	10.99±0.33	-
	10	10.93±0.30	11.07±0.41	-
	11	10.91±0.26	11.15±0.52	-
	12	10.88±0.15	10.74±0.04	-
	13	10.89±0.04	10.77±0.15	-
	14	10.39±0.49	11.28±1.03	-

Table A1.3 (Continued).

Elementary reaction (ε = 78)	Structure number	Distance (Å)		
		$RC_R^{Arg173H^+}-C_R^{Glu277}$	$RC_R^{Arg173H^+}-C_R^{Gln190}$	$RC_R^{Arg173H^+}-C_R^{Glu282}$
	1	10.86±0.08	12.44±1.10	8.49±1.54
	2	10.83±0.04	12.59±0.90	8.80±1.36
	3	10.83±0.04	12.67±0.83	8.85±1.28
	4	10.81±0.02	12.76±0.75	9.04±1.11
	5	10.80±0.02	12.87±0.64	9.25±0.97
	6	10.80±0.01	12.98±0.53	9.54±0.82
	7	10.78±0.01	13.05±0.44	9.78±0.75
(III)→(V)	8	10.76±0.00	13.10±0.37	9.95±0.71
	9	10.75±0.01	13.15±0.30	10.09±0.68
	10	10.74±0.01	13.19±0.26	10.22±0.64
	11	10.73±0.01	13.22±0.24	10.34±0.59
	12	10.71±0.02	13.26±0.24	10.48±0.54
	13	10.70±0.04	13.31±0.25	10.60±0.48
	14	10.69±0.07	13.37±0.29	10.74±0.40

A2 An example for the calculations of the average residue-to-residue distances ($R_{C_R^{Arg173H^+}-C_R^{Glu277}}$ in Tables A1.1 and A.13) and their SD, Equations (A1) and (A2), respectively

$$\overline{R}_{C_R^{Arg173H^+}-C_R^{Glu277}} = \frac{\sum_{i=1}^{n}(R_{C_R^{Arg173H^+}-C_R^{Glu277}})_i}{n} \tag{A1}$$

$$SD = \sqrt{\frac{\sum_{i=1}^{n}[(R_{C_R^{Arg173H^+}-C_R^{Glu277}})_i - (\overline{R}_{C_R^{Arg173H^+}-C_R^{Glu277}})]^2}{n-1}} \tag{A2}$$

For the average residue-to-residue distances made per elementary reaction, n = 14, whereas those made per each model molecular clusters on the NEB potential energy curves, n = 2 for (I)→(II) and n = 3 for (III)→(V).
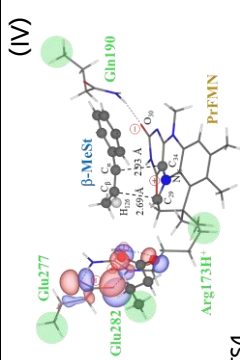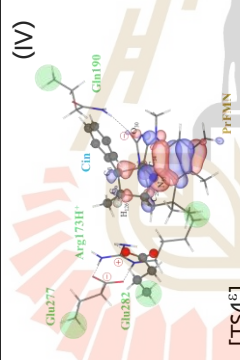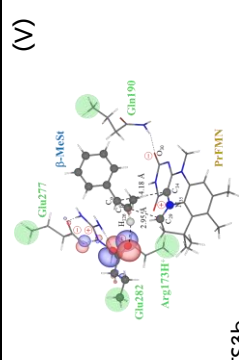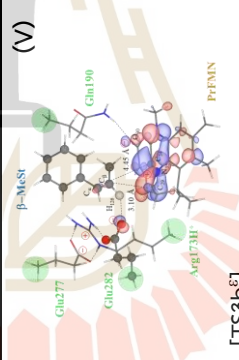
A3 Transition structures, total energies in $\varepsilon = 1$ and 78

Table A3 Transition structures, total energies in $\varepsilon = 1$ and 78 (E^{Total} and $E^{Total,\varepsilon}$, respectively) and solvation energies (ΔE^{Solv}) on the potential energy curves, obtained from the B3LYP/DZP and NEB methods. Spheres are the CH_3 groups substituting backbone atoms of the FDC1 enzyme. E^{Total} and $E^{Total,\varepsilon}$ are in au and ΔE^{Solv} in kJ/mol. [...] = values obtained in $\varepsilon = 78$.

Table A3

Model molecular cluster ε = 1		E^{Total}	Model molecular cluster ε = 78		E^{Total}	ΔE^{Solv}	R
TS1	(I)	−2561.014226	(I) [TS1ε']		[−2561.107670]	−257.3	(1) $R_{C_{\beta}^{Cin}-C_{34}^{PrFMN}} = 3.30\ [3.19]$ (2) $R_{C_{\alpha}^{Cin}-C_{29}^{PrFMN}} = 2.78\ [2.77]$ (3) $R_{C_{\alpha}^{Cin}-C_{43}^{Cin}} = 1.54\ [1.53]$
TS2	(II)	−2561.010601	(II) [TS2ε']		[−2561.108935]	−242.1	(1) $R_{C_{\beta}^{Cin}-C_{34}^{PrFMN}} = 1.74\ [3.02]$ (2) $R_{C_{\alpha}^{Cin}-C_{29}^{PrFMN}} = 1.54\ [1.53]$ (3) $R_{C_{\alpha}^{Cin}-C_{43}^{Cin}} = 1.62\ [2.97]$
TS3	(III)	−2680.059418	(III) [TS3ε']		[−2680.107193]	−222.2	(1) $R_{C_{\beta}^{Cin}-C_{34}^{PrFMN}} = 1.64\ [2.31]$ (2) $R_{C_{\alpha}^{Cin}-C_{29}^{PrFMN}} = 1.53\ [1.55]$ (3) $R_{C_{\alpha}^{Cin}-H_{126}^{Glu282}} = 1.10\ [1.26]$ (4) $R_{O_{125}^{Glu282}-H_{126}^{Glu282}} = 1.99\ [1.66]$

Table A3 (Continued).

Model molecular cluster $\varepsilon = 1$	E^{Total}	Model molecular cluster $\varepsilon = 78$	E^{Total}	ΔE^{Solv}	R

(IV)

TS4

E^{Total} = -2680.049549

(IV)

[TS4$^{\varepsilon}$]

E^{Total} = [-2680.139404]

ΔE^{Solv} = -235.9

(1) $Rc_\beta^{Cin} \_C_{34}^{PrFMN} = 2.93\ [1.81]$
(2) $Rc_\alpha^{Cin} \_C_{29}^{PrFMN} = 2.69\ [1.68]$

(V)

TS3b

E^{Total} = -2680.047799

(V)

[TS3b$^{\varepsilon}$]

E^{Total} = [-2680.141673]

ΔE^{Solv} = -250.0

(1) $Rc_\beta^{Cin} \_C_{34}^{PrFMN} = 4.18\ [4.45]$
(2) $Rc_\alpha^{Cin} \_C_{29}^{PrFMN} = 2.95\ [3.10]$
(3) $Rc_\alpha^{Cin} \_H_{126}^{Glu282} = 1.12\ [1.11]$
(4) $Ro_{125}^{Glu282} \_H_{126}^{Glu282} = 1.88\ [2.05]$

A4 Example for the Calculations of the kinetic and thermodynamic properties (Extracted from ChemShell Output) for the rate determining elementary reaction Int3→TS4 in ε = 1

    A4.1 Model molecular cluster Int3

$E^{Total,Int3}$ = -2680.0803909669999 au

(Total energy of the equilibrium structure Int3)

Thermochemical analysis

Temperature: 300.00 Kelvin

total ZPE ($E^{ZPE,Int3}$)	1.0746681505 au
total E_vib ($E^{Vib,Int3}$)	0.0633498277 au
-T*S	-0.1421675356 au

total vibrational energy correction to E_electronic   0.9958504426 au

total ZPE ($E^{ZPE,Int3}$)	2821540.81983 J/mol
total E vib ($E^{Vib,Int3}$)	166324.94857 J/mol
total S vib ($S^{Vib,Int3}$)	1244.20270 J/mol/K

Crossover temperature for tunnelling   1.50197 K

Writing file qts_reactant.txt

Writing Hessian file qts_hessian_rs.txt

Vibrational adiabatic energy of Int3 ($E^{ZPC,Int3}$ in au)

$E^{ZPC,Int3}$ = $E^{Total,Int3}$ + $E^{ZPE,Int3}$

= -2680.0803909669999 au + 1.07466791273907 au

= -2679.0057230542500 au

A4.2 Model molecular cluster TS4

$E^{Total,Int3}$ = -2680.0495493439998 au

(Total energy of the equilibrium structure TS4)

Thermochemical analysis

Temperature: 300.00 Kelvin

total ZPE ($E^{ZPE,TS4}$)	1.0702864713 au
total E_vib ($E^{Vib,TS4}$)	0.0627030206 au
-T*S	-0.1386259552 au

total vibrational energy correction to E_electronic   0.9943635367 au

total ZPE ($E^{ZPE,TS4}$)	2810036.72294 J/mol
total E vib ($E^{Vib,TS4}$)	164626.75663 J/mol
total S vib ($S^{Vib,TS4}$)	1213.20798 J/mol/K

Crossover temperature for tunnelling   6.53993 K

Writing file qts_ts.txt

Writing Hessian file qts_hessian_ts.txt

Vibrational adiabatic energy of TS4 ($E^{ZPC,TS4}$ in au)

$E^{ZPC,TS4} = E^{Total,TS4} + E^{ZPE,TS4}$

   = -2680.0495493439998 au + 1.07028623457732 au

   = -2678.9792631094100 au

A4.3 Int3→TS4

Calculation of the reaction rate based on harmonic TST

Number of zero modes in RS and TS: 6   6

	Reactant	TS
Number of atoms	126	126
Degrees of freedom	378	378

	Hartree	kJ/mol	eV	K
Potential energy Barrier ($\Delta E^{\ddagger}$)	0.0308416	80.97466944	0.83924324	9739.0026515
ZPE Correction ($\Delta E^{\ddagger,ZPE}$)	-0.00436449	-11.45897673	-0.11876392	-1378.1964844
Vibrational adiabatic barrier ($\Delta E^{\ddagger,ZPC}$)	0.02647713	69.51569271	0.72047933	8360.8061671
Rotational contr. at start T	0.00000000	0.00000000	0.00000000	0.00000000

Crossover Temperature 6.53992787 K

log10 of rates in s^{-1}

Change of log(rate) by the rotational partition function 0.00000000

1000/T	rate classical	quantised vib.	simpl. Wigner	full Wigner
5.00	-4.285	-3.280	-3.280	-3.280
3.61	1.611	2.118	2.118	2.118
3.33	2.765	3.187	3.187	3.187
2.70	5.456	5.705	5.705	5.705

A4.4 Example

Potential energy Barrier ($\Delta E^{\ddagger}$)

$\Delta E^{\ddagger} = E^{Total,TS4} - E^{Total,Int3}$

    = -2680.0495493439998 au – (-2680.0803909669999 au)

    = 0.0308416230 au

    = 80.97466944 kJ/mol

ZPE Correction ($\Delta E^{\ddagger,ZPE}$)

$\Delta E^{\ddagger,ZPE} = E^{ZPE,TS4} - E^{ZPE,Int3}$

    = 2810036.72294 J/mol - 2821540.81983 J/mol

    = -11.45897673 kJ/mol

Vibrational adiabatic barrier ($\Delta E^{\ddagger,ZPC}$)

$\Delta E^{\ddagger,ZPC} = \Delta E^{\ddagger} + \Delta E^{\ddagger,ZPE}$

    = 80.97466944 kJ/mol + (-11.45897673 kJ/mol)

    = 69.51569271 kJ/mol

or

Vibrational adiabatic barrier ($\Delta E^{\ddagger,ZPC}$)

$\Delta E^{\ddagger,ZPC} = \Delta E^{\ddagger,ZPC,TS4} - \Delta E^{\ddagger,ZPC,Int3}$

$\qquad$ = (-2678.9792631094100 au) – (-2679.0057230542500 au)

$\qquad$ = 0.0264599448383 au

$\qquad$ = 69.51569271 kJ/mol

A5 Thermodynamics and kinetics tables of the elementary reactions of the enzymatic decarboxylation of α,β-unsaturated acid in ε = 1 and 78

Table A5.1 Thermodynamics and kinetics of the elementary reactions of the enzymatic decarboxylation of α,β-unsaturated acid in ε = 1. Rate constants, temperatures and energies are in s-1, K and kJ/mol, respectively; $\Delta E^{\ddagger}$ = energy barrier on the optimized reaction path; $\Delta E^{\ddagger,ZPE}$ = difference between $E^{\ddagger,ZPE}$ of the transition structure and precursor; $\Delta E^{\ddagger,ZPC}$ = zero point energy-corrected energy barrier; $\Delta H^{\ddagger}$ = activation enthalpy; T_c = crossover temperature; T = temperature; $k_{f/r}^{Class}$ = rate constant obtained from classical TST; $k_{f/r}^{Q-vib}$ = rate constant obtained with quantized vibrations including the zero-point vibrational energy; $k_{f/r}^{S-Wig}$ = rate constant obtained with quantized vibrations and tunneling correction through the simple Wigner correction; $k_{f/r}^{F-Wig}$ = full Wigner-corrected rate constant at T above Tc; $k_{f/r}^{Arr}$ = Arrhenius rate constant; f/r = forward or reverse direction; $\Delta G^{\ddagger}$ = activation or relative Gibbs free energy; $\Delta S^{\ddagger}$ = activation entropy; f/r = forward or reverse direction.

Table A5.1

Elementary reaction ($\varepsilon = 1$)	$\Delta E^{\ddagger}$	$\Delta E^{\ddagger,ZPE}$	$\Delta E^{\ddagger,ZPC}$	$\Delta H^{\ddagger}$	T_c	T	$k_{f/r}^{Class}$	$k_{f/r}^{Q\text{-}vib}$	$k_{f/r}^{S\text{-}Wig}$	$k_{f/r}^{F\text{-}Wig}$	$k_{f/r}^{Arr}$	$\Delta G^{\ddagger}$	$\Delta S^{\ddagger}$
1,3-dipolar cycloaddition (React→TS1)	50.0	6.1	56.1	58.2	3	200	4.55×10^{-1}	1.88×10^{-1}	1.89×10^{-1}	1.89×10^{-1}	2.16×10^{-2}	51.1	3.6×10^{-2}
						277	5.47×10^{3}	3.43×10^{3}	3.44×10^{3}	3.44×10^{3}	2.75×10^{2}	49.0	3.3×10^{-2}
						300	3.43×10^{4}	2.32×10^{4}	2.32×10^{4}	2.32×10^{4}	1.79×10^{3}	48.4	3.3×10^{-2}
						371	2.50×10^{6}	1.96×10^{6}	1.96×10^{6}	1.96×10^{6}	1.23×10^{5}	46.8	3.1×10^{-2}
1,3-dipolar cycloaddition (TS1←Int1)	51.0	-9.3	41.7	58.0	3	200	2.40×10^{2}	2.41×10^{3}	2.41×10^{3}	2.41×10^{3}	2.72×10^{2}	35.4	1.1×10^{-1}
						277	1.24×10^{6}	4.54×10^{6}	4.54×10^{6}	4.54×10^{6}	3.72×10^{5}	32.4	9.2×10^{-2}
						300	5.08×10^{7}	1.28×10^{8}	1.28×10^{8}	1.28×10^{8}	2.64×10^{6}	30.2	9.3×10^{-2}
						371	3.25×10^{8}	6.96×10^{8}	6.96×10^{8}	6.96×10^{8}	4.36×10^{7}	28.7	7.9×10^{-2}
Decarboxylation (Int1→TS2)	60.2	-5.0	55.2	56.1	4	200	1.58×10^{-7}	1.09×10^{-6}	1.09×10^{-6}	1.09×10^{-6}	1.29×10^{-7}	71.1	-7.5×10^{-2}
						277	3.82×10^{-3}	1.26×10^{-2}	1.26×10^{-2}	1.26×10^{-2}	1.02×10^{-3}	77.8	-7.8×10^{-2}
						300	2.76×10^{-2}	7.92×10^{-2}	7.92×10^{-2}	7.92×10^{-2}	6.10×10^{-3}	79.8	-7.9×10^{-2}
						371	2.77×10^{0}	5.85×10^{0}	5.85×10^{0}	5.85×10^{0}	3.73×10^{-1}	86.0	-8.1×10^{-2}
Decarboxylation (TS2←Int2)	118.3	7.9	126.2	119.8	4	200	6.53×10^{-27}	4.11×10^{-27}	4.11×10^{-27}	4.11×10^{-27}	4.85×10^{-28}	149.3	-1.5×10^{-1}
						277	2.69×10^{-18}	2.49×10^{-18}	2.49×10^{-18}	2.49×10^{-18}	1.91×10^{-19}	161.2	-1.5×10^{-1}
						300	1.30×10^{-16}	1.27×10^{-16}	1.27×10^{-16}	1.27×10^{-16}	9.66×10^{-18}	164.8	-1.5×10^{-1}
						371	1.12×10^{-12}	1.17×10^{-12}	1.17×10^{-12}	1.17×10^{-12}	7.44×10^{-14}	176.2	-1.5×10^{-1}

Table A5.1 (Continued).

Elementary reaction (ε = 1)	$\Delta E^{\ddagger}$	$\Delta E^{\ddagger,ZPE}$	$\Delta E^{\ddagger,ZPC}$	$\Delta H^{\ddagger}$	T_c	T	$k_{f/r}^{Class}$	$k_{f/r}^{Q\text{-}vib}$	$k_{f/r}^{S\text{-}Wig}$	$k_{f/r}^{F\text{-}Wig}$	$k_{f/r}^{Arr}$	$\Delta G^{\ddagger}$	$\Delta S^{\ddagger}$
Acid catalyst (1) (Int2b→TS3)	42.4	7.2	49.6	46.9	15	200	3.30×10^{5}	5.81×10^{4}	5.86×10^{4}	5.86×10^{4}	6.59×10^{3}	30.1	8.4×10^{-2}
						277	4.04×10^{8}	1.70×10^{8}	1.71×10^{8}	1.71×10^{8}	1.37×10^{7}	24.1	8.2×10^{-2}
						300	1.63×10^{9}	7.94×10^{8}	7.97×10^{8}	7.97×10^{8}	6.03×10^{7}	22.4	8.2×10^{-2}
						371	4.18×10^{10}	2.78×10^{10}	2.78×10^{10}	2.78×10^{10}	1.70×10^{9}	17.4	8.0×10^{-2}
Acid catalyst (1) (TS3←Int3)	55.2	-2.9	52.3	53.9	15	200	8.39×10^{6}	1.55×10^{7}	1.56×10^{7}	1.56×10^{7}	1.77×10^{6}	20.8	1.7×10^{-1}
						277	8.78×10^{10}	1.28×10^{11}	1.29×10^{11}	1.29×10^{11}	1.05×10^{10}	8.8	1.6×10^{-1}
						300	5.37×10^{11}	7.53×10^{11}	7.56×10^{11}	7.56×10^{11}	5.72×10^{10}	5.3	1.6×10^{-1}
						371	3.68×10^{13}	4.70×10^{13}	4.72×10^{13}	4.72×10^{13}	2.94×10^{12}	(-5.6)	1.6×10^{-1}
Cycloelimination (Int3→TS4)	81.0	-11.5	69.5	75.2	7	200	5.19×10^{-5}	5.24×10^{-4}	5.25×10^{-4}	5.25×10^{-4}	5.95×10^{-5}	60.9	7.2×10^{-2}
						277	4.08×10^{1}	1.31×10^{2}	1.31×10^{2}	1.31×10^{2}	1.06×10^{1}	56.5	6.8×10^{-2}
						300	5.82×10^{2}	1.54×10^{3}	1.54×10^{3}	1.54×10^{3}	1.17×10^{2}	55.2	6.7×10^{-2}
						371	2.86×10^{5}	5.07×10^{5}	5.07×10^{5}	5.07×10^{5}	3.16×10^{4}	51.0	6.5×10^{-2}
Cycloelimination (TS4←Prod)	50.2	3.5	53.7	52.8	7	200	8.20×10^{-3}	2.04×10^{-3}	2.04×10^{-3}	2.04×10^{-3}	2.37×10^{-4}	58.6	-2.9×10^{-2}
						277	3.71×10^{1}	1.46×10^{1}	1.46×10^{1}	1.46×10^{1}	1.16×10^{0}	61.6	-3.2×10^{-2}
						300	1.93×10^{2}	8.24×10^{1}	8.25×10^{1}	8.25×10^{1}	6.28×10^{0}	62.5	-3.2×10^{-2}
						371	8.99×10^{3}	4.68×10^{3}	4.68×10^{3}	4.68×10^{3}	2.97×10^{2}	65.4	-3.4×10^{-2}

Table A5.1 (Continued).

Elementary reaction ($\varepsilon = 1$)	$\Delta E^{\ddagger}$	$\Delta E^{\ddagger,ZPE}$	$\Delta E^{\ddagger,ZPC}$	$\Delta H^{\ddagger}$	T_c	T	$k_{f/r}^{Class}$	$k_{f/r}^{Q\text{-}vib}$	$k_{f/r}^{S\text{-}Wig}$	$k_{f/r}^{F\text{-}Wig}$	$k_{f/r}^{Arr}$	$\Delta G^{\ddagger}$	$\Delta S^{\ddagger}$
Acid catalyst (2) (Int2b→TS3b)	72.9	-7.5	65.4	71.0	31	200	2.63×10^{5}	5.02×10^{5}	5.21×10^{5}	5.22×10^{5}	5.74×10^{4}	26.5	2.2×10^{-1}
						277	5.37×10^{10}	6.72×10^{10}	6.86×10^{10}	6.86×10^{10}	5.47×10^{9}	10.3	2.2×10^{-1}
						300	5.87×10^{11}	6.90×10^{11}	7.02×10^{11}	7.02×10^{11}	5.28×10^{10}	5.5	2.2×10^{-1}
						371	1.56×10^{14}	1.62×10^{14}	1.64×10^{14}	1.64×10^{14}	1.01×10^{13}	(-9.4)	2.2×10^{-1}
Acid catalyst (2) (TS3b←Prod)	54.7	-2.3	52.4	55.8	31	200	1.10×10^{7}	4.73×10^{6}	4.91×10^{6}	4.92×10^{6}	5.31×10^{5}	22.8	1.7×10^{-1}
						277	1.07×10^{11}	5.17×10^{10}	5.27×10^{10}	5.27×10^{10}	4.22×10^{9}	10.9	1.6×10^{-1}
						300	6.41×10^{11}	3.22×10^{11}	3.28×10^{11}	3.28×10^{11}	2.47×10^{10}	7.4	1.6×10^{-1}
						371	4.23×10^{13}	2.34×10^{13}	2.37×10^{13}	2.37×10^{13}	1.44×10^{12}	(-3.4)	1.6×10^{-1}

Table A5.2 Thermodynamics and kinetics of the elementary reactions of the enzymatic decarboxylation of α,β-unsaturated acid in ε = 78. Rate constants, temperatures and energies are in s-1, K and kJ/mol, respectively; $\Delta E^{\ddagger}$ = energy barrier on the optimized reaction path; $\Delta E^{\ddagger,ZPE}$ = difference between $E^{\ddagger,ZPE}$ of the transition structure and precursor; $\Delta E^{\ddagger,ZPC}$ = zero point energy-corrected energy barrier; $\Delta H^{\ddagger}$ = activation enthalpy; T_c = crossover temperature; T = temperature; $k_{f/r}^{Class}$ = rate constant obtained from classical TST; $k_{f/r}^{Q-vib}$ = rate constant obtained with quantized vibrations including the zero-point vibrational energy; $k_{f/r}^{S-Wig}$ = rate constant obtained with quantized vibrations and tunneling correction through the simple Wigner correction; $k_{f/r}^{F-Wig}$ = full Wigner-corrected rate constant at T above Tc; $k_{f/r}^{Arr}$ = Arrhenius rate constant; f/r = forward or reverse direction; $\Delta G^{\ddagger}$ = activation or relative Gibbs free energy; $\Delta S^{\ddagger}$ = activation entropy; f/r = forward or reverse direction.

Table A5.2

Elementary reaction (ε = 78)	$\Delta E^{\ddagger}$	$\Delta E^{\ddagger,ZPE}$	$\Delta E^{\ddagger,ZPC}$	$\Delta H^{\ddagger}$	T_c	T	$k^{Class}_{f/r}$	$k^{Q\text{-}vib}_{f/r}$	$k^{S\text{-}Wig}_{f/r}$	$k^{F\text{-}Wig}_{f/r}$	$k^{Arr}_{f/r}$	$\Delta G^{\ddagger}$	$\Delta S^{\ddagger}$
1,3-dipolar cycloaddition (React$^{\varepsilon}$→TS1$^{\varepsilon}$)	48.0	-0.4	47.6	48.0	123	200	5.86×10^{-1}	5.92×10^{-1}	9.62×10^{-1}	1.23×10^{0}	6.76×10^{-2}	49.2	-6.0×10^{-3}
						277	1.83×10^{3}	1.84×10^{3}	2.44×10^{3}	2.61×10^{3}	1.50×10^{2}	50.4	-8.7×10^{-3}
						300	8.85×10^{3}	8.89×10^{3}	1.14×10^{4}	1.19×10^{4}	6.84×10^{2}	50.8	-9.3×10^{-3}
						371	3.49×10^{5}	3.50×10^{5}	4.14×10^{5}	4.23×10^{5}	2.21×10^{4}	52.1	-1.1×10^{-2}
1,3-dipolar cycloaddition (TS1$^{\varepsilon}$←Int1$^{\varepsilon}$)	43.8	-0.3	43.5	43.8	43	200	5.07×10^{0}	5.09×10^{0}	5.48×10^{0}	5.50×10^{0}	5.89×10^{-1}	45.6	-9.0×10^{-3}
						277	7.81×10^{3}	7.83×10^{3}	8.14×10^{3}	8.16×10^{3}	6.28×10^{2}	47.1	-1.2×10^{-2}
						300	3.28×10^{4}	3.29×10^{4}	3.40×10^{4}	3.40×10^{4}	2.57×10^{3}	47.5	-1.2×10^{-2}
						371	9.37×10^{5}	9.38×10^{5}	9.59×10^{5}	9.59×10^{5}	5.85×10^{4}	49.1	-1.4×10^{-2}
Decarboxylation (Int1$^{\varepsilon}$→TS2$^{\varepsilon}$)	38.8	-14.7	24.1	31.7	44	200	3.86×10^{6}	7.25×10^{7}	7.83×10^{7}	7.86×10^{7}	8.45×10^{6}	18.2	6.8×10^{-2}
						277	2.56×10^{9}	1.16×10^{10}	1.21×10^{10}	1.21×10^{10}	9.63×10^{8}	14.3	6.3×10^{-2}
						300	9.14×10^{9}	3.27×10^{10}	3.39×10^{10}	3.39×10^{10}	2.51×10^{9}	13.1	6.2×10^{-2}
						371	1.78×10^{11}	3.92×10^{11}	4.01×10^{11}	4.01×10^{11}	2.43×10^{10}	9.2	6.1×10^{-2}
Decarboxylation (TS2$^{\varepsilon}$←Int2$^{\varepsilon}$)	69.3	5.9	75.2	75.0	44	200	4.71×10^{-9}	1.74×10^{-10}	1.88×10^{-10}	1.89×10^{-10}	1.98×10^{-11}	85.7	-5.4×10^{-2}
						277	5.25×10^{-4}	4.92×10^{-5}	5.12×10^{-5}	5.13×10^{-5}	3.94×10^{-6}	90.6	-5.6×10^{-2}
						300	5.10×10^{-3}	5.75×10^{-4}	5.96×10^{-4}	5.96×10^{-4}	4.40×10^{-5}	92.1	-5.7×10^{-2}
						371	1.03×10^{0}	1.80×10^{-1}	1.85×10^{-1}	1.85×10^{-1}	1.12×10^{-6}	96.8	-5.9×10^{-2}

Table A5.2 (Continued).

Elementary reaction (ε = 78)	$\Delta E^{\ddagger}$	$\Delta E^{\ddagger,ZPE}$	$\Delta E^{\ddagger,ZPC}$	$\Delta H^{\ddagger}$	T_c	T	$k_{f/r}^{Class}$	$k_{f/r}^{Q\text{-}vib}$	$k_{f/r}^{S\text{-}Wig}$	$k_{f/r}^{F\text{-}Wig}$	$k_{f/r}^{Arr}$	$\Delta G^{\ddagger}$	$\Delta S^{\ddagger}$
Acid catalyst (1) ($Int2b^{\varepsilon} \rightarrow TS3^{\varepsilon}$)	136.6	-7.4	129.2	127.9	61	200	3.40×10^{-25}	4.11×10^{-23}	4.73×10^{-23}	4.80×10^{-23}	4.81×10^{-24}	134.0	-3.1×10^{-2}
						277	2.98×10^{-15}	8.90×10^{-14}	9.60×10^{-14}	9.64×10^{-14}	7.00×10^{-15}	137.0	-3.3×10^{-2}
						300	2.63×10^{-13}	5.91×10^{-12}	6.31×10^{-12}	6.33×10^{-12}	4.48×10^{-13}	138.0	-3.4×10^{-2}
						371	9.11×10^{-9}	1.04×10^{-7}	1.09×10^{-7}	1.09×10^{-7}	6.51×10^{-9}	141.1	-3.6×10^{-2}
Acid catalyst (1) ($TS3^{\varepsilon} \leftarrow Int3^{\varepsilon}$)	161.7	-22.1	139.6	142.5	61	200	5.88×10^{-30}	9.89×10^{-26}	1.14×10^{-25}	1.16×10^{-25}	1.11×10^{-26}	144.1	-8.0×10^{-3}
						277	3.48×10^{-18}	2.12×10^{-15}	2.29×10^{-15}	2.30×10^{-15}	1.60×10^{-16}	145.7	-1.2×10^{-2}
						300	7.00×10^{-16}	2.26×10^{-13}	2.41×10^{-13}	2.42×10^{-13}	1.74×10^{-14}	146.1	-1.2×10^{-2}
						371	1.66×10^{-10}	1.26×10^{-8}	1.32×10^{-8}	1.32×10^{-8}	7.91×10^{-10}	147.6	-1.4×10^{-2}
Cycloelimination ($Int3^{\varepsilon} \rightarrow TS4^{\varepsilon}$)	77.4	-10.0	67.4	69.8	51	200	1.36×10^{-7}	4.66×10^{-6}	5.15×10^{-6}	5.19×10^{-6}	5.46×10^{-7}	68.7	5.5×10^{-3}
						277	5.89×10^{-2}	5.06×10^{-1}	5.34×10^{-1}	5.35×10^{-1}	4.09×10^{-2}	69.3	1.8×10^{-3}
						300	7.46×10^{-1}	4.97×10^{0}	5.21×10^{0}	5.22×10^{0}	3.79×10^{-1}	69.5	1.0×10^{-3}
						371	2.79×10^{2}	1.06×10^{3}	1.10×10^{3}	1.10×10^{3}	6.67×10^{1}	70.0	-5.4×10^{-4}
Cycloelimination ($TS3^{\varepsilon} \leftarrow Prod^{\varepsilon}$)	44.3	6.9	51.2	47.3	51	200	2.59×10^{-4}	6.57×10^{-5}	7.27×10^{-5}	7.32×10^{-5}	7.70×10^{-6}	64.3	-8.5×10^{-2}
						277	4.33×10^{-1}	1.98×10^{-1}	2.09×10^{-1}	2.09×10^{-1}	1.57×10^{-2}	71.5	-8.7×10^{-2}
						300	1.85×10^{0}	9.35×10^{-1}	9.79×10^{-1}	9.80×10^{-1}	7.04×10^{-2}	73.7	-8.8×10^{-2}
						371	5.48×10^{1}	3.41×10^{1}	3.52×10^{1}	3.52×10^{1}	2.15×10^{0}	80.6	-9.0×10^{-2}

Table A5.2 (Continued).

Elementary reaction ($\varepsilon = 78$)	$\Delta E^{\ddagger}$	$\Delta E^{\ddagger,ZPE}$	$\Delta E^{\ddagger,ZPC}$	$\Delta H^{\ddagger}$	T_c	T	$k_{f/r}^{Class}$	$k_{f/r}^{Q\text{-}vib}$	$k_{f/r}^{S\text{-}Wig}$	$k_{f/r}^{F\text{-}Wig}$	$k_{f/r}^{Arr}$	$\Delta G^{\ddagger}$	$\Delta S^{\ddagger}$
Acid catalyst (2) ($Int2b^{\varepsilon} \rightarrow TS3b^{\varepsilon}$)	46.6	-5.2	41.4	44.5	55	200	9.60×10^{2}	2.61×10^{3}	2.93×10^{3}	2.96×10^{3}	3.07×10^{2}	35.2	4.7×10^{-2}
						277	2.37×10^{6}	4.26×10^{6}	4.53×10^{6}	4.54×10^{6}	3.41×10^{5}	32.6	4.3×10^{-2}
						300	1.09×10^{7}	1.83×10^{7}	1.93×10^{7}	1.93×10^{7}	1.39×10^{6}	31.8	4.2×10^{-2}
						371	3.87×10^{8}	5.59×10^{8}	5.78×10^{8}	5.79×10^{8}	3.47×10^{7}	29.4	4.1×10^{-2}
Acid catalyst (2) ($TS3b^{\varepsilon} \leftarrow Prod^{\varepsilon}$)	38.1	-1.7	36.4	37.3	55	200	9.43×10^{2}	1.33×10^{3}	1.50×10^{3}	1.52×10^{3}	1.49×10^{6}	36.4	4.5×10^{-3}
						277	5.59×10^{5}	6.85×10^{5}	7.31×10^{5}	7.33×10^{5}	5.50×10^{4}	36.8	1.8×10^{-3}
						300	1.95×10^{6}	2.33×10^{6}	2.46×10^{6}	2.47×10^{6}	1.80×10^{5}	36.9	1.3×10^{-3}
						371	3.60×10^{7}	4.08×10^{7}	4.23×10^{7}	4.24×10^{7}	2.51×10^{6}	37.5	-5.4×10^{-4}

APPENDIX B

PUBLICATION

PAPER

Check for updates

Kinetics and thermodynamics of enzymatic decarboxylation of α,β-unsaturated acid: a theoretical study†

Phorntep Promma,[a] Charoensak Lao-ngam,[b] Rung-Yi Lai [ID][a] and Kritsana Sagarik [ID] *[a]

Enzymatic decarboxylation of α,β-unsaturated acid through ferulic acid decarboxylase (**FDC1**) has been of interest because this reaction has been anticipated to be a promising, environmentally friendly industrial process for producing styrene and its derivatives from natural resources. Because the local dielectric constant at the active site is not exactly known, enzymatic decarboxylation to generate β-methylstyrene (**β-MeSt**) was studied under two extreme conditions ($\varepsilon = 1$ and 78 in the gas phase and aqueous solution, respectively) using the B3LYP/DZP method and transition state theory (TST). The model molecular clusters consisted of an α-methylcinnamate (**Cin**) substrate, a prenylated flavin mononucleotide (**PrFMN**) cofactor and all relevant residues of **FDC1**. Analysis of the equilibrium structures showed that the **FDC1** backbone does not play the most important role in the decarboxylation process. The potential energy profiles confirmed that the increase in the polarity of the solvent could lead to significant changes in the energy barriers, especially for the transition states that involve proton transfer. Analysis of the rate constants confirmed the low/no quantum mechanical tunneling effect in the studied temperature range and that inclusion of the fluctuation of the local dielectric environment in the mechanistic model was essential. Because the computed rate constants are not compatible with the time resolution of the stopped-flow spectrophotometric experiment, the direct route for generating **β-MeSt** after CO₂ elimination (acid catalyst (2)) is unlikely to be utilized, thereby confirming that indirect cycloelimination in a low local dielectric environment is the rate determining step. The thermodynamic results showed that the elementary reactions that involve charge (proton) transfer are affected by solvent polarity, thereby leading to the conclusion that overall, the enzymatic decarboxylation of α,β-unsaturated acid is thermodynamically controlled at high ε. The entropy changes due to the generation of molecules in the active site appeared more pronounced than that due to only covalent bond breaking/ formation or structural reorientation. This work examined in detail for the first time the scenarios in each elementary reaction and provided insight into the effect of the fluctuations in the local dielectric environment on the enzymatic decarboxylation of α,β-unsaturated acids. These results could be used as guidelines for further theoretical and experimental studies on the same and similar systems.

Introduction

Decarboxylation has long been known in organic synthesis, in which the formation of a carbanion intermediate and carbon dioxide product controls the reaction rate.[1] Therefore, decarboxylation reactions require organic or metal ion catalysts to stabilize the intermediates.[2] Enzymatic decarboxylation of α,β-unsaturated acid using ferulic acid decarboxylase (**FDC1**)

has been of interest in recent decades[1,3–5] because the reaction has been anticipated to be a promising, environmentally friendly industrial process for producing styrene and its derivatives from natural resources. Biosynthesis of styrene from this nonoxidative decarboxylation could start from biological sugars (*e.g.*, glucose) to produce ʟ-phenylalanine and *trans*-cinnamate through the shikimate pathway and coexpression of genes that encode phenylalanine ammonia lyase (PAL),[6] respectively. Enzymatic decarboxylation using **FDC1** is accomplished through the 1,3-dipolar cycloaddition reaction between the substrate (an α,β-unsaturated acid, such as α-methylcinnamic acid) and an appropriate enzyme cofactor.[1]

Experiments have shown that decarboxylation of aromatic carboxylic acids using **FDC1** is reversible.[1] However, in the presence of a hydroxyl (OH) group at the α position of the substrate (*e.g.*, α-hydroxycinnamic acid), the enzyme activity of

[a]*School of Chemistry, Institute of Science, Suranaree University of Technology, Nakhon Ratchasima 30000, Thailand. E-mail: kritsana@sut.ac.th; Fax: +66 44 224635; Tel: +66 44 224635*

[b]*Chemistry Program, Faculty of Science and Technology, Nakhon Ratchasima Rajabhat University, Nakhon Ratchasima 30000, Thailand*

FDC1 is inhibited, and the reaction becomes irreversible.[5] Although various cofactors have been suggested, *e.g.*, pyridoxal phosphate and pyridine pyrophosphate,[2] biosynthesis of styrene using modified flavin cofactors seems to have received special attention, *e.g.*, the prenylated flavin mononucleotide (**PrFMN**).[1,3–5,7,8] Because the mechanisms of the enzymatic decarboxylation of α,β-unsaturated acids have been extensively studied using theoretical and experimental methods, only the results that are relevant to the present study will be discussed in detail. To facilitate discussion, the abbreviations for the molecules that are used in this work are summarized in Table S1.†

Several mechanisms for the enzymatic decarboxylation of α,β-unsaturated acids using **PrFMN** have been reported, among which that proposed by Payne *et al.*[1] has been widely accepted and further studied in detail. Because the enzyme-catalyzed 1,3-dipolar cycloaddition of **PrFMN** and an α,β-unsaturated acid was unprecedented, the reaction was confirmed using a mechanism-based inhibitor.[4] Based on the theoretical and experimental data in ref. 1, two forms of **PrFMN** with different ring structures were considered, namely the iminium and ketimine forms, which are abbreviated **PrFMN**^iminium and **PrFMN**^ketimine, respectively, in Table S1.† It was suggested that through **PrFMN**^iminium, the decarboxylation of cinnamic acid occurs *via* 1,3-dipolar cycloaddition, whereas the reaction with **PrFMN**^ketimine occurs *via* Michael addition.

Although mass spectroscopic data cannot differentiate these two forms, because the reaction is stereospecific, the enzyme activity was suggested to be higher using **PrFMN**^iminium; therefore, the reaction using **PrFMN**^iminium has been further studied in detail.[1] Based on the density functional theory (DFT) method with the Becke, 3-parameter, and Lee–Yang–Parr hybrid functionals and 6-311++G(d,p) basis set (abbreviated B3LYP/6-311++G(d,p)),[1] the equilibrium structures of **PrFMN**^ketimine with bent-down and bent-up forms are -41.5 and -36.9 kJ mol^{-1} more stable, respectively, than those of **PrFMN**^iminium. The mechanism that was proposed by Payne *et al.*[1] consists of four consecutive elementary steps (Scheme 1): (**I**) 1,3-dipolar cycloaddition, (**II**) Grob-type decarboxylation, (**III**) protonation and (**IV**) *retro* 1,3-dipolar cycloaddition. Based on spectroscopic methods and kinetic isotope effects, Ferguson *et al.* studied the enzyme activity of **FDC1** by following the depletion of the substrate.[3] The results showed that cycloelimination (**IV**) could represent the rate-determining step.

The roles of residues in **FDC1** in **PrFMN** oxidative maturation, cofactor isomerization and enzyme catalysis were studied using *Aspergillus niger* **FDC1** as a model system.[9] Analysis of the high-resolution crystal structures, mass spectrometric and kinetic data indicated that the isomerization of **PrFMN**^iminium to **PrFMN**^ketimine is an irreversible light-dependent process and is independent of the **Glu277**–**Arg173**–**Glu282** residue network. Most importantly, while irreversible isomerization leads to loss of enzyme activity, the efficiency of enzymatic decarboxylation through the **PrFMN**^iminium cofactor is dependent on the conserved **Glu277**–**Arg173**–**Glu282** residue network; the network was suggested to facilitate the oxidative maturation of the **PrFMN**^iminium cofactor and to act as a key acid–base during catalysis. The need for the **Glu277** and

Glu282 acid residues in the enzymatic decarboxylation of α,β-unsaturated acid was confirmed using NMR spectroscopy.

To study the stability of the transient intermediates, Kaneshiro *et al.*[10] performed kinetic experiments to investigate the formation of the **PrFMN**^iminium–styrene cycloadduct that accumulated on the **FDC1** enzyme in 0.1 M potassium phosphate buffer (pH = 7.0). Analysis of the stopped-flow UV-vis spectrophotometric results at 277 K and the half-of-sites model revealed that in the active site, a **PrFMN**^iminium–cinnamic acid cycloadduct is formed with $k = 131$ s^{-1} and is converted to a **PrFMN**^iminium–styrene cycloadduct with $k = 75$ s^{-1}. These results led to the suggestion that both cycloelimination (**IV**) of the **PrFMN**^iminium–styrene cycloadduct and diffusion from the active site represent the rate-determining step, with $k = 11$ s^{-1}.

The enzymatic decarboxylation of an α,β-unsaturated acid using **FDC1** was theoretically studied by the quantum mechanics/molecular mechanics (QM/MM) method,[8] in which the original crystal structure in the protein data bank (PDB), including the **FDC1** enzyme, α-methylcinnamic acid, **PrFMN**^iminium and **PrFMN**^ketimine, was used as the model system. In QM/MM simulations, the substrate, a part of **PrFMN** and the side chains of **Glu282** and **Arg173** were included in the QM region, whereas the remaining part of **FDC1** and 8103 TIP3 water molecules were included in the MM region. To study the effect of hydrogen bonding (H-bonding), two water molecules were included in the QM region. The results that were obtained by scanning over the potential energy curves (B3LYP/6-311++G(2d,2p)) suggested that the Michael addition through **PrFMN**^ketimine involves a rather high energy barrier ($\Delta E^{\ddagger} = 166$ kJ mol^{-1}), whereas **PrFMN**^iminium can easily form the cofactor-substrate adduct ($\Delta E^{\ddagger} = 65$ kJ mol^{-1}) in the 1,3-dipolar cycloaddition process and, therefore, is more relevant to the enzymatic reaction. Although decarboxylation of the pyrrolidine adduct intermediate and subsequent protonation involve low energy barriers (58 and 27 kJ mol^{-1}, respectively), the overall energy barrier is $\Delta E^{\ddagger} = 98$ kJ mol^{-1}.

In this work, because the information on the kinetic and thermodynamic aspects was limited, the proposed elementary reactions of the enzymatic decarboxylation of α,β-unsaturated acid were further studied using the DFT method with B3LYP functionals and transition state theory (TST). While previous theoretical studies focused only on potential energy profiles in low local dielectric environments,[5,7] this theoretical study focused on the scenarios (progress) in the elementary reactions and on the kinetic and thermodynamic properties in two extreme local dielectric environments, namely, the gas phase and aqueous solution with $\varepsilon = 1$ and 78, respectively. This theoretical study began with geometry optimizations of the proposed model molecular clusters,[5] which consisted of the α-methylcinnamate (**Cin**) substrate, **PrFMN**^iminium cofactor (abbreviated **PrFMN** hereafter) and all relevant residues in the active site of **FDC1**. The kinetic and thermodynamic aspects of the elementary reactions at $\varepsilon = 1$ and 78 were analyzed in detail based on the TST results and were included in the proposed mechanisms. The results were discussed in comparison with the reported theoretical and experimental data.
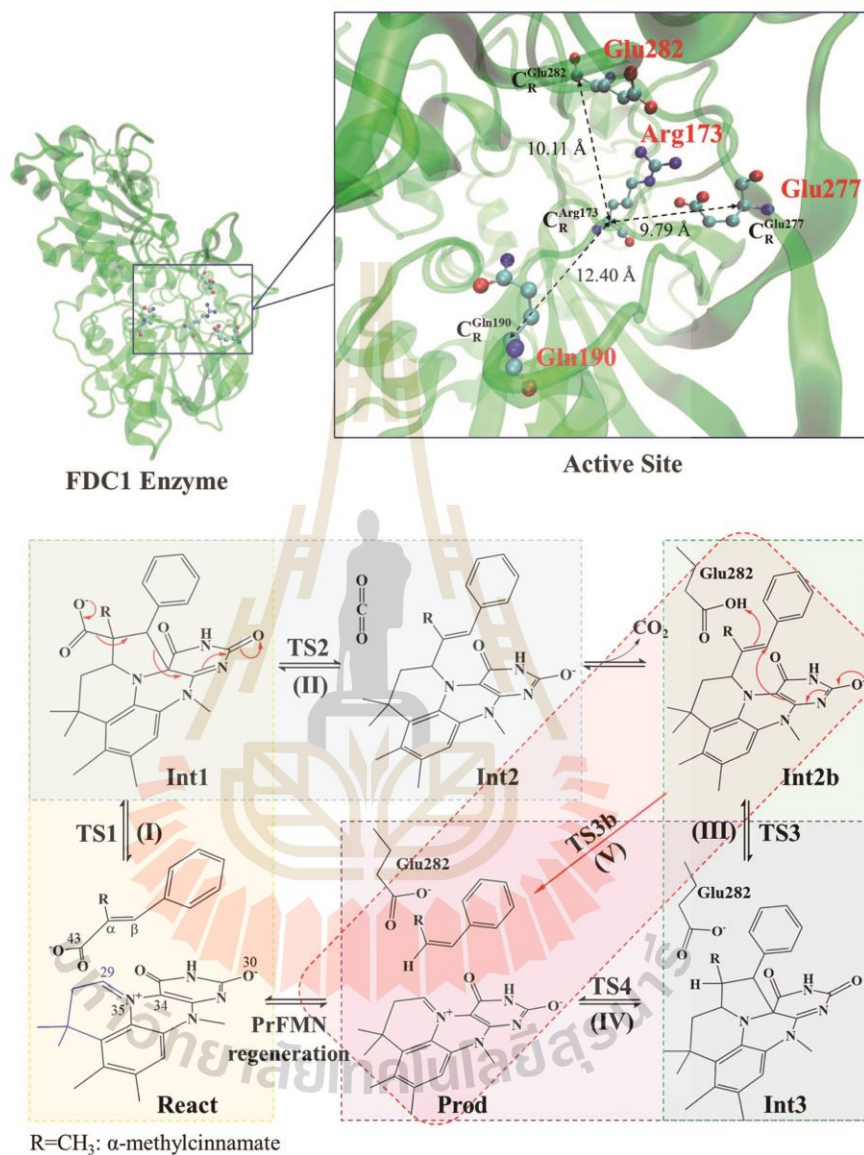
Scheme 1 Structure of the **FDC1** enzyme and the proposed catalytic pathways for the decarboxylation of α,β-unsaturated acid.[1]

Computational methods

Quantum chemical methods

Because the **FDC1** enzyme is exceedingly large for high-level *ab initio* methods and because our previous studies showed that the mechanisms for proton transfer in heterocyclic aromatic systems can be studied reasonably well using the B3LYP method with the DZP basis set,[11–13] the B3LYP/DZP method was used in this study; our benchmark calculations on bifunctional proton transfers in poly(benzimidazole) (PBI) H-bond systems[14] confirmed that the B3LYP/DZP method yields approximately the same equilibrium and transition structures and relative interaction energies as the B3LYP/TZP method with reasonable computational resources. In this study, the model molecular clusters that were hypothesized in ref. 5 were chosen as model systems, which consist of all important active site residues, the substrate and the cofactor. The model molecular clusters were constructed by substituting the carbon atoms of **FDC1**$^{\text{Backbone}}$ that connect the residues with methyl (CH$_3$) groups (Table S2†); for example, C$_{\text{R}}^{\text{Glu277}}$ is the carbon atom of the CH$_3$ group that substitutes the carbon atom of the **FDC1**$^{\text{Backbone}}$ that connects the **Glu277** residue (Scheme 1).

Because our previous studies showed that the local dielectric environment (microenvironment) can affect the structures and energetics of elementary processes[11,13,14] and because enzymatic decarboxylation occurs in aqueous solution, the conductor-like screening model (COSMO) was used to simulate the effect of the aqueous environment. COSMO was used successfully in our previous studies on proton transfer processes in H-bond systems.[11,13,14] Previous theoretical studies used $\varepsilon = 4$ (ref. 5) and 5.7 (ref. 7) to model the local dielectric environment at the active site of FDC1. In this work, because the local dielectric constant was not exactly known and we wanted to study the elementary reactions in extreme local dielectric conditions, the lowest and highest possible values (and fluctuation) were used, namely, $\varepsilon = 1$ and 78, in the gas phase and bulk water, respectively. All B3LYP/DZP calculations were performed using the TURBOMOLE 7.50 software package.[15]

Equilibrium structures and potential energy curves

The six model molecular clusters that were hypothesized in the previous study[5] were considered in this work (Table S2†), in which α-methylcinnamate (**Cin**) was chosen as the substrate for generating β-methylstyrene (**β-MeSt**). The active site of FDC1 consists of **Glu277**, **Arg173** and **Gln190**, in which the salt bridge between protonated **Arg173** (**Arg173H$^+$**) and the carboxylate group (COO$^-$) of **Cin** is responsible for the enzyme–substrate interaction (the docking site); **Glu277** is the proton source of **Arg173H$^+$**. The interaction between **PrFMN** and the **Gln190** residue is an N–H···O$^-$ H-bond, *e.g.*, in the precursor **React**; **Cin** only weakly interacts with **PrFMN** through a π–π interaction. The five hypothesized elementary reactions, which are presented in Scheme 1, are (**I**) 1,3-dipolar cycloaddition, **React → TS1 → Int1**; (**II**) decarboxylation, **Int1 → TS2 → Int2**; (**III**) acid catalyst (**1**), **Int2b → TS3 → Int3**; (**IV**) cycloelimination, **Int3 → TS4 → Prod**; and (**V**) acid catalyst (**2**), **Int2b → TS3b → Prod**.

The symbols that are used in this manuscript (*e.g.*, **React**, **TS1** and **Int1**) correspond to ref. 5.

The structures of the molecules in the model molecular clusters were fully optimized without any geometrical constraint using the B3LYP/DZP method before they were included in the model molecular clusters (Table S1†). The Newton–Raphson method was used with the converge criterion for the total energies and energy gradients, 1.0×10^{-6} and 1.0×10^{-4} au, respectively. Then, the structures of the six model molecular clusters (including the residues, cofactor and substrate) were reoptimized using the same method (Table S2†). The equilibrium structures of the model molecular clusters were employed in the elementary reaction path optimizations using the nudged elastic band (NEB) method with the limited-memory Broyden–Fletcher–Goldfarb–Shanno (L-BFGS) optimizer in the ChemShell software package.[16] In the elementary reaction path optimizations, fourteen structures that connected the precursor, transition structure and product were optimized. The relative energies with respect to the precursor (ΔE^{Rel}) along the optimized reaction path were plotted. The effect of the aqueous environment was studied using the solvation energy (ΔE^{Solv}), which was defined as the difference between the total energies of the model molecular clusters at $\varepsilon = 78$ and $\varepsilon = 1$, namely, $E^{\text{Total},\varepsilon}$ and E^{Total}.

Kinetics of elementary reactions

Characteristic structures of the model molecular clusters on the potential energy curves were used in the calculations of the rate constants based on the TST method.[17–19] To study the effect of quantum mechanical tunneling, the classical (k^{Class}) and quantized-vibrational ($k^{\text{Q-vib}}$) rate constants were initially computed over the temperature range of 200–371 K. k^{Class} was calculated using eqn (1):[20]

$$k^{\text{Class}}(T) = \frac{k_{\text{B}}T}{\hbar}\frac{Q^{\ddagger}}{Q^{\text{R}}}e^{-\Delta E^{\ddagger}/k_{\text{B}}T}. \tag{1}$$

Q^{R} and $Q^{\ddagger}$ are the partition functions of the precursor and transition structures, respectively. $\Delta E^{\ddagger}$ is the energy barrier obtained from the NEB method. k_{B} and $\hbar$ are the Boltzmann and Planck constants ($\hbar = h/2\pi$), respectively. $k^{\text{Q-vib}}$ was obtained with the zero point energy-corrected energy barrier ($\Delta E^{\ddagger,\text{ZPC}}$):

$$k^{\text{Q-vib}}(T) = \frac{k_{\text{B}}T}{\hbar}\frac{Q^{\ddagger,\text{ZPC}}}{Q^{\text{R,ZPC}}}e^{-\Delta E^{\ddagger,\text{ZPC}}/k_{\text{B}}T}. \tag{2}$$

$Q^{\text{R,ZPC}}$ and $Q^{\ddagger,\text{ZPC}}$ in eqn (2) are the partition functions of the precursor and transition structures, respectively, that were obtained with ZPC. $\Delta E^{\ddagger,\text{ZPC}}$ was obtained by including the zero-point correction energy (ΔE^{ZPE}) to $\Delta E^{\ddagger}$. The definitions and methods to calculate the energy barriers in eqn (1) and (2) are illustrated as an example in ESI.† The temperatures below which quantum mechanical tunneling dominates were approximated using the crossover temperature (T_{c}):[21,22]

$$T_{\text{c}} = \frac{\hbar \Omega^{\ddagger}}{2\pi k_{\text{B}}}. \tag{3}$$

$\Omega^{\ddagger}$ in eqn (3) is the imaginary frequency of the transition structure. To approximate the effect of quantum mechanical tunneling, the Wigner corrections were made by multiplying $k^{Q\text{-vib}}(T)$ by the Wigner transmission coefficient ($\kappa^{F\text{-Wig}}$) in eqn (4):[21,22]

$$\kappa^{F\text{-Wig}}(T) = \frac{\hbar\Omega^{\ddagger}/2k_B T}{\sin(\hbar\Omega^{\ddagger}/2k_B T)}. \quad (4)$$

In this work, $\kappa^{F\text{-Wig}}$ is regarded as the full Wigner transmission coefficient. Because $\kappa^{F\text{-Wig}}$ diverges near T_c, without a theoretical foundation, the simple Wigner transmission coefficient ($\kappa^{S\text{-Wig}}$) in eqn (5) is recommended to avoid the divergence:[17]

$$\kappa^{S\text{-Wig}}(T) = 1 + \frac{1}{24}\left(\frac{\hbar\Omega^{\ddagger}}{k_B T}\right)^2. \quad (5)$$

$\kappa^{S\text{-Wig}}$ is a Taylor series expansion of $\kappa^{F\text{-Wig}}$ around $1/k_B T = 0$, maintaining only the first two terms. The Wigner corrected rate constants ($k^{F\text{-Wig}}$ and $k^{S\text{-Wig}}$) were computed using eqn (6):

$$k^{F(S)\text{-Wig}}(T) = \kappa^{F(S)\text{-Wig}}(T)k^{Q\text{-vib}}(T). \quad (6)$$

$\kappa^{F\text{-Wig}}$ and $\kappa^{S\text{-Wig}}$ equal to 1 at the classical limit ($\hbar = 0$). The activation free energies ($\Delta G^{\ddagger}$) were computed from the rate constant using $k(T) = (k_B T/h)e^{-\Delta G^{\ddagger}/RT}$. To correlate $k^{S\text{-Wig}}$ with the experimental data,[10] the Eyring equation (eqn (7)) was primarily used to calculate the activation enthalpy ($\Delta H^{\ddagger}$):[20]

$$\ln k^{S\text{-Wig}}(T) = \ln A + \frac{\Delta S^{\ddagger}}{R} - \frac{\Delta H^{\ddagger}}{RT}. \quad (7)$$

$\Delta S^{\ddagger}$ is the activation entropy and R is the gas constant. $\Delta H^{\ddagger}$ in eqn (7) was obtained from the linear relationship between $\ln k^{S\text{-Wig}}(T)$ and $1000/T$. $\Delta G^{\ddagger}$ obtained from the TST method were used to determine $\Delta S^{\ddagger}$ using $\Delta G^{\ddagger} = \Delta H^{\ddagger} - T\Delta S^{\ddagger}$. All the kinetic and thermodynamic calculations were performed using the DL-FIND program[23] included in the ChemShell package.[16]

Results and discussion

To facilitate discussion, additional character codes are used. To characterize the scenarios (progress) in the elementary reactions, lowercase letters in parentheses are used. For example, for 1,3-dipolar cycloaddition (**React → TS1 → Int1**) in Fig. 1, the three consecutive steps, namely, π–π stacking, dipolarophile iminium pair and pyrrolidine cycloadduct formations, are labeled (a), (b), and (c), respectively. The properties/processes with superscript "ε" correspond to a high local dielectric environment. For example, **TS1$^{\varepsilon}$** in and (a)$^{\varepsilon}$ in Fig. 1 and S1b† are the transition structure and π–π stacking, respectively, that were observed on the potential energy curve at $\varepsilon = 78$.

Equilibrium structures of the model molecular clusters

The equilibrium structures and total energies of the model molecular clusters that are involved in the elementary reactions
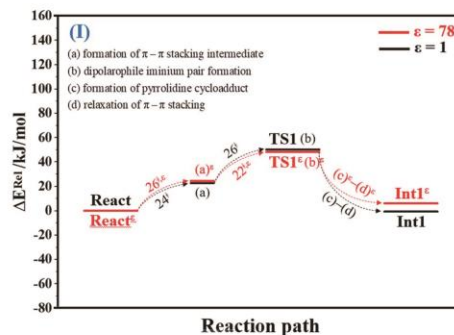

Fig. 1 Potential energy profiles for 1,3-dipolar cycloaddition (**I**) simplified based on the B3LYP/DZP and NEB results in $\varepsilon = 1$ and 78 (Fig. S1†). Energies are in kJ mol. (...) and (...)$^{\varepsilon}$ = scenarios in the elementary reactions in $\varepsilon = 1$ and 78, respectively; $\ddagger$ = energy barrier.

are presented in Table S2.† The B3LYP/DZP results show that the equilibrium structures of the model molecular clusters and the shapes of the active sites therein are not significantly different at $\varepsilon = 1$ versus 78. The average residue-to-residue distances (Table S3†) reveal small standard deviations (SD) for all elementary reactions; the average residue-to-residue distances were approximated using the distances between the carbon atoms of the CH_3 groups that substituted the carbon atom of **FDC1^{Backbone}** (Scheme 1). For example, for **React → TS1 → Int1** at $\varepsilon = 1$, $R_{C_R^{Arg173H^+}-C_R^{Glu277}} = 10.41 \pm 0.48$, $R_{C_R^{Arg173H^+}-C_R^{Gln190}} = 11.07 \pm 0.49$ and $R_{C_R^{Glu277}-C_R^{Gln190}} = 17.08 \pm 0.50$ Å (Table S3a†) and for **Int2b → TS3 → Int3**, $R_{C_R^{Arg173H^+}-C_R^{Glu277}} = 10.78 \pm 0.04$, $R_{C_R^{Arg173H^+}-C_R^{Gln190}} = 13.00 \pm 0.59$ and $R_{C_R^{Arg173H^+}-C_R^{Glu282}} = 8.95 \pm 0.83$ Å. It appears that the highest SD are for elementary reactions that involve proton transfer, in which formation of π–π stacking leads to an increase in $R_{C_R^{Glu277}-C_R^{Gln190}}$. For example, at $\varepsilon = 1$, $R_{C_R^{Glu277}-C_R^{Gln190}} = 13.46 \pm 1.94$ and 13.43 ± 1.86 Å are for acid catalyst (1) (**III**) and acid catalyst (2) (**V**), respectively.

These average residue-to-residue distances (Table S3a and b†) are in good agreement with the PDB crystallographic data (code 4ZA7) in Scheme 1, in which $R_{C_R^{Arg173}-C_R^{Glu277}} = 9.79$, $R_{C_R^{Arg173}-C_R^{Gln190}} = 12.40$, $R_{C_R^{Glu277}-C_R^{Gln190}} = 17.47$ and $R_{C_R^{Arg173}-C_R^{Glu282}} = 10.11$ Å. Similar results were obtained from the analysis of the average residue-to-residue distances per each model molecular structure on the optimized reaction paths. They are also not significantly different; for example, for structure 1 of elementary reactions (**I**) and (**II**) (Table S3c†), $R_{C_R^{Arg173H^+}-C_R^{Glu277}} = 10.31 \pm 0.99$ Å and that for elementary reactions (**III**) and (**IV**) is 10.82 ± 0.07 Å.

The above results suggest that in the enzymatic decarboxylation reaction, the active site structure and volume do not significantly change. These results also imply that the motion of **FDC1^{Backbone}** can be neglected in the model systems. These findings are in accordance with the results in ref. 9, in which the **Glu277–Arg173–Glu282** residue network was suggested to be conserved in the enzymatic decarboxylation reaction; the residues help immobilize the substrate and cofactor in the active

site. In addition, because the computed residue-to-residue distances are in good agreement with the PDB crystallographic data (code 4ZA7), one can conclude that the model molecular clusters are appropriate for representing the active site of **FDC1**.

Elementary reactions

The structures and energetics of the model molecular clusters on the potential energy curves of elementary reactions (**I**)–(**V**) that were obtained *via* the NEB method at $\varepsilon = 1$ and $\varepsilon = 78$ are included in Fig. S1–S5,† together with the relative total energies (ΔE^{Rel} and $\Delta E^{\text{Rel},\varepsilon}$). The transition structures on the potential energy curves are summarized in Table S4.† To keep the manuscript concise, the scenarios, interactions among molecules, and energetic effect of the local dielectric environment on the elementary reactions are explained in detail in ESI.† Only the simplified potential energy profiles are included in the manuscript (Fig. 1–5).

1,3-Dipolar cycloaddition (I). For 1,3-dipolar cycloaddition (**I**), the potential energy profile in Fig. 1 and potential energy curve Fig. S1c† reveal that at $\varepsilon = 1$, **React → TS1** is a two-step process, in which the formation of π–π stacking (a) occurs first ($\Delta E^{\ddagger} = 24$ kJ mol^{-1}), followed by dipolarophile–iminum pair formation (b) in the transition structure **TS1** ($\Delta E^{\ddagger} = 50$ kJ mol^{-1}). **TS1** is characterized by the α,β-double bond of **Cin** staying exactly above the iminium ion (C_{29}^{PrFMN}–$N_{35}^{\text{PrFMN,+}}$–C_{34}^{PrFMN}, 1,3-dipole) of **PrFMN** (Fig. S1a†). It appears that pyrrolidine cycloadduct formation (c) and relaxation of π–π stacking (d) occur instantly in **TS1 → Int1**, thereby leading to the transformation of the enolate anion to a C=O group at the O_{30}^{PrFMN} atom.

At $\varepsilon = 78$, the potential energy profile in Fig. 1 and potential energy curve in Fig. S1c† are almost the same as those at $\varepsilon = 1$. The energy barriers for π–π stacking (a)$^{\varepsilon}$ and **TS1**$^{\varepsilon}$ formation (b)$^{\varepsilon}$ are slightly different, namely, $\Delta E^{\ddagger} = 26$ and 48 kJ mol^{-1}, respectively. This could be because cycloadduct formation (**React**$^{\varepsilon}$ **→ TS1**$^{\varepsilon}$ **→ Int1**$^{\varepsilon}$) does not involve direct charge (proton)

transfer (Fig. S1b†). Therefore, the electric field that is induced by the aqueous solvent ($\varepsilon = 78$) does not have a strong influence on the energy barriers.

Decarboxylation (II). At $\varepsilon = 1$, the potential energy profile in Fig. 2 and structures of the model molecular clusters on the potential energy curve in Fig. S2a† reveal that decarboxylation (**II**) (**Int1 → TS2 → Int2**) is a four-step process, in which the C_{α}^{Cin}–C_{43}^{Cin} bond extension (a) occurs in **Int1 → TS2** ($\Delta E^{\ddagger} = 60$ kJ mol^{-1}), followed by CO$_2$ elimination (b), C_{β}^{Cin}–C_{34}^{PrFMN} dissociation (c) and reorientation of the aromatic ring of **Cin** away from **PrFMN** (d) in **TS2 → Int2**. The potential energy profile in Fig. 2 and potential energy curve in Fig. S2c† show that at $\varepsilon = 78$, although the consecutive reaction scheme is not different from that at $\varepsilon = 1$, the C_{α}^{Cin}–C_{43}^{Cin} bond extension (a)$^{\varepsilon}$, CO$_2$ elimination (b)$^{\varepsilon}$ and C_{β}^{Cin}–C_{34}^{PrFMN} dissociation (c)$^{\varepsilon}$ occur readily in **Int1**$^{\varepsilon}$ **→ TS2**$^{\varepsilon}$ with a significantly lower energy barrier ($\Delta E^{\ddagger} = 39$ kJ mol^{-1}).

Acid catalyst (1) (III). The potential energy profile in Fig. 3 and precursor and transition structures of the model molecular clusters on the potential energy curves in Fig. S3a† indicate that at $\varepsilon = 1$, proton transfer from the COOH group of **Glu282** to C_{α}^{Cin} (a) and formation of the pyrrolidine cycloadduct (b) are associated with a low energy barrier; for **Int2b → TS3**, $\Delta E^{\ddagger} = 42$ kJ mol^{-1}. The formation of π–π stacking between **Cin** and **PrFMN** (c) is partly responsible for the stability of **Int3**.

The scenario is slightly different at $\varepsilon = 78$ (Fig. 3, S3b and c†), in which proton transfer from the COOH group of **Glu282** to C_{α}^{Cin} (a)$^{\varepsilon}$ instantly produces the transition state (**TS3**$^{\varepsilon}$); for **Int2b**$^{\varepsilon}$ **→ TS3**$^{\varepsilon}$, $\Delta E^{\ddagger} = 137$ kJ mol^{-1}. At $\varepsilon = 78$, acid catalyst (1) is accomplished through the formation of pyrrolidine cycloadduct (b)$^{\varepsilon}$ and π–π stacking intermediate (c)$^{\varepsilon}$ (**Int3**$^{\varepsilon}$).

Cycloelimination (IV). To complete the enzymatic reaction cycle, **β-MeSt** and **PrFMN** are formed through cycloelimination (**IV**). In **Int3 → TS4 → Prod** at $\varepsilon = 1$ (Fig. 4), the C_{β}^{Cin}–C_{34}^{PrFMN} extension (a) and dissociation (b) and C_{α}^{Cin}–C_{29}^{PrFMN} dissociation (c) occur consecutively in **Int3 → TS4** ($\Delta E^{\ddagger} = 81$ kJ mol^{-1}),

Fig. 2 Potential energy profiles for decarboxylation (II) simplified based on the B3LYP/DZP and NEB results in $\varepsilon = 1$ and 78 (Fig. S2†). Energies are in kJ mol. (…) and (…)$^{\varepsilon}$ = scenarios in the elementary reactions in $\varepsilon = 1$ and 78, respectively; ‡ = energy barrier.

Fig. 3 Potential energy profiles for acid catalyst (1) (III) simplified based on the B3LYP/DZP and NEB results in $\varepsilon = 1$ and 78 (Fig. S3†). Energies are in kJ mol. (…) and (…)$^{\varepsilon}$ = scenarios in the elementary reactions in $\varepsilon = 1$ and 78, respectively; ‡ = energy barrier.

Fig. 4 Potential energy profiles for cycloelimination (IV) simplified based on the B3LYP/DZP and NEB results in $\varepsilon = 1$ and 78 (Fig. S4†). Energies are in kJ mol. (…) and (…)$^{\varepsilon}$ = scenarios in the elementary reactions in $\varepsilon = 1$ and 78, respectively; ‡ = energy barrier.

whereas β-MeSt leaves the iminium ion (**TS4 → Prod**) on a barrierless potential curve; the model molecular cluster **Prod** consists of free β-MeSt and the regenerated **PrFMN, Glu277, Arg173H$^+$** and **Gln190** (Fig. S4a†), as in **React**.

The scenarios are slightly different at $\varepsilon = 78$ (Fig. 4 and S4b†), in which the C_β^{Cin}–C_{34}^{PrFMN} extension (a)$^{\varepsilon}$ takes place first in **Int3$^{\varepsilon}$ → TS4$^{\varepsilon}$** with a comparable energy barrier ($\Delta E^{\ddagger} = 77$ kJ mol^{-1}), followed by the C_β^{Cin}–C_{34}^{PrFMN} (b)$^{\varepsilon}$ and C_α^{Cin}–C_{29}^{PrFMN} dissociations (c)$^{\varepsilon}$.

Acid catalyst (2) (V). Based on the potential energy profiles and potential energy curves that have been discussed up to this point, the highest energy barrier at $\varepsilon = 1$ is for cycloelimination (**IV**) ($\Delta E^{\ddagger} = 81$ kJ mol^{-1}), whereas that at $\varepsilon = 78$ is for acid catalyst (1) (**III**) ($\Delta E^{\ddagger} = 137$ kJ mol^{-1}). To complete the discussion on the potential energy profiles and potential energy curves of the elementary reactions, the route for generating **Prod** directly from
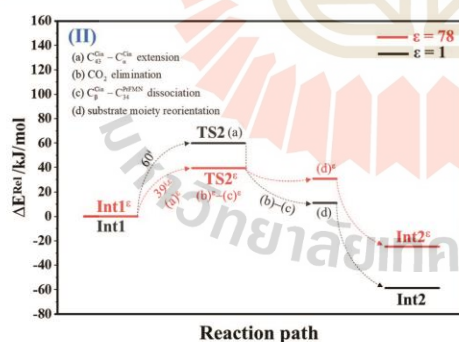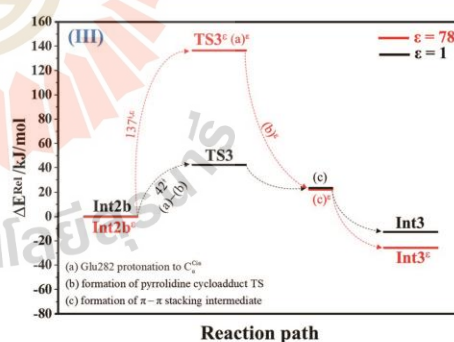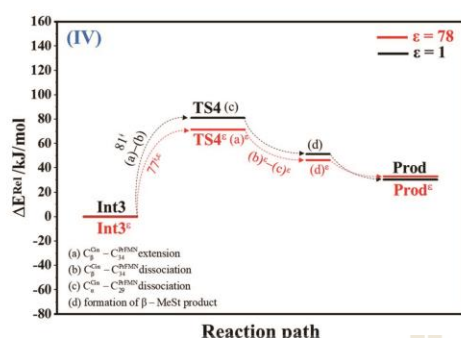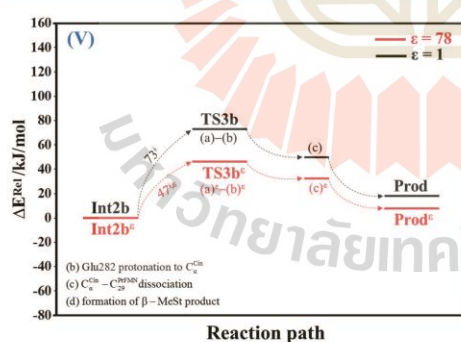

Fig. 5 Potential energy profiles for acid catalyst (2) (V) simplified based on the B3LYP/DZP and NEB results in $\varepsilon = 1$ and 78 (Fig. S5†). Energies are in kJ mol. (…) and (…)$^{\varepsilon}$ = scenarios in the elementary reactions in $\varepsilon = 1$ and 78, respectively; ‡ = energy barrier.

Int2b without the formation of pyrrolidine cycloadduct (Fig. 5 and S5†) is discussed. At $\varepsilon = 1$, the proton transfer from the COOH group of **Glu282** to C_α^{Cin} (a) instantly leads to C_α^{Cin}–C_{29}^{PrFMN} dissociation (b) and the formation of β-MeSt (c) with a slightly lower energy barrier ($\Delta E^{\ddagger} = 73$ kJ mol^{-1}) compared with **Int3 → TS4 → Prod** ($\Delta E^{\ddagger} = 81$ kJ mol^{-1}), whereas at $\varepsilon = 78$, **Int2b$^{\varepsilon}$ → TS3b$^{\varepsilon}$ → Prod$^{\varepsilon}$** involves a considerably lower energy barrier ($\Delta E^{\ddagger} = 47$ kJ mol^{-1}). Therefore, the direct route at $\varepsilon = 78$ should also be considered in further discussion.

The effect of a high local dielectric environment

The potential energy profiles for the enzymatic decarboxylation of α,β-unsaturated acid that were obtained in this and previous studies are presented in Fig. 6. To verify the theoretical results, our potential energy profiles at $\varepsilon = 1$ are compared with profiles at $\varepsilon = 4$ (ref. 5) (Fig. 6a) that were obtained from B3LYP/6-311+G(2d,2p)//6-31G(d,p) calculations with the intrinsic reaction coordinate (IRC) and conductor-like polarizable continuum model (CPCM) methods. Because **React** and **Int2b** possess different number of atoms (115 and 126 atoms, respectively), the elementary reactions are categorized into two groups, namely, the decarboxylation/CO$_2$ elimination (**React → TS1 → Int1 → TS2 → Int2**) and β-MeSt formation/cofactor regeneration on the indirect (**Int2b → TS3 → Int3 → TS4 → Prod**) and direct routes (**Int2b → TS3b → Prod**). Comparison of the potential energy profiles in Fig. 6a reveals similar energy barriers at $\varepsilon = 1$ and 4,[5] except for acid catalyst (1) (**III**), for which $\Delta E^{\ddagger}$ at $\varepsilon = 4$ is ∼17 kJ mol^{-1} higher than that at $\varepsilon = 1$, thereby implying that a slight increase in ε could result in a significant change in the energy barrier for the elementary reaction involving proton transfer.

The potential energy profiles in Fig. 6b confirm the above observation by showing that the increase in the polarity of the solvent from $\varepsilon = 1$ to 78 leads to significant changes in $\Delta E^{\ddagger}$, especially for the transition states that involve proton transfer; $\Delta E^{\ddagger}$ for acid catalyst (1) (**III**) increases from 42 to 137 kJ mol^{-1}, whereas that of acid catalyst (2) (**V**) decreases from 73 to 47 kJ mol^{-1}. It appears that due to the regeneration of the positive and negative charges at **PrFMN**, the **Glu277, Arg173H$^+$** and **Gln190** residues, the end-product cluster (**Prod**) is more stable at $\varepsilon = 78$ than at $\varepsilon = 1$.

Kinetics and thermodynamics of the elementary reactions

All the kinetic and thermodynamic results at $\varepsilon = 1$ and 78 that were obtained based on the TST method are presented in Tables S5 and S6,† respectively. The emphasis will be on the results at 277 K in Tables 1 and 2, which is the temperature at which the stopped-flow spectrophotometric experiment[10] was performed. Comparison of the rate constants that were obtained using different methods reveals considerable differences only for k_{tr}^{Class}. This confirms that for large biological molecules, at least the zero-point vibrational energies must be included in TST calculations. The values for $T_c = 3$–123 K suggest a low/no quantum mechanical tunneling effect in the studied temperature range. At $\varepsilon = 1$, $k_{tr}^{Q\text{-vib}}$, $k_{tr}^{S\text{-Wig}}$ and $k_{tr}^{F\text{-Wig}}$ are almost the same over the temperature range of 200–371 K. At $\varepsilon = 78$, $k_{tr}^{Q\text{-vib}}$, $k_{tr}^{S\text{-Wig}}$ and $k_{tr}^{F\text{-Wig}}$ are approximately the same, except for
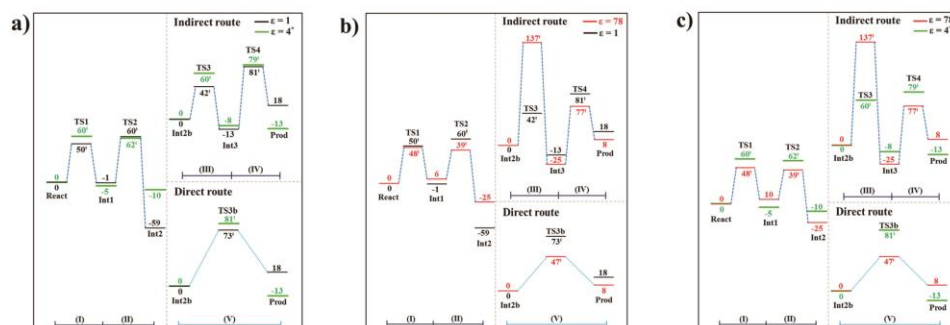
Fig. 6 Comparison of the potential energy profiles for enzymatic decarboxylation of α,β-unsaturated acid obtained in this and previous studies. Energy barriers are in kJ mol⁻¹. (I) = 1,3-dipolar cycloaddition; (II) = decarboxylation; (III) = acid catalyst (1); (IV) = cycloelimination; (V) = acid catalyst (2). (a) The B3LYP/DZP results in $\varepsilon = 1$ (black solid lines) compared with those obtained using the B3LYP/6-311+G(2d,2p)//6-31G(d,p) and CPCM methods ($\varepsilon = 4$) in ref. 5 (green solid lines). (b) The B3LYP/DZP results in $\varepsilon = 1$ and 78 (black and red solid lines, respectively). (c) The B3LYP/DZP results in $\varepsilon = 78$ compared with those obtained using the B3LYP/6-311+G(2d,2p)//6-31G(d,p) and CPCM methods ($\varepsilon = 4$) in ref. 5 (red and green solid lines, respectively).

Table 1 Thermodynamics and kinetics of the elementary reactions of the enzymatic decarboxylation of α,β-unsaturated acid in $\varepsilon = 1$ at 277 K. Rate constants, temperatures and energies are in s⁻¹, K and kJ mol⁻¹, respectively; $\Delta E^{\ddagger}$ = energy barrier on the optimized reaction path; $\Delta E^{\ddagger,ZPE}$ = difference between E^{ZPE} of the transition structure and precursor; $\Delta E^{\ddagger,ZPC}$ = zero point energy-corrected energy barrier; $\Delta H^{\ddagger}$ = activation enthalpy; T_c = crossover temperature; $k_{f/r}^{S\text{-Wig}}$ = rate constant obtained with quantized vibrations and quantum mechanical tunneling through the simple Wigner correction; $k_{f/r}^{Arr}$ = Arrhenius rate constant; $\Delta G^{\ddagger}$ = activation free energy; $\Delta S^{\ddagger}$ = activation entropy; f/r = forward or reverse direction

Elementary reaction ($\varepsilon = 1$)	$\Delta E^{\ddagger}$	$\Delta E^{\ddagger,ZPE}$	$\Delta E^{\ddagger,ZPC}$	$\Delta H^{\ddagger}$	T_c	$k_{f/r}^{S\text{-Wig}}$	$k_{f/r}^{Arr}$	$\Delta G^{\ddagger}$	$\Delta S^{\ddagger}$
1,3-Dipolar cycloaddition (React → TS1)	50.0	6.1	56.1	58.2	3	3.44×10^3	2.75×10^2	49.0	3.3×10^{-2}
1,3-Dipolar cycloaddition (TS1 ← Int1)	51.0	−9.3	41.7	58.0	3	4.77×10^8	3.72×10^5	32.4	9.2×10^{-2}
Decarboxylation (Int1 → TS2)	60.2	−5.0	55.2	56.1	4	1.26×10^{-2}	1.02×10^{-3}	77.8	-7.8×10^{-2}
Decarboxylation (TS2 ← Int2)	118.3	7.9	126.2	119.8	4	2.49×10^{-18}	1.91×10^{-19}	161.2	-1.5×10^{-1}
Acid catalyst (1) (Int2b → TS3)	42.4	7.2	49.6	46.9	15	1.71×10^8	1.37×10^7	24.1	8.2×10^{-2}
Acid catalyst (1) (TS3 ← Int3)	55.2	−2.9	52.3	53.9	15	1.29×10^{11}	1.05×10^{10}	8.8	1.6×10^{-1}
Cycloelimination (Int3 → TS4)	81.0	−11.5	69.5	75.2	7	1.31×10^2	1.06×10^1	56.5	6.8×10^{-2}
Cycloelimination (TS4 ← Prod)	50.2	3.5	53.7	52.8	7	1.46×10^1	1.16×10^0	61.6	-3.2×10^{-2}
Acid catalyst (2) (Int2b → TS3b)	72.9	−7.5	65.4	71.0	31	6.86×10^{10}	5.47×10^9	10.3	2.2×10^{-1}
Acid catalyst (2) (TS3b ← Prod)	54.7	−2.3	52.4	55.8	31	5.27×10^{10}	4.22×10^9	10.9	1.6×10^{-1}

1,3-dipolar cycloaddition (I) and acid catalyst (1) (III), for which $k_{f/r}^{S\text{-Wig}}$ and $k_{f/r}^{E\text{-Wig}}$ are slightly higher than $k_{f/r}^{Q\text{-vib}}$ at low temperatures. Therefore, further discussion focuses only on $k_{f/r}^{S\text{-Wig}}$.

Analysis of $k_{f/r}^{S\text{-Wig}}$ at 277 K confirms that the fluctuation of the local dielectric environment must be included in the mechanistic model; otherwise, some of the hypothesized elementary reactions are too slow to be monitored in the stopped-flow spectroscopic experiment. For example, decarboxylation (II) (Int1$^\varepsilon$ → TS2$^\varepsilon$ → Int2$^\varepsilon$) is kinetically favorable at $\varepsilon = 78$, with $k_{f}^{S\text{-Wig},\varepsilon} = 1.21 \times 10^{10}$ s⁻¹, whereas at $\varepsilon = 1$, $k_{f/r}^{S\text{-Wig}} = 1.26 \times 10^{-2}$ s⁻¹. In contrast, for acid catalyst (1) (III) at $\varepsilon = 78$ (Int2b$^\varepsilon$ → TS3$^\varepsilon$ → Int3$^\varepsilon$), $k_{f}^{S\text{-Wig},\varepsilon} = 9.60 \times 10^{-14}$ s⁻¹, whereas for the same reaction at $\varepsilon = 1$ (Int2b → TS3 → Int3), $k_{f}^{S\text{-Wig}} = 1.71 \times 10^8$ s⁻¹, which indicates that acid catalyst (1) (III) is kinetically favorable in a low local dielectric environment. This is in accordance with our previous work,[11,14,24] in which the fluctuation of the local dielectric environment was confirmed to govern the kinetics of

proton transfer processes; based on this analysis, **React → TS1 → Int1** (1,3-dipolar cycloaddition (I)) is kinetically more favorable than **React$^\varepsilon$ → TS1$^\varepsilon$ → Int1$^\varepsilon$** ($k_{f}^{S\text{-Wig}} = 3.44 \times 10^3$ and $k_{f}^{S\text{-Wig},\varepsilon} = 2.44 \times 10^3$ s⁻¹, respectively).

Attempt was made to correlate the rate constants obtained from the TST method with the experimental data.[10] Because the experiments on enzyme kinetics are complex due to several factors, such as experimental conditions (e.g., temperature, pH and ionic strength), sensitivity of the spectroscopic equipment and measurement timescale (time resolution), it is not straightforward to compare our theoretical results with the experimental data. In this work, the Arrhenius rate constants (k^{Arr}) were calculated in terms of $\Delta G^{\ddagger}$, which were obtained from the TST method (Tables S5 and S6†), using $k^{Arr} = Ae^{-\Delta G^{\ddagger}/k_B T}$.

Because the pre-exponential constant (A) in the Arrhenius equation is not known for this enzyme system, the value was tentatively approximated using the highest rate constants

Table 2 Thermodynamics and kinetics of the elementary reactions of the enzymatic decarboxylation of α,β-unsaturated acid in $\varepsilon = 78$ at 277 K. Rate constants, temperatures and energies are in s^{-1}, K and kJ mol^{-1}, respectively; $\Delta E^{\ddagger,\varepsilon}$ = energy barrier on the optimized reaction path; $\Delta E^{\ddagger,\text{ZPE},\varepsilon}$ = difference between $E^{\text{ZPE},\varepsilon}$ of the transition structure and precursor; $\Delta E^{\ddagger,\text{ZPC},\varepsilon}$ = zero point energy-corrected energy barrier; $\Delta H^{\ddagger,\varepsilon}$ = activation enthalpy; T_c = crossover temperature; $k_{f/r}^{\text{S-Wig},\varepsilon}$ = rate constant obtained with quantized vibrations and quantum mechanical tunneling through the simple Wigner correction; $k_{f/r}^{\text{Arr},\varepsilon}$ = Arrhenius rate constant; $\Delta G^{\ddagger,\varepsilon}$ = activation free energy; $\Delta S^{\ddagger,\varepsilon}$ = activation entropy; f/r = forward or reverse direction

Elementary reaction ($\varepsilon = 78$)	$\Delta E^{\ddagger,\varepsilon}$	$\Delta E^{\ddagger,\text{ZPE},\varepsilon}$	$\Delta E^{\ddagger,\text{ZPC},\varepsilon}$	$\Delta H^{\ddagger,\varepsilon}$	T_c	$k_{f/r}^{\text{S-Wig},\varepsilon}$	$k_{f/r}^{\text{Arr},\varepsilon}$	$\Delta G^{\ddagger,\varepsilon}$	$\Delta S^{\ddagger,\varepsilon}$
1,3-Dipolar cycloaddition (**React**$^\varepsilon$ → **TS1**$^\varepsilon$)	48.0	−0.4	47.6	48.0	123	2.44×10^3	1.50×10^2	50.4	-8.7×10^{-3}
1,3-Dipolar cycloaddition (**TS1**$^\varepsilon$ ← **Int1**$^\varepsilon$)	43.8	−0.3	43.5	43.8	43	8.14×10^3	6.28×10^2	47.1	-1.2×10^{-2}
Decarboxylation (**Int1**$^\varepsilon$ → **TS2**$^\varepsilon$)	38.8	−14.7	24.1	31.7	44	1.21×10^{10}	9.63×10^8	14.3	6.3×10^{-2}
Decarboxylation (**TS2**$^\varepsilon$ ← **Int2**$^\varepsilon$)	69.3	5.9	75.2	75.0	44	5.12×10^{-5}	3.94×10^{-6}	90.6	-5.6×10^{-2}
Acid catalyst (1) (**Int2b**$^\varepsilon$ → **TS3**$^\varepsilon$)	136.6	−7.4	129.2	127.9	61	9.60×10^{-14}	7.00×10^{-15}	137.0	-3.3×10^{-2}
Acid catalyst (1) (**TS3**$^\varepsilon$ ← **Int3**$^\varepsilon$)	161.7	−22.1	139.6	142.5	61	2.29×10^{-15}	1.60×10^{-16}	145.7	-1.2×10^{-2}
Cycloelimination (**Int3**$^\varepsilon$ → **TS4**$^\varepsilon$)	77.4	−10.0	67.4	69.8	51	5.34×10^{-1}	4.09×10^{-2}	69.3	1.8×10^{-3}
Cycloelimination (**TS4**$^\varepsilon$ ← **Prod**$^\varepsilon$)	44.3	6.9	51.2	47.3	51	2.09×10^{-1}	1.57×10^{-2}	71.5	-8.7×10^{-2}
Acid catalyst (2) (**Int2b**$^\varepsilon$ → **TS3b**$^\varepsilon$)	46.6	−5.2	41.4	44.5	55	4.53×10^6	3.41×10^5	32.6	4.3×10^{-2}
Acid catalyst (2) (**TS3b**$^\varepsilon$ ← **Prod**$^\varepsilon$)	38.1	−1.7	36.4	37.3	55	7.31×10^5	5.50×10^4	36.8	1.8×10^{-3}

($\sim 10^{11}$ s^{-1}) with low $\Delta G^\ddagger$ (Tables S5 and S6†). Investigation of Tables S5 and S6† revealed that the highest rate constants at 277 and 300 K are $k_{f/r}^{\text{S-Wig}}$ = 7.56×10^{11}, 7.02×10^{11}, 3.28×10^{11} and 1.29×10^{11} s^{-1}, and the average value is 4.79×10^{11} s^{-1}. Based on this approximated pre-exponential constant and the values of $\Delta G^\ddagger$, $k_{f/r}^{\text{Arr}}$ were computed and included in Tables S5 and S6.† The values at 277 K in Tables 1 and 2 will be used in further discussion.

To correlate k_f^{Arr} and $k_f^{\text{Arr},\varepsilon}$ with the experimental rate constants,[10] the elementary reactions that occur within the time resolution of stopped-flow spectrophotometry ($\sim 10^{-3}$ s) are considered.[10] Based on the assumption that the two active sites on **FDC1** react with different rates (denoted (a) and (b) for the fast and slow sites, respectively),[10] the stopped-flow spectrophotometric results at 277 K and the half-of-sites model suggested that for the fast site (a), the **PrFMN**$^{\text{iminium}}$–cinnamic acid cycloadduct is formed with $k_{1(a)}$ = 131 s^{-1} and is converted to the **PrFMN**$^{\text{iminium}}$–styrene cycloadduct with $k_{2(a)}$ = 75 s^{-1}. However, cycloelimination to generate the styrene product and free **FDC1** appeared to be the slowest process, with k_{cat} = 11 s^{-1}. Because the observed rete constants were reported to be in the range of k_{obs} = 0.75–2.0 × 10^2 s^{-1}, only the elementary reactions with k_f^{Arr} larger than k_{obs} are included in the proposed mechanism. Based on the analysis of all the rate constants (k_f^{Arr} and $k_f^{\text{Arr},\varepsilon}$) and activation free energies ($\Delta G^\ddagger$) in Tables 1 and 2, the kinetically controlled paths for the enzymatic decarboxylation of α,β-unsaturated acid (long rightwards blue arrows) are proposed in Fig. 7a.

Comparison of the rate constants of the proposed elementary reactions (long rightwards blue arrows in Fig. 7a) with those that were obtained in the experiment suggests that within the time resolution of stopped-flow spectrophotometry, k_f^{Arr} of 1,3-dipolar cycloaddition (**I**) is compatible (associated) with $k_{1(a)}$; for **React**$^\varepsilon$ → **TS1**$^\varepsilon$ → **Int1**$^\varepsilon$ and **React** → **TS1** → **Int1**, $k_f^{\text{Arr},\varepsilon}$ = 1.50×10^2 and k_f^{Arr} = 2.75×10^2 s^{-1} at $\varepsilon = 78$ and 1, respectively. However, because decarboxylation (**II**) at $\varepsilon = 1$ is slower than the time resolution of stopped-flow spectrophotometry (k_f^{Arr} = 1.02×10^{-3} s^{-1}), decarboxylation (**II**) is likely to occur in a high local dielectric environment. Likewise, although the direct route for

generating **β-MeSt** (acid catalyst (2) (**V**)) is kinetically very favorable ($k_f^{\text{Arr},\varepsilon}$ = 3.41×10^5 and k_f^{Arr} = 5.47×10^9 s^{-1} at $\varepsilon = 78$ and 1, respectively), it is too fast to be monitored in the stopped-flow spectroscopic experiment. Because the indirect route at $\varepsilon = 1$ (**Int3** → **TS4** → **Prod**) is within the time resolution of stopped-flow spectrophotometry (k_f^{Arr} = 1.06×10^1 s^{-1}), cycloelimination (**IV**), which includes **β-MeSt** formation and cofactor regeneration, could be the rate-determining step. This analysis is in accordance with the conclusion of ref. 3 and is in good agreement with the kinetics results in ref. 10, in which cycloelimination (**IV**) of the **PrFMN**$^{\text{iminium}}$–**β-MeSt** cycloadduct and diffusion from the active site represent the slowest processes, k_{cat} = 1.13×10^1 s^{-1}.

To examine whether the proposed kinetically controlled (favorable) mechanisms in Fig. 7a (long rightward blue arrows) are also thermodynamically controlled, the standard free energy changes (ΔG^0 and $\Delta G^{0,\varepsilon}$) of each elementary reaction were calculated from the difference between the activation free energies ($\Delta G^\ddagger$) in the forward and reverse directions. In addition, because the entropic effect has been suggested to play an important role in enzymatic reactions,[25] an attempt was made to study the entropy changes of the system (the model molecular clusters); although several known and unknown factors contribute to the entropy change, e.g., the entropy change of the surrounding, we tentatively consider only the entropy change in the system. The standard entropy changes of each elementary reaction (ΔS^0 and $\Delta S^{0,\varepsilon}$) were computed in the studied temperature range (200–371 K). These thermodynamic data are listed in Table 3, and the values at 277 K are presented in Fig. 7b.

The results reveal similar trends for ΔG^0 and $\Delta G^{0,\varepsilon}$ (Table 3), except for acid catalyst (1) (**III**), in which $\Delta G^{0,\varepsilon}$ is negative, whereas ΔG^0 is positive; at 277 K, ΔG^0 and $\Delta G^{0,\varepsilon}$ for 1,3-dipolar cycloaddition (**I**) are both positive, whereas those for decarboxylation (**II**), cycloelimination (**IV**) and acid catalyst (2) (**V**) are all negative. Analysis of the scenarios in the elementary reactions in Fig. S1–S5† suggests that at least three factors affect the standard free energy and entropy changes of the systems, namely, the disorder/order due to breaking/formation of covalent bonds,
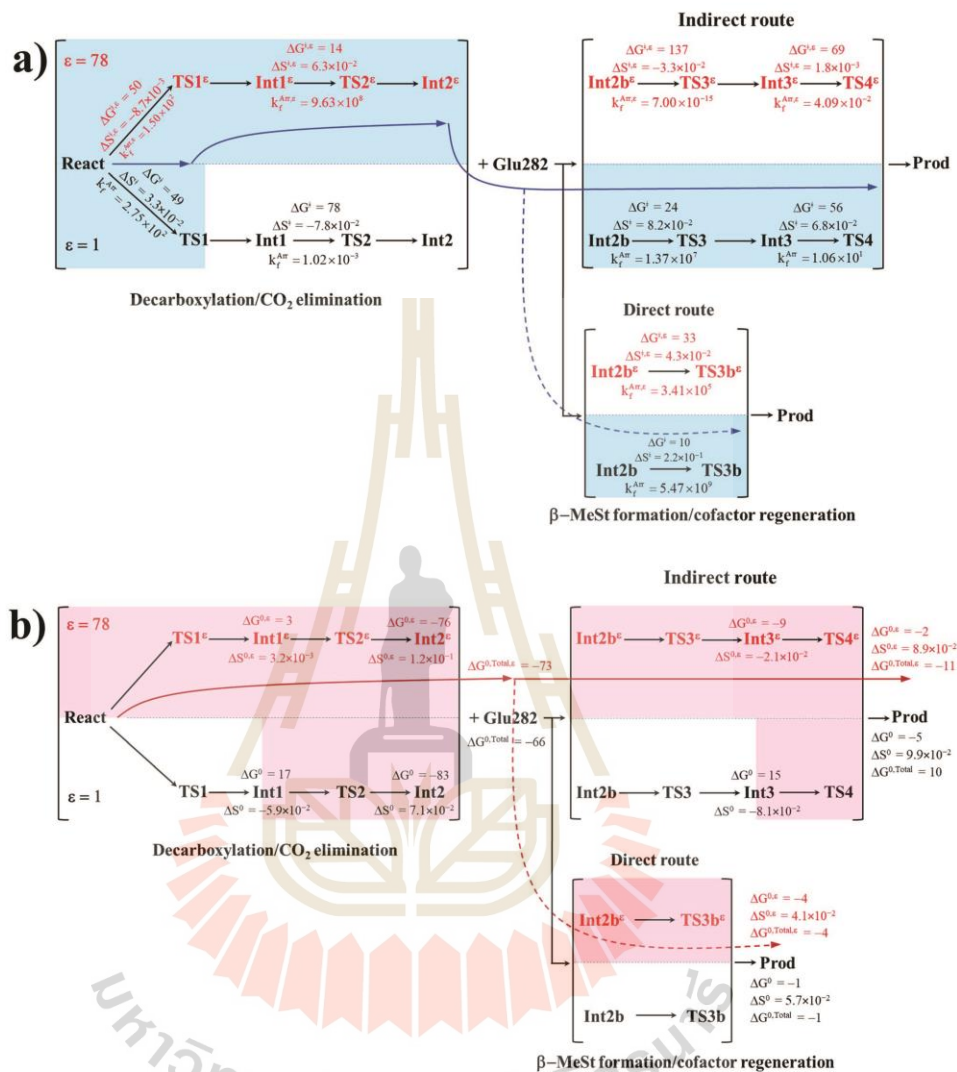
Fig. 7 (a) The kinetically controlled paths (long rightwards blue arrows) for the enzymatic decarboxylation of α,β-unsaturated acid at 277 K, proposed based on the potential energy profiles (Fig. 6), Arrhenius rate constants (k_f^{Arr} and $k_f^{Arr,\varepsilon}$) and activation free energies ($\Delta G^{\ddagger}$ and $\Delta G^{\ddagger,\varepsilon}$) obtained from the TST method. Energies and rate constants are in kJ mol^{-1} and s^{-1}, respectively. Long rightwards blue dashed line arrow is an alternative kinetically controlled path, which is too fast to be monitored using the stopped-flow spectroscopic method. (b) The thermodynamically controlled paths (long rightwards red arrows) for the enzymatic decarboxylation of α,β-unsaturated acid at 277 K, proposed based on the standard free energy (ΔG^0 and $\Delta G^{0,\varepsilon}$) and entropy (ΔS^0 and $\Delta S^{0,\varepsilon}$) changes of the elementary reactions. Energies are in kJ mol^{-1}. Long rightwards red dashed line arrow is an alternative thermodynamic controlled path. $\Delta G^{\ddagger}$ and $\Delta G^{\ddagger,\varepsilon}$ = activation free energies; $\Delta S^{\ddagger}$ and $\Delta S^{\ddagger,\varepsilon}$ = activation entropies; k_f^{Arr} and $k_f^{Arr,\varepsilon}$ = Arrhenius rate constants. ΔG^0 and $\Delta G^{0,\varepsilon}$ = standard free energy changes of the elementary reactions; ΔS^0 and $\Delta S^{0,\varepsilon}$ = standard entropies of reaction; $\Delta G^{0,Total}$ and $\Delta G^{0,Total,\varepsilon}$ = total standard free energy changes.

Table 3 Standard free energies and entropies of the elementary reactions in $\varepsilon = 1$ and 78, obtained from TST calculations. Energies and temperatures are in kJ mol^{-1} and K, respectively. ΔG^0 and $\Delta G^{0,\varepsilon}$ = standard free energies; ΔS^0 and $\Delta S^{0,\varepsilon}$ = standard entropies

Elementary reaction	T	ΔG^0	$\Delta G^{0,\varepsilon}$	ΔS^0	$\Delta S^{0,\varepsilon}$
1,3-Dipolar cycloaddition (**I**)	200	15.7	3.4	-7.8×10^{-2}	3.0×10^{-3}
	277	16.6	3.3	-5.9×10^{-2}	3.3×10^{-3}
	300	16.9	3.3	-6.0×10^{-2}	3.0×10^{-3}
	371	18.1	3.0	-4.8×10^{-2}	3.2×10^{-3}
Decarboxylation (**II**)	200	-78.2	-67.5	7.2×10^{-2}	1.2×10^{-1}
	277	-83.4	-76.3	7.1×10^{-2}	1.2×10^{-1}
	300	-85.0	-79.0	7.1×10^{-2}	1.2×10^{-1}
	371	-90.1	-87.6	7.1×10^{-2}	1.2×10^{-1}
Acid catalyst (1) (**III**)	200	9.3	-10.0	-8.2×10^{-2}	-2.3×10^{-2}
	277	15.3	-8.6	-8.1×10^{-2}	-2.1×10^{-2}
	300	17.1	-8.1	-8.0×10^{-2}	-2.2×10^{-2}
	371	22.9	-6.5	-8.1×10^{-2}	-2.2×10^{-2}
Cycloelimination (**IV**)	200	2.3	4.4	1.0×10^{-1}	9.1×10^{-2}
	277	-5.1	-2.2	9.9×10^{-2}	8.9×10^{-2}
	300	-7.3	-4.2	9.9×10^{-2}	8.9×10^{-2}
	371	-14.4	-10.6	9.9×10^{-2}	8.9×10^{-2}
Acid catalyst (2) (**V**)	200	3.7	-1.1	5.8×10^{-2}	4.2×10^{-2}
	277	-0.6	-4.2	5.7×10^{-2}	4.1×10^{-2}
	300	-1.9	-5.1	5.7×10^{-2}	4.1×10^{-2}
	371	-6.0	-8.1	5.7×10^{-2}	4.1×10^{-2}

increase/decrease in the number of molecules, and charge (proton) transfer at the active site. For example, for 1,3-dipolar cycloaddition (**I**), ΔS^0 and $\Delta S^{0,\varepsilon}$ are only slightly changed due to the formation of the pyrrolidine cycloadduct, whereas the values for decarboxylation (**II**), cycloelimination (**IV**) and acid catalyst (2) (**V**) are all positive because these elementary reactions involve both net covalent bond breaking and an increase in the number of molecules in the active site, e.g., decarboxylation (**II**) involving C_α^{Cin}–C_β^{Cin} and C_β^{Cin}–C_{34}^{PrFMN} covalent bond dissociations and formations of free CO_2 molecule.

It appears that the entropy changes for the elementary reactions that generate molecules, e.g., decarboxylation (**II**) and cycloelimination (**IV**), are more pronounced than those for the reactions that involve only charge (proton) transfer, covalent bond breaking/formation and structural reorientation, e.g., 1,3-dipolar cycloaddition (**I**) and catalyst (1) (**III**) at $\varepsilon = 78$. Based on the total free energy changes ($\Delta G^{0,\text{Total}}$ and $\Delta G^{0,\text{Total},\varepsilon}$ in Fig. 7b), the decarboxylation/CO_2 elimination reaction ((**I**) and (**II**)) at $\varepsilon = 78$ is slightly more favorable than at $\varepsilon = 1$ ($\Delta G^{0,\text{Total},\varepsilon} = -73$ and $\Delta G^{0,\text{Total}} = -66$ kJ mol^{-1}). Likewise, the **β-MeSt** formation/cofactor regenerations in the indirect route ((**III**) and (**IV**)) at $\varepsilon = 78$ are significantly more favorable than at $\varepsilon = 1$, ($\Delta G^{0,\text{Total},\varepsilon} = -11$ and $\Delta G^{0,\text{Total}} = 10$ kJ mol^{-1}). These results lead to the conclusion that elementary reactions that involve charge (proton) transfer favor a high local dielectric environment. The proposed thermodynamically favorable paths are illustrated in Fig. 7b (long rightwards red arrows).

Conclusions

Enzymatic decarboxylation of α,β-unsaturated acid through ferulic acid decarboxylase (**FDC1**) has been of interest because the reaction is anticipated to be a promising, environmentally friendly industrial process for producing styrene and its derivatives from natural resources. In this study, the proposed mechanisms for the enzymatic decarboxylation of α,β-unsaturated acid were theoretically studied using the B3LYP/DZP method and TST. The present study began with geometry optimizations of the proposed model molecular clusters in extreme local dielectric environments ($\varepsilon = 1$ and 78). The model molecular clusters consisted of the **Cin** substrate, **PrFMN** cofactor and all relevant residues of **FDC1** at the active site. These moderate model molecular clusters made it possible to calculate kinetic and thermodynamic properties with reasonable computational resources.

Analysis of the B3LYP/DZP results showed that the active site structure and volume are not significantly changed in the enzymatic decarboxylation reaction, which suggested that the **FDC1** backbone does not play the most important role in enzymatic decarboxylation processes. These findings are in accordance with the experimental result that the **Glu277–Arg173–Glu282** residue network was conserved in the enzymatic decarboxylation reaction. These findings confirmed that the selected model molecular clusters (including the active site) are reasonable. Comparison of the potential energy profiles that were obtained via the NEB method revealed similar energy barriers at $\varepsilon = 1$ and 4,[5] except for acid catalyst (1), for which $\Delta E^{\ddagger}$ at $\varepsilon = 4$ is higher than that at $\varepsilon = 1$, thereby implying that an increase in the local dielectric environment could result in a significant change in the energy barrier for the elementary reaction that involves proton transfer. The potential energy profiles at $\varepsilon = 78$ confirmed that the increase in the polarity of the solvent could lead to significant changes in $\Delta E^{\ddagger}$, especially for the transition states that involve charge (proton) transfer.

Comparison of the rate constants that were obtained based on various methods revealed that the zero-point vibrational energies are important and cannot be neglected in TST calculations. Although the values of the crossover temperatures suggested a low or no quantum mechanical tunneling effect on the

enzymatic decarboxylation of α,β-unsaturated acid, it is advisable to include this effect in the theoretical study on every enzymatic reaction to assure that the effect can be neglected at least in the studied temperature range. Analysis of the rate constants at $\varepsilon = 1$ and 78 confirmed that the inclusion of the fluctuation of the local dielectric environment in the mechanistic model is essential; otherwise, some of the hypothesized elementary reactions are too slow to be monitored using the stopped-flow spectroscopic method. Because the rate constants at $\varepsilon = 1$ and 78 are not compatible with the time resolution of stopped-flow spectro-photometry, the direct route for generating **Prod** through acid catalyst (2) is unlikely to be utilized, whereas the cycloelimination that occurs in the indirect route in a low local dielectric environment is the rate determining step.

To examine the entropic effect and determine whether the proposed kinetically controlled (favorable) mechanisms are also thermodynamically controlled, the standard free energy and entropy changes of the elementary reactions were calculated. The results showed that at 277 K, the thermodynamic properties of the elementary reactions that involve charge (proton) transfer ((**III**) and (**IV**)) are strongly affected by a high local dielectric environment, which led to the conclusion that overall, the enzymatic decarboxylation of α,β-unsaturated acid is thermodynamically controlled in a high local dielectric environment. It appeared that the factors that affect the standard entropy changes are the disorder/order due to breaking/formation of covalent bonds and charge (proton) transfer in the active site; the standard entropy changes due to generation of molecules are the most significant (pronounced). The results that are reported in this work illustrate for the first time scenarios in each elementary reaction and provide insight into the effect of the local dielectric environment on the kinetics and thermodynamics of the enzymatic decarboxylation process of α,β-unsaturated acid, which could be used as guidelines for further theoretical and experimental studies on the same and similar systems.

Conflicts of interest

There are no conflicts to declare.

Acknowledgements

References

1 K. A. Payne, M. D. White, K. Fisher, B. Khara, S. S. Bailey, D. Parker, N. J. Rattray, D. K. Trivedi, R. Goodacre and R. Beveridge, *Nature*, 2015, **522**, 497–501.

2 T. Li, L. Huo, C. Pulley and A. Liu, *Bioorg. Chem.*, 2012, **43**, 2–14.

3 K. L. Ferguson, N. Arunrattanamook and E. N. G. Marsh, *Biochemistry*, 2016, **55**, 2857–2863.

4 K. L. Ferguson, J. D. Eschweiler, B. T. Ruotolo and E. N. G. Marsh, *J. Am. Chem. Soc.*, 2017, **139**, 10972–10975.

5 C.-L. Lan and S.-L. Chen, *J. Org. Chem.*, 2016, **81**, 9289–9295.

6 R. McKenna and D. R. Nielsen, *Metab. Eng.*, 2011, **13**, 544–554.

7 S. S. Bailey, K. A. P. Payne, A. Saaret, S. A. Marshall, I. Gostimskaya, I. Kosov, K. Fisher, S. Hay and D. Leys, *Nat. Chem.*, 2019, **11**, 1049–1057.

8 G. Tian and Y. Liu, *Phys. Chem. Chem. Phys.*, 2017, **19**, 7733–7742.

9 S. S. Bailey, K. A. P. Payne, K. Fisher, S. A. Marshall, M. J. Cliff, R. Spiess, D. A. Parker, S. E. J. Rigby and D. Leys, *J. Biol. Chem.*, 2018, **293**, 2272–2287.

10 A. K. Kaneshiro, K. J. Koebke, C. Zhao, K. L. Ferguson, D. P. Ballou, B. A. Palfey, B. T. Ruotolo and E. N. G. Marsh, *Biochemistry*, 2020, **60**, 125–134.

11 W. Bua-ngern, S. Chaiwongwattana, P. Suwannakham and K. Sagarik, *RSC Adv.*, 2016, **6**, 99391–99403.

12 K. Sagarik, P. Panajapo, M. Phonyiem and J. Thisuwan, *Int. J. Quantum Chem.*, 2015, **115**, 1161–1174.

13 J. Thisuwan and K. Sagarik, *RSC Adv.*, 2014, **4**, 61992.

14 J. Thisuwan, P. Promma and K. Sagarik, *R. Soc. Open Sci.*, 2021, **8**, 211168.

15 *TURBOMOLE V 7.5 2020, a development of University of Karlsruhe and Forschungszentrum Karlsruhe GmbH*, V7.5 edn, https://BIOVIA.TURBOMOLE@3ds.com, 2019.

16 *ChemShell, a Computational Chemistry Shell*, see https://www.chemshell.org.

17 J. Kästner, *WIREs*, 2014, **4**, 158–168.

18 P. Hänggi, P. Talkner and M. Borkovec, *Rev. Mod. Phys.*, 1990, **62**, 251–341.

19 E. Pollak and P. Talkner, *Chaos*, 2005, **15**, 026116.

20 J. E. House, *Principles of Chemical Kinetics*, 2nd edn, Elsevier, USA, 2007.

21 E. Wigner, *Z. Phys. Chem.*, 1932, **15**, 203–216.

22 E. Wigner, *Trans. Faraday Soc.*, 1938, **34**, 29–41.

23 J. Kästner, J. M. Carr, T. W. Keal, W. Thiel, A. Wander and P. Sherwood, *J. Phys. Chem. A*, 2009, **113**, 11856–11865.

24 P. Suwannakham and K. Sagarik, *RSC Adv.*, 2017, **7**, 21492–21506.

25 J. Villà, M. Štrajbl, T. M. Glennon, Y. Y. Sham, Z. T. Chu and A. Warshel, *Proc. Natl. Acad. Sci. U. S. A.*, 2000, **97**, 11899–11904.

CURRICULUM VITAE

Name: Phorntep Promma

Education

2014–2018   B.Ed. (Chemistry), Nakhon Ratchasima Rajabhat University, Thailand.

2019–2022   Ph.D. candidate in Chemistry, Suranaree University of Technology, Thailand.

Scholarship

2019 – 2023   Kittibandit Scholarship, Suranaree University of Technology, Thailand.

Publications

Promma, P., Lao-Ngam, C., Lai, R. Y., and Sagarik, K. (2022). Kinetics and thermodynamics of enzymatic decarboxylation of α,β-unsaturated acid: a theoretical study. *RSC advances*, *12*(22), 14223-14234.